3-1986

Transient Response Of A Packed Bed For Both Sensible And Latent Thermal Energy Storage

Shi-Hong Ji
University of Tennessee, Knoxville

Follow this and additional works at: https://trace.tennessee.edu/utk_graddiss

Part of the Mechanical Engineering Commons

Recommended Citation

To the Graduate Council:

I am submitting herewith a dissertation written by Shi-Hong Ji entitled "Transient Response Of A Packed Bed For Both Sensible And Latent Thermal Energy Storage." I have examined the final electronic copy of this dissertation for form and content and recommend that it be accepted in partial fulfillment of the requirements for the degree of Doctor of Philosophy, with a major in Engineering Science.

Donald R. Pitts, Major Professor

We have read this dissertation and recommend its acceptance:

Jeffrey W. Hodgson, Robert J. Krane, Joseph J. Perona

Accepted for the Council:

Carolyn R. Hodges

Vice Provost and Dean of the Graduate School

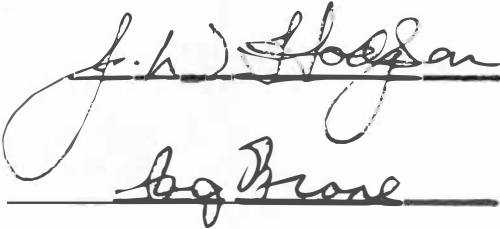(Original signatures are on file with official student records.)

To the Graduate Council:

I am submitting herewith a dissertation written by Shi-Hong Ji
entitled "Transient Response Of A Packed Bed For Both Sensible
And Latent Thermal Energy Storage." I have examined the final
copy of this dissertation for form and content and recommend
that it be accepted in partial fulfillment of the requirements
for the degree of Doctor of Philosophy, with a major in
Mechanical Engineering.

_____

Donald R.Pitts, Major Professor

We have read this dissertation
and recommend its acceptance:

Accepted for the Council:

_____

Vice Provost
and Dean of The Graduate School

TRANSIENT RESPONSE OF A PACKED BED

FOR BOTH SENSIBLE AND LATENT THERMAL ENERGY STORAGE

A dissertation

Presented for the

Doctor of Philosophy

Degree

The University of Tennessee, Knoxville

Shi-Hong Ji

March, 1986

ACKNOWLEDGEMENTS

ABSTRACT

The present work was undertaken to provide a model which accurately predicts the performance of a packed bed energy storage system utilizing spherically encapsulated phase-change material (PCM). Two models were developed which are refered to as the first-order and second-order models. Both models involve modeling of the phase-change material as a conduction problem with both sensible and latent energy storage and include consideration of the temperature gradients in both phases. Both models include the solution of the energy equation for the fluid passing through the packed bed. In the second-order model, both the intra-particle conduction and the dispersion effects in the energy transporting fluid are considered, whereas in the first-order model only the intra-particle conduction effects are considered.

Numerical results obtained with both models have been compared with experimental results available in the published literaature and with experimental data previously obtained at University of Tennessee. Of major importance to any computation is the treatment of the convective heat transfer coefficient between the fluid and the packed bed particles. It was determined that existing correlation equation for the heat transfer coefficient are

quite suitable. Also, confirmation of the convective heat transfer coefficient between the capsules and the fluid can be accurately determined by matching the exiting fluid temperature variation with time at the exit obtained with the second-order model with that obtained by experiment. A specific feature of both models is the use of a physically correct treatment of the exiting fluid temperature boundary condition.

Both analytical models accommodate subcooling and superheating for PCM melting and freezing situations, respectively, as well as supercooling of the PCM in the computer simulation. The significance of subcooling or superheating depends upon the magnitude of the subcooling or superheating. For example, when using NA HPO .12H O as the PCM, and a ratio of the length to the diameter of the bed larger than 1.0.the neglecting of subcooling would result in an error in the total energy stored of about 1/2 percent for each degree of subcooling. Previously reported analyses in the literature do not include the effect of subcooling or superheating.

Both the first-order and second-order models of the present study can be used to predict the melting/freezing time, the melting/freezing front location in the packed bed, and the temperature history of both the transporting

fluid and the PCM in the bed. For the case of small Peclet numbers, comparison with experiment indicates that the first-order model results in significantly greater error than does the second-order model; it does, however, provide an adequate approximation for the latent heat storage in the bed. For Peclet number greater than 200, the difference between the results from the two models is typically less than 10%. The use of the first-order model requires only about one-fourth as much computer time as does the second-order model. The second-order model is shown to provide very accurate results when compared with experimental data in the published literature.

TABLE OF CONTENTS

LIST OF FIGURES

NOMENCLATURE

A = total surface area of heat storage material inside packed bed

c = specific heat

d = inner diameter of packed bed

D = diameter of spherical heat storage material

E = radial length fraction of / R used in determination of phase-change interface

Fr= Floude number

g = gravity accelaration

h = heat transfer coefficient between working fluid and thermal storage material

h_ω= heat transfer coefficient between working fluid and packed bed wall

j = Colburn-J factor

K = coefficient of thermal conductivity

L = latent heat of PCM

Lf= latent heat of two-phase working fluid

Lu = length of packed bed

M = mass flowrate of working fluid

Nu = Nusselt number

Pr = Prandtl number

r = radius of packed bed

r_0= inner radius of packed bed

$\bar{r}$ = non-dimensional radius of packed bed

R = radius of spherical thermal storage material

R_o = outside radius of spherical thermal
  storage material

$\bar{R}$ = non-dimensional radius of heat storage material

$\bar{R}_1 = (1 - \bar{R})$

R^* = radius of melting/freezing front

$\bar{R}^*$ = non-dimensional radius of melting/freezing front

Re = Reynolds number

Rem = modified Reynolds number

Sfr = total frontal cross-sectional area of
  packed bed

St = Stanton number

Ste = Stefen number

t = time

T' = temperature

T = non-dimensional temperature

V_o = superficial veocity

x = distance along packed bed

X = non-dimensional distance used in sensible
  thermal storage packed bed

X' = non-dimensional distance used in packed
  bed with two-phase working fluid

$\bar{X}$ = non-dimensional distance used in latent
  thermal storage packed bed

<x> = thermodynamic quality

Greek Symbols

ε = void fraction of packed bed

ν = coefficient of dynamic viscosity

ρ = density

η = non-dimensional time

$\tilde{\eta}$ = non-dimensional time

$\bar{\tilde{\eta}}$ = non-dimensional time

η' = non-dimensional time

α = thermal diffusivity

Subscripts

c = PCM

f = fluid

fre= freezing

fi = inlet working fluid condition

g = gas

l = liquid region in PCM

m = melting /freezing front

o = initial

p = glass sphere or capsule

s = solid region in PCM

sur = surface of thermal storage material

v = vapor

w = bed wall

1ϕ = single-phase

2ϕ = two-phase

xvi

Superscripts

r = in r-direction

x = in x-direction

CHAPTER 1

INTRODUCTION

The motivation of the work reported herein was thermal energy storage applications in cyclical heating or cooling problems. Any substance which has heat capacity can be used as a heat storage material, but this does not mean that it is suitable for practical engineering applications. Energy storage in general, although not actually reducing energy needs, does play an inportant role in energy conservation strategies, thereby reducing energy comsumption. It also enhances the use of renewable energy sources and permits the more efficient use of high capital cost, energy conversion plants.

The energy crisis in the early 1970's prompted many industrial countries to develop new energy sources and conservation techniques in order to reduce reliance on foreign oil while continuing to increase their industrial productivities. One of these general developments, the energy storage unit, can greatly assist in improving the overall efficiency of some energy conversion units through load leveling, may decrease energy demands by the use of waste energy recovery, and can enhance utilization of alternative sources of energy.

As early as 1975, the U.S. Energy Research and Development Administration (ERDA) requested the National Research Council to undertake a study on the potential of advanced energy storage systems [1]. One of the resulting analyses showed that a better designed heat storage unit would be economically attractive.

One example of energy storage unit utilization is seen in solar energy engineering where thermal energy storage units are an integral part of many solar energy systems. These are used to supply heat not only during the night when no solar energy is collected but also for periods of time, say two or three days, when incident solar radiation is low due to clouds. In industry, thermal storage systems also play an important role in the recovery of waste heat in situations where a large percentage of energy is otherwise discharged to the surroundings as waste heat. An additional application of thermal storage devices is the use of their stored thermal energy, obtained in off peak hours, during periods of high demand when conventional energy sources may be expensive or even unavailable.

Presently, most thermal storage devices use sensible thermal energy where good technology has been developed for designing such systems [2]. A great amount of

research has been done on sensible thermal energy storage packed beds, and, in particular, in rock-beds. This is hardly surprising, considering that over three-quarters of all single family dwellings in the U.S. are provided with warm air heating systems. The use of solar collectors has enabled these types of building heating units to operate without the need for heat exchangers other than the packed bed.

In recent years thermal storage units that utilize the latent heat of the storage material have received considerable attention [3,4], because these offer advantages over materials whose thermal storage capacity is based exclusively on sensible heat. These advantages consist of: (1) high energy storage densities (which means a reduction in storage volume for a given capacity); (2) smaller overall system temperature differentials (which means that the heat capacity of the storage unit is concentrated in a narrow temperature range thereby promising an improvement of solar heating system performance as the mean inlet temperature is expected to be lower); and (3) higher heat collection efficiency. However, very little literature has been found which deals with the study of thermal storage packed beds with phase-change occuring in the thermal storage material, and

no literature was found for both the thermal storage material and working fluid undergoing phase-change.

In solar engineering for residential or commercial heating purposes, air, water and Freon are the best potential candidates for the working fluid. The selection of the phase change thermal storage material has generally involved the following selection criteria: temperature of transition between 25 and 70° C; high latent heat and specific heat; long term stability under temperature cycling conditions; good thermal conductivity; abundant supply; and low cost. The ideal material which satisfies all of these selection criteria has not yet been found, but the list in Table 1 summarizes the materials which have been studied most intensively. To a large extent, good design of a thermal storage device depends upon the choice of the working fluid and phase-change material (PCM) for energy storage.

To know whether a particular latent heat thermal energy storage system can achieve the required storage and withdrawal rates as well as the total heat capacity is the major design problem. Proper design rests upon understanding the phase-change processes in the PCM and, hence, on modeling the process. current PCM technology focuses on encapsulated or pelletized phase-change

TABLE 1 SOME PHASE-CHANGE MATERIALS

AND SELECTED PROPERTIES

Material	Cost(c/kg)	L(kj/kg)	Phase-Change Temperature	Appl.Temp.
$Na_2S_2O_3 5H_2O$	26	119	49 C(119 F)	Active Heating (35-36°C)
Wax P116	44	146	47 C(116 F)	
Na_2HPO_4 $12H_2O$	44	264	36 C(97 F)	
$Na_2SO_4/NaCO_3$ $10H_2O/BORAX$	10-22	209	23 C(84 F)	Passive Heating (23-30°C)
$NaCl_2 \cdot 6H_2O$	9	188	29 C(84 F)	"

material. In such case, the heat transfer from the fluid to the PCM pellets can be generally assumed to be controlled by either forced convection to or conduction in the pellets. In a typical packed bed, the pellets usually are so small that natural convection in the PCM melt region is not important, and conduction is indeed the dominating heat transfer process there.

The prediction of the melting or freezing front within the pelletized PCM is important in order to estimate the amount and rate of thermal energy stored in or withdrawn from the bed. This is a moving boundary problem of the Stefan type best solved by numerical methods.

Most important in any packed bed thermal storage unit analysis is the determination of the heat transfer coefficient. This determination is a very complicated problem influenced by many factors including properties and superficial velocities of the energy transporting fluid, the voidage of the packed bed, and the geometry and size of the pellets in the bed. It is impossible to formulate a general mathematical equation for the heat transfer coefficient solely by an analytical method, even for the packed bed with a single phase fluid. But, fortunately, this has been the topic of many preceding

investigations, and some empirical and semi-empirical correlation equations are available.

The latent heat packed bed with working fluid undergoing phase-change should be so designed that the quality of the fluid should be near zero (for condensing) or near 1.0 (for boiling) at the exit of the bed during bed charging. Such a condition would mean that most of the working fluid's latent heat has been absorbed by the thermal storage material. Although the temperature in the two-phase flow regime is almost constant, the change of fluid quality with length causes the heat transfer coefficient to be a function of bed length position.

The present study focuses on an analysis of a phase-change type storage system intended for use with a heat pump in residential solar heating. The following chapters specify the particular problems of interest.

CHAPTER   2

SURVEY OF PREVIOUS WORKS

Over the years, a great amount of practical work on sensible thermal storage in packed beds, and particularly in rock beds, has been undertaken in many countries throughout the world. The relative published literature is very extensive, including structural aspects of packed beds, the mechanism of fluid flow, the gross performance parameters such as pressure drop and overall heat transfer coefficient between the working fluid and thermal storage materials, and some work concerning phase-change thermal storage materials.   But there exist very few references about packed beds with encapsulated phase change materials.   No publication has been found treating packed beds involving phase-change in both the working fluid and the thermal storage material.

In this survey, no attempt is made to report on all of the related publications, but it is intended to include sufficient coverage of the more important related works. This survey may be divided into four aspects: (1) work relative to fluid flow in packed beds; (2) heat transfer coefficient in the packed pad; (3) sensible thermal energy storage packed bed systems intended for solar energy

applications, in which some form of thermal storage device is essential to accommodate system demands which are often out of phase with direct solar energy availability, and (4) latent heat storage in packed beds utilizing the latent heat of fusion in suitable substances that undergo melting and freezing at a desired temperature level.

(1) Fluid Flow in Packed Beds

Three major models for flow through a packed bed were developed in the past.

(1.A) Model 1:

In 1952, S.Ergun [5] proposed a so-called "channel model", which envisages the packed bed as consisting of an assembly of tortuous conduits. From this model he postulated a well-known and widely used expression to calculate the pressure drop caused by the friction between the fluid and particles, and expansion and contraction along the packed bed.

Ergun's equation is

$$\frac{\Delta p}{Lu} g_c = 150 \; \frac{(1-\varepsilon)^2}{\varepsilon^3} \cdot \frac{\mu V_o}{D} + 1.75 \; \frac{(1-\varepsilon)}{\varepsilon^3} \frac{M_f \cdot V_o}{S_{fr} \cdot D}$$

I.F.MacDonald, et al., [6] introduced a modified Ergun equation, where the constants 1.75 and 150 are replaced by packing geometry dependent parameters A' and B' which were determined by comparison with extensive data. In general, this modified equation is used to calculate pressure drop across the bed in terms of the Fanning friction factor.

(1.B) Model 2:

W.E.Ranz [7] suggested a discrete particle model which regards the system as consisting of an assembly of particles submerged in the flowing fluid, each possessing its own individual boundary layer. He pointed out that there is no continuous channel along which the fluid flows; most of the pressure drop occurs on the forward face of each individual particle and a relationship between the actual average velocity and the superficial velocity is built.

Both of the above models provide reasonably good pressure drop predictions for spherical, or near-spherical shapes, but are inadequate for particles of low sphericity.

(1.C) Model 3:

In 1962, C.L.Kusik and J.Happel [8] proposed another model, based on the consideration that the particle wake effectively decreases the area available for flow. This area reduction creates stagnant regions in the fluid, which are represented by a stagnant void fraction . T.R.Galloway and B.H.Sage [9] reported the values of for different particle shapes from available experimental data on single particles and on packed beds.

W.H.Gauvin and S.Katta [10] developed a theoretical approach based on the concept of stagnant void fraction and the principle of drag additivity to estimate stagnant voidages for various particle shapes arranged in a packed bed. A new type of friction factor based on this approach was correlated satisfactorily with a shape factor. The momentum transfer data were also correlated with the sphericity of the particles.

In seeking theoretical models to describe the fluid transport process in the bed medium, two main approaches have been followed. In the first [11], the flow is described as a random process in which the progress of the fluid is assumed to creep over the surface of the packing elements. In the second approach [12,13,14], a differential form of the modified Ergun equation is used.

(2) Heat Transfer Correlation in Packed Beds

Much literature about heat transfer correlations for single-phase flow in a packed bed has been published. Most of the reported investigations have presented anddiscussed empirical equations for the heat transfer coefficient. Because of the different experimental set-ups and different heating metdods used in the experiments, however,many of the results apply only to situations similar to those of the specific experiment for which a correlation was obtained. However, all of those results still offer some useful guidelines for constructing a heat transfer coefficient correlation as a first approximation for calculations in a single-phase flow, packed bed.

In 1965, J.J.Barker [15] presented an extensive survey of heat transfer coefficient correletions available up to 1964. A considerable spread in the data was found when the Colburn J factor was ploted versus the Reynolds number, which was an expected result. It is unreasonable to think that a correlation of J as a function of Reynolds number only could be obtained, because the data were obtained from different beds differing in geometric parameters, etc.

H. S. Mickley and K. A. Smith [16] studied the local property effect on heat transfer by making basic fluid flow measurements. Their results showed that the low heat transfer coefficient regions near the contact points between the particles correspond to low velocity and low turbulent intensity regions.

Empirical correlations are generally useful for the particular purpose for which they are made. For the sake of clarity in the application and use of the data obtained in packed beds, it seems desirable to develop expressions in a comprehensive form applicable to all types of flow. In doing so, theoretical developments, as well as empirical approaches , have been considered.

In 1968, D.Handley and P.J.Heggs in their article [17] on the momentum and heat transfer mechanisms in regular shaped packed beds, experimentally determined the heat transfer coefficient by using a transient method based on an iterative solution of Schumann's mathematical model [18]. The advantage of this method is that the heat transfer coefficient correlation thus obtained includes consideration of the effects of the dispersion and intraparticle conduction. Schumann's model assumes that there are no thermal gradients within the particles; in fact, it is a uniform temperature model.

W. E. Ranz op.cit., developed a method of analysis based on properties of a single particle for estimating and characterizing heat transfer rates in packed beds. Equations for estimating effective thermal conductivity and diffusivity are derived, and parametric constants relating the actual fluid velocity and average lateral velocity to the superficial velocity, which is defined as the velocity of the working fluid passing through a completely void bed, are shown to characterize the performance of a packed bed. This method reveals the mechanisms by which energy is lost and heat transfer occurs. The simple correlation equation developed by Ranz can be used up to a value of Reynolds number of 10^6 and for values of Pr between 0.6 and 400.

This correlation is

$$Nu = 2.0 + 0.6 \cdot Pr^{1/3} \cdot Re^{1/2} \qquad (2\text{-}1)$$

where Re is based on the actual velocity and the diameter of spheres. The relationship between actual velocity and superficial velocity, as an approximation for the packed bed, can be given by

$$V = 10.73 \cdot V_o$$

where V_o is the superficial velocity.

15

D. E. Beasley and J. A. Clark [19] adapted the heat transfer correlation developed by Galloway and Saze [9]. That correlation has the following form:

$$N_u = 2.0 + C_1 Re^{1/2} \cdot Pr^{1/3} + C_2 \cdot Re_o \cdot Pr^{1/2}$$ (2-2)

Where $Re_o = V_o d/ v$
$C_1 = 1.354$
$C_2 = 0.0326$

B. T. Kulakowski and F. W. Schmidt [20] used Dunkle and Ellul's [21] correlation in their packed bed design. This is

$$\frac{hDS_{fr}}{C_f M_f} = 2.4 Re^{-0.3}$$ (2-3)

Where

$$Re = \frac{M_f d}{\mu_f S_{fr}}$$

This correlation is based on an equivalent sphere diameter D where the sphere volume is equal to that of the packed particles.

Hanley and Hegg [17] expressed the heat transfer correction in the following form.

$$J = St \cdot (Pr)^{2/3} = \frac{C_1 (Rem)^{C_2}}{\varepsilon}$$ (2-4)

where Re is a modified Reynold's number, and given by

$$Re_m = \frac{2}{3} \frac{D\rho_f V_f}{(1-\varepsilon)\mu_f}$$

and the Stanton number, St, is

$$St = \frac{h \cdot S_{fr}}{C_f \cdot M_f}$$

Many other equations are available for calculating the heat transfer coefficient in a packed bed. For example, Timofeev, as reported by S.S.Zabrodsky [22], proposed the following empirical formula which describes the experimental data for heat transfer coefficients for a fixed bed of any material.

$$N_u = 0.106 \cdot Re \qquad 20 < Re < 200$$

(2-5)

$$N_u = 0.61 \cdot Re^{0.67} \qquad Re > 2000$$

where Re is based on the superficial velocity and the sphere diameter.

It is obvious that these equations are simple, but they do not have very high accuracy and do not cover a sufficient range of Reynolds number.

Another Russian worker, Chechetkin, as also reported by S.S.Zabrodsky [22], obtained the following empirical formula for nonmetallic packings:

$$N_u = 0.123 \cdot Re^{0.83} \qquad 50 < Re < 2000 \qquad (2-6)$$

In calculating the value of the Reynolds number in both this and the Timofeev equation, the superficial velocity and equivalent diameter (De= void fraction / surface area of the particles per unit volume of the bed) are used.

The heat transfer coefficient between the working fluid and the wall of a packed bed is much different from that between the working fluid and the particles inside the bed. Yagi and Kunii [23] obtained coefficients for heat transfer on the inner surface, as well as the mean effective thermal conductivities, of a packed bed in terms of a theoretical model of heat transfer. The model was then applied to the prediction of wall film coefficient, especially for low Reynolds number.

All of the heat transfer correlation expressions mentioned in the preceding discussion are empirical and dependent on the specific physical parameters involved in obtaining the particular correlation.

(3) Sensible Thermal Energy Storage Packed Bed

B. T. Kulakowski and F. W. Schmidt [1] presented a method for the design and sizing of a packed bed thermal storage unit for a heating system. The characteristics of

the design are suh that a controlled bypass of the thermal storage unit during the retrieval process is used in order to maintain the fluid temperature leaving the system at a constant value.

D. E. Beasley and J. A. Clark [19] conducted an analytical and experimentudy of a packed bed, sensible heat thermal storage unit; both charging and recovery modes were included in their study. Spatial variations in void fraction were found to have some effect on the dynamic response of both fluid and solid temperatures. A uniform temperature model for the thermal storage material was assumed. This is a reasonable approach because the thermal storage material used was aluminum with high thermal conductivity.

R. F. Benenati and C. B. Brosilow [24] studied the radial variation of void fraction within a packed bed of uniform spheres. They found that the voidage distribution takes the form of a damped oscillatory wave with the oscilations damped out at about 4.5 to 5 sphere diameters from the wall.

(4) Latent Heat Packed Bed

Latent heat storage at low temperature is of interest for a variety of residential and commercial applications. The development of dependable thermal storage systems for

such purposes requires a better understanding of the melting and freezing characteristics of thermal storage materials. The low thermal conductivity of organic PCM's such as paraffin wax and the almost total absence of convective enhancement of heat transfer in phase-stabilized salt hydrates have resulted in the need for heat exchangers with large surface area per unit storage volume. The use of encapsulated phase-change materials in packed beds offers a simple solution to this problem.

(4.A) Melting and Freezing Process of Phase-Change Materials.

In 1958, P. A. Longwell [25] used a graphical method for obtaining a numerical solution to Stefan-type problems involving a moving boundary which can be described in terms of one space coordinate. In that reference, the equations are derived and are applied to two examples involving solidification. The method used takes into account both sensible heat and latent heat.

W. D. Murray and F. Landis [26] improved the previous methods for the solution of one-dimensional heat conduction problems with melting and freezing. Two new and more generally applicable numerical methods suitable for digital and analog computation were developed in 1959.

Their approaches utilize a traveling space network where the fusion point travel can be accurately determined, instead of the stationary space network used in previous methods.

J. E. Sunderland and R. J. Grosh [27] considered superheating and subcooling. Their method consisted of calculating the temperature distribution before the phase-change occurs, during the transient process of phase-change, and after steady-state conditions are obtained, if such steady state is attained.

A simple algorithm incorporating the equivalent heat capacity model is described for the finite difference heat capacity analysis with phase-change by J. S. Hsiao [28]. The specific heat associated with those nodes adjacent to the fusion front are determined using a linear interpolation of nodal temperatures to properly account for the latent heat effect. This scheme was proven to be insensitive to the selection of the temperature interval assumed for phase change to take place. Therefore, very small or large temperature intervals can be used to properly simulate the fusion of phase-change materials.

L. C. Tao [29] developed a numerical method and graphs of generalized solutions for the moving interface problem of freezing a saturated liquid inside a cylinder

or a sphere. Before his work, all other generalized analytical solutions were not readily applicable to cylinders and spheres.

In order to improve the thermal conductivity of the solidified material, R. Siegel [30] suggested that some fine particles of high conductivity material should be dispersed in the salt, which certainly aids the solidification rate. However, some effective volume is occupied by these particles that do not melt, so the heat of fusion per unit volume is diminished.

A. D. Solomon [31] has undertaken extensive research concerning phase change materials at the United States Oak Ridge National Laboratory. He developed simple equations for evaluation of the melting time of phase change materials having a slab shape and a convective boundary condition. A comparison of his analytical results with numerical computations shows a relative discrepancy of less than 7% in all cases.

Due to the nonlinearity associated with the moving boundary condition at the solid-liquid interface, it is difficult to obtain analytical solutions of phase-change problems. J. Y. Ku [32] developed a systematic approach whereby the standard Laplace transform technique is extended to yield exact solutions for some simple

(4.B) Latent Heat Storage System

L. G. Marianowski and H. C. Maru [33] studied a latent heat thermal energy storage system above $450^{o}C$ (840 F). They placed emphasis on the choice of the salts. The main factors they considered were thermal properties, physical properties, the change in melting point, and volumetric expansion on melting. Their work selected a salt of 35% Li_2Co_3 and 65% K_2Co_3 mixture as a model system for experimental effort in the temperature range of their interest. A mathematical analysis was described and compared with the experimental results. The analysis was based on the slab geometry.

The major problem in using salt hydrates as PCMs is their poor nucleating properties which result in supercooling of the liquid salt hydrate prior to freezing. Suitable measures must be adopted to eliminate supercooling or reduce it to a minimun. A typical method suggested in the literature for this purpose is to add some nucleating agents to the salt, or to use metallic heat exchanging surfaces immersed in the salt hydrates. See,for example, Lou [34].

At the Electrotechnical Laboratory, Ibaraki, Japan, a direct contact latent heat thermal energy storage unit which consists of a bundle of vertically arranged, thin

HDPE (high density Polythylene) rods was developed by Abe, et el., [35] for the purpose of studing charge and discharge characteristics. Of particular interest are the effects of low charge/discharge rate and of varing inlet and initial temperatures.

Up to now, only a few published papers dealing with a packed bed of encapsulated, phase-change material have been found. R. J. Wood , S. D. Gladwell, et al., [36] have reported experimental and simulation results for a latent heat thermal energy storage system using a small scale, experimental packed bed of 20 mm diameter, wax filled, high density polypropylene spheres. A packed bed heat transfer correlation was also developed. A charateristic of their analytical method for predicting the thermal performance of the storage unit is that no temperature gradient exists inside the capsules. It is obvious that this assumption of uniform temperature in the capsules is not valid because the thermal storage material has a poor conductivity, and thus the Biot number is usually much larger than 1.0. Certainly in this case significant errors will be caused by the assumption of uniform temperature in the storage material.

T.Saitoh and K.Hirose [37] carried out an experimental and theoretical investigation of the unsteady thermal charateristics of a latent heat, thermal energy storage unit using spherical capsules. Particular attention was focused on developing a method for predicting the thermal performance of a latent heat thermal energy storage system unit for design purposes. A simulation program that rigorously considers transient aspects of both the surrounding heat transfer fluid and the phase-change material packed inside the spherical capsules was developed. The experimental thermal responses under various conditions were obtained for both charging and discharging processes. For the charging process, the experimental results were coincident with the modelling results. But superheating, subcooling, and supercooling were not considered in modelling, and a quasi-steady approximation for heat transmission inside the spherical capsules was assumed. These flaws limit the use of their simulation method.

Much of the past work concerning the use of phase-change materials in latent heat thermal energy storage units deals with the behavior of freezing and melting, the location of melting front, and how to choose a suitable phase-change material for a particular thermal

energy storage system so that the process of phase-change takes place in the operating temperature range of the total system. Natural convection inside the capsule is usually neglected because the small size of the capsule and small variation of the density of the PCM with temperature results in low convective effects in the PCM. It may be that natural convection should be considered in a rather large size PCM capsule.

CHAPTER   3

MATHEMATICAL MODEL OF THERMAL STORAGE PACKED BED

(1) Sensible Thermal Storage in a Packed Bed

Two models for determination of the transient response of packed bed thermal storage units will be presented in this section. The first takes the intraparticle conduction and the dispersion effects in the working fluid into consideration. The temperature of the surface in contact with the fluid depends on the convective film coefficient and the intraparticle conduction. As the fluid flows through the packed bed, small eddies are generated in the fluid thereby causing extensive mixing of the fluid particles. This mixing and the effect of the axial molecular conduction of heat within the fluid are classified as the dispersion effects. This model is called a second-order model in the present study.

If the dispersion effects in the fluid are neglected, only intraparticle conduction is considered. The equation for the fluid in the second-order model will then be degraded into a first-order differential equation, and we call the resulting model the first-order model.

(1.A) The Second-Order Model

The transient response of the thermal storage packed bed is governed by (i) the two-dimensional conservation of energy equation in cylindrical coordinates for the working fluid, accounting for temperature gradients in both axial and radial directions, and by (ii) the one-dimensional transient heat conduction equation in spherical coordinates for the phase-change thermal storage material.

The governing equation for the working fluid in non-dimensional form is as follows (see Appendix A)

$$\frac{1}{PE} \frac{\partial^2 T_f}{\partial X^2} - \frac{\partial T_f}{\partial X} - \frac{\partial T_f}{\partial \eta} - (T_f - T_{sur}) + \beta \left(\frac{1}{\bar{r}} \frac{\partial T_f}{\partial \bar{r}} + \frac{\partial^2 T_f}{\partial \bar{r}^2} \right) = 0 \qquad (3\text{-}1)$$

where

$$X = \frac{hA \cdot x}{M_f \cdot C_f \cdot Lu}$$

$$\eta = \frac{h \cdot A \cdot t}{S_{fr} \cdot \rho_f \cdot C_f \cdot Lu \cdot \varepsilon}$$

$$T = \frac{T' - T_o'}{T_{fi}' - T_o'}$$

$$\bar{r} = \frac{r}{r_o}$$

$$\beta = \frac{\varepsilon \cdot K_f^R \cdot Lu \cdot S_{fr}}{h A R_o}$$

$$PE = \frac{(\rho_f V_f C_f)^2 S_{fr} \ Lu \cdot \varepsilon}{h \cdot A \cdot K_f^x}$$

The boundary conditions are

$$T_f = T_{fi}(\eta) \qquad\qquad at \quad X = 0$$

$$\frac{\partial T_f}{\partial X} = 0 \qquad\qquad at \quad X \to \infty$$

$$\frac{\partial T_f}{\partial \bar{r}} = 0 \qquad\qquad at \quad \bar{r} = 0$$

$$(T_f - T_w) = \frac{-2}{(Bi)w} \frac{\partial T_w}{\partial \bar{r}} \Bigg|_{\bar{r}=1} \qquad\qquad at \; \bar{r} = 1.0$$

where

$$(Bi)\,w = \frac{hw \cdot d}{Kw}$$

and the initial condition

$$T_f = T_o(X) \qquad\qquad at \quad \eta = 0$$

In some of the thermal storage packed beds (see Appendix A), the wall is well insulated, and, therefore, the temperature gradient in the radial direction becomes unimportment. In this case the governing equations can be simplified into the following form

$$\frac{1}{PE} \frac{\partial^2 T_f}{\partial X^2} - \frac{\partial T_f}{\partial X} - \frac{\partial T_f}{\partial \eta} - (T_f - T_{sur}) = 0 \qquad\qquad (3\text{-}2)$$

with boundary conditions

$$T_f = T_{fi}(\eta) \qquad\qquad at \quad X = 0$$

$$\frac{\partial T_f}{\partial X} = 0 \qquad\qquad as \quad X \to \infty$$

and the initial condition is unchanged.

The governing equations for spherical particles (see Appendix B) is

$$\frac{\partial T_p}{\partial \bar{\eta}} = \frac{\partial^2 T_p}{\partial \bar{R}^2} + \frac{2}{\bar{R}} \frac{\partial T_p}{\partial \bar{R}} \qquad\qquad (3-3)$$

where

$$\bar{\eta} = \frac{K_p \cdot t}{r_o^2 \cdot \rho_p \cdot C_p}$$

$$T_p = \frac{T_p' - T_o'}{T_{fi}' - T_o'}$$

$$\bar{R} = \frac{R}{R_0}$$

the boundary conditions for equation (3-3) are

$$\frac{\partial T_p}{\partial \bar{R}} = 0 \qquad\qquad at \, \bar{R} = 0$$

$$(T_f - T_{sur}) = \frac{-2}{(Bi)p} \frac{\partial T_p}{\partial \bar{r}} \bigg|_{\bar{r}=1} \qquad\qquad at \, \bar{R} = 1$$

where

$$(Bi)p = \frac{h\,D}{K_p}$$

and the initial condition is

$$T_p = T_o(X) \qquad at \quad \eta = 0$$

Some previous investigators have used different boundary conditions for the fluid, particularly for the condition at the exit. T. Saitoh op.cit., chose

$$\left.\frac{\partial T_f}{\partial X}\right|^{+} = \left.\frac{\partial T_f}{\partial X}\right|^{-}$$

at the exit and Beasley and Clark [19] used

$$\frac{\partial T_f}{\partial X} = 0$$

at the exit.

In fact, both dT /dx and T at the exit are varying with time during the thermal charging and discharging processes. Rather than use either of the preceding, We chose $\dfrac{\partial T_f}{\partial X} = 0$ as $X \to \infty$

as a more realistic, physical boundary condition.

Equations (3-2) and (3-3) are a set of coupled, second-order, time-dependent, partial differential equations which can be solved by the implicit finite-difference method.

(1.B) The First-Order Model:

If the dispersion effects in the fluid are neglected, the energy equation for the fluid reduces to a first-order partial differential equation. The complete mathematical model of the packed bed in terms of the dimensionless parameters becomes

For the fluid:

$$\frac{\partial T_f}{\partial X} + \frac{\partial T_f}{\partial \eta} + (T_f - T_{sur}) = 0 \qquad (3-4)$$

with

$$T_f = T_{fi}(\eta) \qquad at \quad X = 0$$

and

$$T_f = T_o(X) \qquad at \quad \eta = 0$$

The governing equation and the boundary and the initial conditions for the spherical particles remains unchanged.

Compared with the second-order model, only the second-order, X-direction derivative term in the governing equation for the working fluid has been omitted. The error caused by this omission depends on the value of the Peclet number. If the size of the packed bed has already been decided, the Peclet number is a function of the

properties of the fluid and thermal storage material, and the flowrate of the working fluid. In the case with Freon 113 as the working fluid, a glass sphere diameter of 0.625 in, and a packed bed inner diameter of 5 in, the Peclet number as a function of flowrate is presented in "TABLE 2".

TABLE 2   Peclet Number Versus Flowrate of Working Fluid

Flowrate (Gallon/min)	Re (Based on Sphere Dia.)	PE
0.1	17.5	>2500
0.2	34.1	>5000
0.5	85.5	>13961
1.00	170.5	>39315
2.00	341.5	>110000
4.00	682.4	>310000

(2) Latent Heat Storage in a Packed Bed

The latent heat storage packed bed requires the use of a phase-change substance as the thermal storage material. This material for the case under study is encapsulated in thin wall, spherical capsules which are surrounded by a flowing working fluid. It is the purpose of this section to concentrate mainly on building a mathematical model for the transient thermal performance of a latent heat, thermal energy storage unit of the spherical capsule type. Throughout this work, a moving boundary problem will be taken to mean a time-dependent problem represented by a parabolic partial differential equation together with a prescribed initial condition and boundary conditions. One of these conditions is given on a boundary which moves in a way that depends on the solution of the partial differential equation, or, in other words, such a problem is characterized by the fact that the domain in which the partial differential equation is to be solved constitutes one of the unknowns of the problem. The problem is non-linear, and due to the unknown and transient nature of the boundary, it is difficult to solve by common numerical methods.

The greatest difficulty in solving a moving boundary problem lies in tracking the unknown phase-change boundary. The approach used is based on energy conservation in the material from which the phase-change boundary location is a natural consequence of solving the energy conservation laws for the system. The following assumptions are made in the approach:

(a) the melting front is sharp, that is, there is no mushy region between the solid and the liquid phases.

(b) Natural convection effects inside the capsule are negligible.

(c) Spherically symmetrical melting and freezing can be assmed , i.e. heat conduction is dominant.

(d) The volumetric increase and decrease due to phase-change is negligible.

(2.A) Second-Order Model

The non-dimensional variables defined for the analysis of the spherical phase-change material (PCM) are

$$STe = \frac{C_l \cdot (T_m' - T_o')}{L}$$

$$\eta = \frac{K_l \ (T_m' - T_o') \cdot \ t}{R_o^{2} \cdot \rho_l \cdot L}$$

$$\overline{R} = \frac{R}{R_o}$$

$$\zeta_1 = \frac{\rho_s \ C_s \ K_l}{\rho_l \cdot \ C_l \cdot \ K_s}$$

$$\zeta_2 = \frac{K_s}{K_l}$$

$$\zeta_3 = \frac{\rho_l K_s}{\rho_s K_l} = \frac{\rho_l}{\rho_s} \zeta_2$$

The other non-dimensional parameters are the same as in the preceding section.

The energy conservation equations for the PCM are:
In the liquid region

$$STe \cdot \frac{\partial T_l}{\partial \overline{\overline{\eta}}} = \frac{\partial^2 T_l}{\partial \overline{R}^2} + \frac{2}{\overline{R}} \frac{\partial T_l}{\partial \overline{R}} \qquad (3-5)$$

which is valid for $R^* < R < 1$ (melting case) or for $0 < R < R^*$ (freezing case).
In the solid region

$$STe \cdot \frac{\partial T_s}{\partial \overline{\overline{\eta}}} = \zeta_1 \cdot \left(\frac{\partial^2 T_s}{\partial R^2} + \frac{2}{\overline{R}} \frac{\partial T_s}{\partial \overline{R}} \right) \qquad (3-6)$$

which is valid for $0 < R < R^*$ (melting case) or for $R^* < R < 1$ (freezing case)

The two coupling conditions at the phase-change interface are

$$T_l = Ts = Tm \tag{3-7}$$

and for the melting case

$$\frac{\partial \overline{R}^*}{\partial \overline{\eta}} = -\frac{\partial T_l}{\partial \overline{R}}\bigg|^-_{\overline{R}=\overline{R}^*} + \zeta_2 \cdot \frac{\partial T_s}{\partial \overline{R}}\bigg|_{\overline{R}=\overline{R}^*} \tag{3-8}$$

or for the freezing case

$$\frac{\partial R^*}{\partial \overline{\eta}} = -\zeta_3 \frac{\partial T_s}{\partial \overline{R}}\bigg|_{\overline{R}=\overline{R}^*} + \frac{\zeta_3}{\zeta_2} \cdot \frac{\partial T_l}{\partial \overline{R}}\bigg|_{\overline{R}=\overline{R}^*} \tag{3-9}$$

In these expressions the subscripts l and s indicate the liquid and solid phases, respectively, Tm is the melting temperature, and r* is the location of the melting front. Other boundary conditions on equations (3-5) and (3-6) are

$$\frac{\partial T}{\partial R} = 0 \qquad\qquad \overline{R} = 0$$

and the surface temperature of the PCM is (see Fig d-2)

$$T_1 = \frac{\dfrac{-(1+E)}{E}T_2 - \dfrac{K_p}{K_c} \cdot \dfrac{T_{sur}}{1.39}}{\dfrac{(2+E)}{(1+E)} - \dfrac{K_p}{1.39 \cdot K_c}}$$

where the Tsur can be obtained by the convection boundary condition on the surface of the capsules.

The energy equation for the working fluid remains the same as that in the sensible thermal storage packed bed, i.e.,

$$\frac{1}{PE} \frac{\partial^2 T_f}{\partial X^2} - \frac{\partial T_f}{\partial X} - \frac{\partial T_f}{\partial \eta} - (T_f - T_{sur}) = 0 \qquad (3\text{-}2)$$

and the boundary conditions on the fluid are also unchanged.

Equations (3-2), (3-5) and (3-6), together with coupling conditions (3-7) and (3-8) or (3-9) and the boundary conditions, constitute a set of coupled partial differential equations which can only be solved numerically.

(2.B) First-Order Model

(a) If the energy dispersion in the fluid is neglected, the energy equation for the fluid simplifies to a first order differential equation, just as we discussed in section (1.B). The equations for the spherical PCM remain the same as the equations in the preceding section.

(b) For the melting/freezing case with the assumption that the phase-change material is initially at the melting point, equations (3-8) to (3-9) simplify to the following: For the melting case where R < R < 1

$$\frac{\partial \overline{R}^*}{\partial \overline{\eta}} = - \frac{\partial T_l}{\partial \overline{R}} \bigg|_{\overline{R} = \overline{R}^*}^{-} \qquad (3\text{-}10)$$

For the freezing case where $0 < R < R^*$

$$\frac{\partial R^*}{\partial \bar{\bar{\eta}}} = -\zeta_3 \frac{\partial T_s}{\partial \bar{R}} \bigg|_{\bar{R} = \bar{R}^*} \tag{3-11}$$

Virtually this assumption ignores the sensible heat of the packed bed below the melting temperature (for the melting case), or above the melting temperature (for the freezing case). If the initial temperature of the bed is not too much lower or higher than the melting temperature, this assumption will not cause significant error. It should be noted that for the phase-change material 'NA$_2$HPO$_3 \cdot$12H$_2$O' and in the temperature application range of 20° to 50° celsius, neglecting subcooling or superheating will cause an error of approximately 0.5% in total thermal storage per degree celsius of subcooling or supercooling.

(2.C)Supercooling

In the freezing process, solidification does not start until the temperature of the phase-change material reaches a point considerablly lower than the freezing temperature. This is known as supercooling. The amount of supercooling depends on a number of factors and can not be determined by analysis. As soon as the solidification begins, the temperature at the phase-change interface

jumps to the freezing point value. The heat of fusion released is not only transferred to the fluid but also to the interior to heat the supercooled liquid phase-change material. This is depicted in figures (3-1) and (3-2).

The temperature distribution in both the liquid and solid phases and the location of the solidification front is of primary concern in analysis. The sets of equations used for computating the temperature distribution are as follows.

(2.C.1)Before Freezing Starts ($t < t_{fre}$):

As the temperature is higher than the temperature of supercooling, the solidification will not start and equation (3-2) and equation (3-5) will be used for the working fluid and the PCM, respectively. A major characteristic of this case is that the temperature of the PCM is below the melting temperature, but higher than the temperature of supercooling. A typical temperature distribution before the moment of freezing is shown in figure (3-1).

(2.C.2) After Freezing Starting ($t > t_{fre}$):

The energy balance equation for the phase-change interface changes into the following forms

$$\frac{\partial R^*}{\partial \bar{\eta}} = -\zeta_3 \frac{\partial T_s}{\partial R} \bigg|_{\bar{R} = \bar{R}^*} - \frac{\zeta_3}{\zeta_2} \cdot \frac{\partial T_l}{\partial R} \bigg|_{\bar{R} = \bar{R}^*} \qquad (3-12)$$
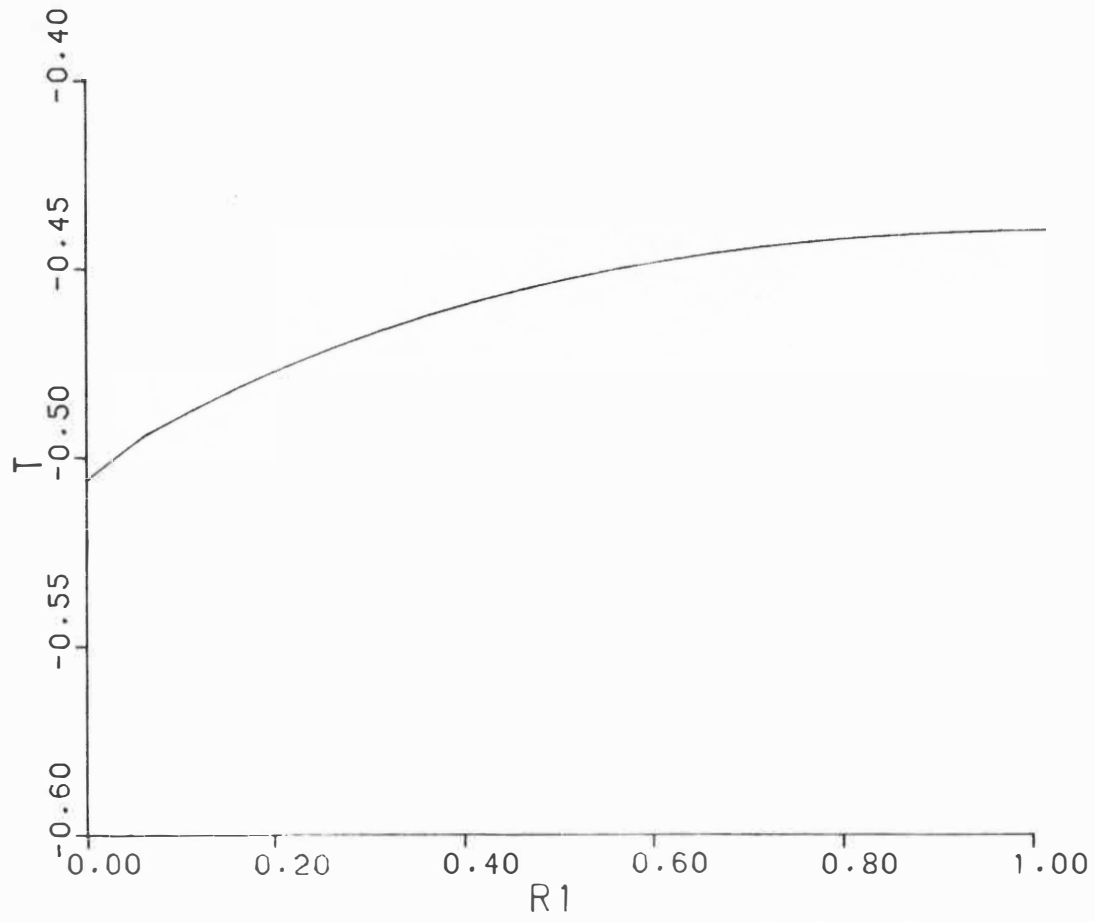
3-1   Temperature Distribution inside Capsule at
       Moment before Freezing Starts; MF=119.9 Kg/hr
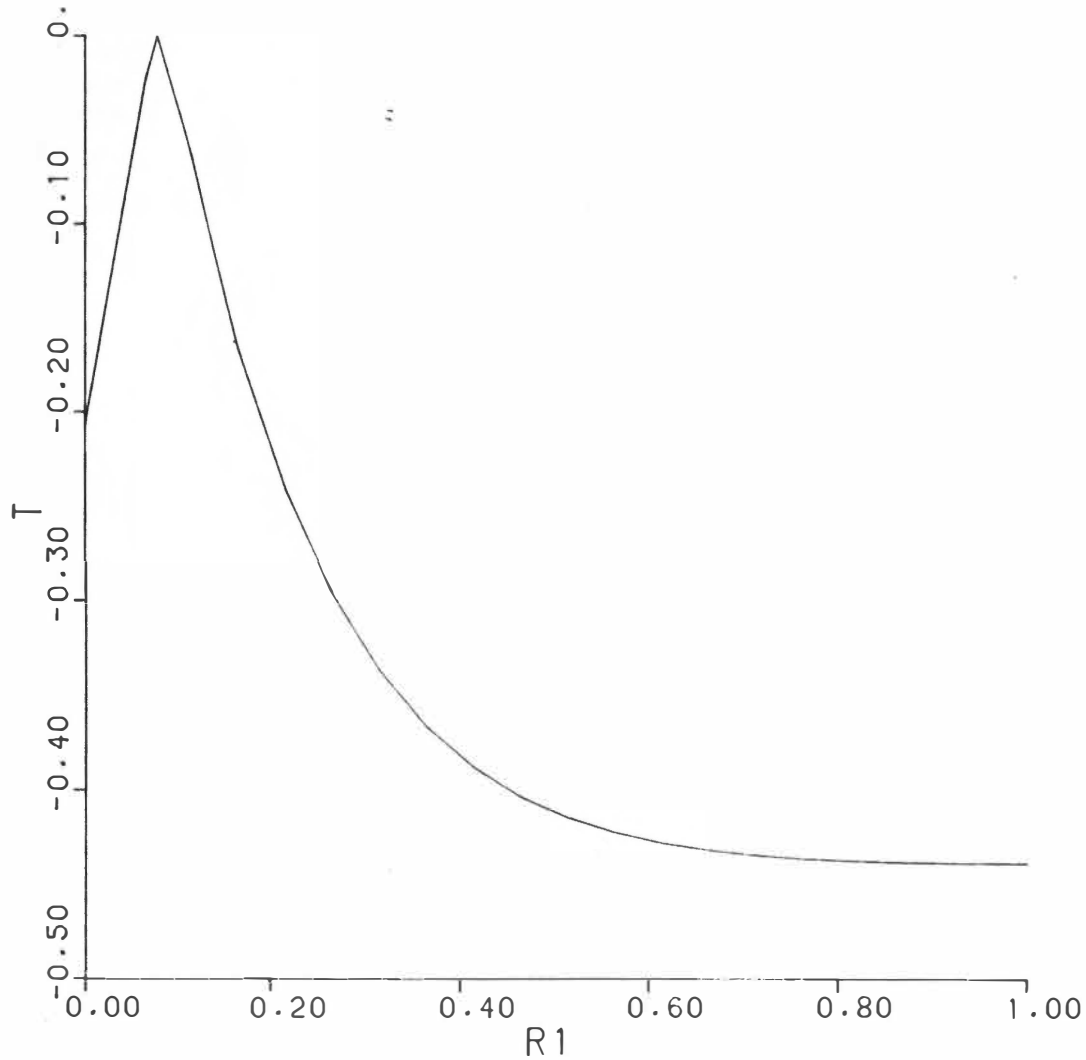
3-2   Temperature Distribution inside Capsule at
       Moment after Freezing Started ;MF=119.9 Kg/hr

After the temperature at the center of the sphere reaches the melting temperature, the energy balance equation at the phase-change interface reduces to

$$\frac{\partial \overline{R}^*}{\partial \overline{\overline{\eta}}} = - \; \zeta_3 \cdot \; \frac{\partial T_s}{\partial \overline{R}} \; \Bigg|_{\overline{R} = \overline{R}^*} \qquad (3\text{-}13)$$

The temperature distribution after the moment of freezing is shown in figure (3-2).

(2.C.3) At the Moment of the Freezing ($t = t_{fre}$):

A temperature jump happens at the phase-change interface; at this moment the temperature at the interface is discontinuous, and the temperature gradient at the phase-change interface is infinite.

As will be shown in a later chapter, the computer simulation results with consideration of supercooling obtained with this set of partial differential equations and a special boundary condition to handle the temperature discontinuty at the initial phase-change interface compare very closely to the experimental data of T. Saitoh [37].

(3)The Packed Bed with Two-Phase Working Fluid

(3.A)Governing Equation

Phase-change of the working fluid is considered in this analysis while the thermal storage material might be either a latent heat (PCM) or a sensible thermal storage material such as solid glass spheres. Since the working fluid temperature in the phase-change region remains relatively constant, the infinite heat capacity model for the working fluid appears to be reasonable. This feature simplifies the modelling and calculation process. However, the thermodynamic quality of the working fluid varies with the distance from the entrance. With the following non-dimensional parameters

$$X' = \frac{h \cdot A \cdot x \cdot (T_m' - T_o')}{M_f \cdot L_f \cdot Lu}$$

$$\eta' = \frac{h A \cdot t (T_m' - T_o')}{\rho_f \cdot L_f \cdot S_{fr} \cdot Lu \cdot \varepsilon}$$

$$T = \frac{T_f' - T_m'}{T_m' - T_o'}$$

the governing equation for the two-phase fluid can be written in the following form

$$\frac{\partial <x>}{\partial X'} + \frac{\partial <x>}{\partial \eta'} + (T_f - T_{sur}) = 0 \qquad\qquad (3\text{-}14)$$

having the boundary condition

$<x> = <x>_i (\eta')$ $X' = 0$

and the initial condition:

  For the working fluid

$<x> = <x>_o (X')$ $\eta' = 0$

  For the thermal storage material

$T = T (X')$ at $\eta' = 0$

(3.B) Heat Transfer Coefficient

The determination of the heat transfer coefficient between the thermal storage material and the two-phase working fluid is very difficult. No published work has been found which applies directly to this problem. In the following section, two different cases are discussed.

(3.B.1) Boiling Situation

The energy transporting fluid absorbs heat from the thermal storage material and undergoes boiling over at least a part of the length of the packed bed. The entering fluid usually is liquid and at a temperature below saturation. Before the saturation temperature is reached, the heat transfer process is that of single-phase

forced convection. At the point where the saturation value of temperature is reached, forced convective boiling occurs. Usually in a boiling situation, before the saturated boiling region is encountered there is a subcooled boiling region. But in a typical packed bed, the transition from subcooled to saturated boiling flow happens in a short distance. This is because the hydraulic diameter is small, and no clearly defined core region appears in the working fluid. Near the exit of the bed "dryout" may occur, the location of which depends on the operational time, flowrate and the kind of thermal storage material.

One forced convective boiling heat transfer correlation presented by R.T. Lahey and F.J.Moody [38] for two phase flow is of the form

$$\frac{h_{2\phi}}{h_{1\phi}} = A \cdot \left(\frac{1}{X_{tt}}\right)^n \tag{3-15}$$

where Xtt is the Martinelli parameter.

From G. B. Wallis and J. G. Collier [39], the Martinelli parameter is given by

$$\frac{1}{X_{tt}} = \left(\frac{<x>}{1-<x>}\right)^{0.9} \cdot \left(\frac{\rho_f}{\rho_g}\right)^{0.5} \cdot \left(\frac{\mu_g}{\mu_f}\right)^{0.1} \tag{3-16}$$

where <x> is the quality of the working fluid.

In equation (3-15), A and n are undetermined constants which can be obtained by a curve fitting method using experimental data. The equation (3-15) can be transformed by taking the logarithm, term by term, into

$$ln(h_{2\phi}/h_{1\phi}) = ln(A) + n \cdot ln(1/X_{tt}) \tag{3-17}$$

For m experimental data points, this equation can be expressed in the following form. (See reference 40 for details concerning this approach.)

$$m \, ln \, A + n \sum_{i=1}^{m} ln\left(\frac{1}{X_{tt}}\right)_i = \sum_{i=1}^{m} \left(\frac{h_{2\phi}}{h_{1\phi}}\right)_i$$

$$ln \, A \cdot \sum_{i=1}^{m} \left(\frac{1}{X_{tt}}\right) + n \sum_{i=1}^{m} \left(\frac{1}{X_{tt}}\right)_i^2 = \sum_{i=1}^{m} \left(\frac{1}{X_{tt}}\right)_i \left(\frac{h_{2\phi}}{h_{1\phi}}\right)_i$$

The solutions of these two normal equations for the unknowns n and A are

$$n = \frac{m \sum_{i=1}^{m} \left(\frac{1}{X_{tt}}\right)_i \left(\frac{h_{2\phi}}{h_{1\phi}}\right)_i - \left[\sum_{i=1}^{m} \left(\frac{1}{X_{tt}}\right)_i \cdot \sum_{i=1}^{m} \left(\frac{h_{2\phi}}{h_{1\phi}}\right)_i\right]}{m \sum_{i=1}^{m} (X_{tt})_i^2 - \left[\sum \left(\frac{1}{X_{tt}}\right)_i\right]^2} \tag{3-18}$$

and

$$A = e^{\left[\frac{1}{m}\sum_{i=1}^{m} \left(\frac{h_{2\phi}}{h_{1\phi}}\right)_i - \frac{n}{m}\sum_{i=1}^{m} \left(\frac{1}{X_{tt}}\right)_i\right]} \tag{3-19}$$

(3.B.2) Condensing Situation

During the charging process, the working fluid vapor releases heat to the thermal storage material by condensing as it flows through the packed bed. J. W. Yang [41] formed a boundary layer analysis for laminar film condensation on a sphere and obtained expressions for the heat transfer coefficient and the condensation rate. His analysis was based on the condition of zero vapor velocity. In 1979, S. S. Kulateladze, N. I. Gogonin, A. R. Dorokhov and V. I. Sosunov [42] reported on a study of film condensation of flowing vapor over a bundle of horizontal tubes. They presented the following equation for the ratio of the heat transfer coefficient for flowing vapor,h, to that for quiescent vapor,h0, on a bundle of horizontal tubes.

$$\frac{h}{h_o} = (1 + 3.62 \cdot z^4 \cdot Fr / Pr \cdot k)^{1/4} \tag{3-20}$$

where

$$z = 0.9 \cdot (1 + Pr \cdot k/R')^{1/3}$$

$$Fr = w^2/g \cdot d$$

$$R' = \rho_f \cdot \mu_f/\rho_v \cdot \mu_v$$

$$k = L_v/C \cdot \Delta t$$

In the above equations, w is the velocity of the vapor, D is the tube diameter, L is the latent heat of vapor, C is the specific heat, h is the heat transfer coefficient in quiescent vapor, t is the temperature difference between vapor and tube wall, and the subscripts f and v indicate liquid and vapor states, respectively.

The value of h can be obtained from Yang [41], viz.

$$h_o = 0.803 \left[\frac{g (\rho_f - \rho_v) \cdot L_v \cdot K^3}{d \cdot v \cdot (t_v - t_w)} \right] \tag{3-21}$$

(4)Energy Stored in the Packed Bed

In the evaluation of the performance of a thermal storage unit, the fraction of available energy that is stored is of major interest since it can be thought of as an indication of the effectiveness of the storage system as an energy recovery device.

The amount of energy added to or extracted from the fluid stream during the time interval 't' is

$$Q = (t_m - t_o) \int_o^t m_f \cdot C_f \cdot \left(T_{fe} - T_{fi} \right) dt$$

$$+ \int_o^t m_f \cdot L_f \cdot (<x>_e - <x>_i) \cdot dt \qquad (3-22)$$

Q is equal to the energy lost or obtained by the fluid as it passes through the packed bed.

The maximum possible energy storage occurs when the final temperature of the thermal storage material is equal to the temperature of the fluid entering the unit, or whenever the thermodynamic quality of a two-phase working fluid at the exit is equal to that at the entrance. Thus,

$$Q_{max} = Q_1 + Q_2 + Q_3 + Q_4$$

where Q1 is the latent heat obsorbed or released by the PCM, Q2 is the sensible heat change of the PCM, Q3 is the latent heat change of the working fluid within the packed bed, and Q4 is the sensible heat change of the fluid within the packed bed.

$$Q_1 = \rho_m (1 - \varepsilon) \cdot S_{fr} \cdot Lu \cdot L$$

$$Q_2 = \left[\rho_m (1 - \varepsilon) \cdot S_{fR} \cdot Lu \cdot C_m \cdot (T_i - T_o) \right] \cdot (T_m' - T_o')$$

$$Q_3 = \left[S_{fR} \cdot Lu \cdot \varepsilon \cdot L_f (\rho_{fi} <x>_i - \rho_{fo} <x>_o) \right]$$

$$Q_4 = \left[\rho_f \cdot S_{fr} \cdot Lu \cdot \varepsilon \cdot C_f \cdot (T_i - T_o) \right] (T_m' - T_o')$$

The fraction of the useful energy stored, $\overline{Q}$, is given by the ratio of Q(actual) to Qmax, i.e.,

$$\overline{Q} = \frac{Q}{Q_1 + Q_2 + Q_3 + Q_4} \tag{3-23}$$

CHAPTER 4

NUMERICAL SOLUTION

The numerical method chosen in the present study is the finite difference, implicit formulation approach.

The usual way of solving the heat flow equation over a fixed domain using finite difference representations of the derivatives is to evaluate the temperatures at discrete points on a fixed grid. For the sensible thermal storage packed bed, the traditional finite difference method can be used to solve the governing equations for both the working fluid and the thermal storage material. In the case of a phase-change material used for the purpose of storing thermal energy, a modified finite difference formula based on unequal space intervals near the moving phase-change front within the spherical pellet is suitable. The complication associated with a moving boundary is that at any time it will be located at an initially unknown position between two neighboring grid points. The governing differential equations for both the PCM and the working fluid are non-linear, and due to the unknown and transient nature of the boundary, it is difficult to solve this set by most methods. Two finite difference methods referred to as the strong solution method and weak solution method by Solomon [33], have

already been developed. The weak solution method avoids
tracking the unknown moving boundary. In the strong
solution method, the boundary location is determined by
the phase-change process which is dependent upon the
latent heat energy of the material, and the boundary
location is a natural consequence of solving the energy
conservation law of the system. Control of charging and
discharging rate of a thermal energy storage packed bed
rests upon the understanding of the phase-change process
in the PCM, and particularly on the estimation of the
location of the melting and solidification front in the
PCM.

In this chapter the finite difference equations for
the sensible thermal storage packed bed and the latent
thermal storage packed bed are discussed separately.

(1) Sensible Thermal Storage Packed Bed

The solution of the coupled set of equations of the
sensible thermal storage packed bed is accomplished by
utilizing a fully implicit, finite difference scheme. The
finite difference equations in non-dimensional form are

For the fluid:(with j denoting node and n denoting time step)

$$(T_f)_j^{n+1} = A_1(T_f)_{J+1}^{n+1} + B_1(T_f)_{J-1}^{n+1} + C_1(T_f)_J^n + D_1(T_f)_J^{n+1} \qquad (4\text{-}1)$$

where:

$$A_1 = \frac{\dfrac{\Delta\eta}{\Delta X}\left(\dfrac{1}{PE\cdot\ \Delta X} - \dfrac{1}{2}\right)}{\left(\dfrac{2\Delta\eta}{PE\cdot\ \Delta X^2} + \Delta\eta + 1\right)}$$

$$B_1 = \frac{\dfrac{\Delta\eta}{\Delta X}\left(\dfrac{1}{PE\cdot\ \Delta X} + \dfrac{1}{2}\right)}{\left(\dfrac{2\Delta\eta}{PE\cdot\ \Delta X^2} + \Delta\eta + 1\right)}$$

$$C_1 = 1$$

$$D_1 = \Delta\eta$$

For the glass spheres:

$$T_i^{n+1} = A_2 T_{i+1}^{n+1} + B_2 T_{i-1}^{n+1} + C_2 T_i^n \qquad (4\text{-}2)$$

where:

$$A_2 = \frac{\dfrac{\Delta\overline{\eta}}{\Delta\overline{R}^2}\left(1 + \dfrac{1}{K-i}\right)}{\left(\dfrac{2\Delta\overline{\eta}}{\Delta\overline{R}^2} + 1\right)}$$

$$B_2 = \frac{-\dfrac{\Delta\overline{\eta}}{\Delta\overline{R}^2}\left(1 - \dfrac{1}{K-i}\right)}{\left(\dfrac{2\Delta\overline{\eta}}{\Delta\overline{R}^2} + 1\right)}$$

$$C_2 = 1$$

In the above expressions for A2 and B2, K indicates the number of nodes of the sphere, and i indicates the location of the node. Equation (4-2) is not valid at i=1 and at i=21; these special cases are discussed in Appendix D .

The initial condition simply involves assigning the initial solid and fluid temperature at each node. The boundary conditions for the fluid, however, are not obvious. For the exit condition, several differential and numerical forms have been employed in the past. In fact, the temperature and temperature gradient at the exit varies for all time, and it is impossible to assign fixed values for both fluid temperature and fluid temperature gradient at the exit.

The truncation error in the above difference formulations is $O(\Delta\eta + \Delta R$).

(2) Latent Heat Storage Packed Bed

The equation that prescribes the working fluid temperature field in a latent heat storage packed bed is the same as that used in a sensible heat packed bed. But the equations for the phase-change thermal storage material are much more complicated. The applicable governing differential equations for the spherical capsule of the phase-change material with constant thermal

properties in both the solid and liquid regions have already been shown in Chapter 3. Equation (3-5) is for the solid and equation (3-4) is for the liquid. Equation (3-6) is the energy balance at the melting front, and this expression couples equations (3-4) and (3-5). The (3-6) represents the rate of travel of the interface, and L is the latent heat of fusion, which is positive for a freezing process and negative for a melting process.

In the computation method employed, the total region of PCM is divided into **N** equally spaced intervals of thickness ΔR, and the melting/freezing front is traced only between two nodes. The regions between all other nodes are either all liquid or all solid. The method leads to a simple and accurate computation of the melting/freezing front travel. The method developed in this work focuses attention on the melting/freezing interface and the node immediately adjacent on each side of the front.

Appendix D presents a detailed development of each of the finite difference equations. These equations are also presented in this section, and four different cases will be discussed.

Case 1: The phase-change interface lies between two points 'i', and 'i+1' (2 < i < 20)

The resulting finite difference equations are

At point 'i'

$$
T_i^{n+1} = \frac{2\Delta\bar{\bar{\eta}}}{Ste \cdot \Delta\bar{R}^2} \left[\left[\frac{2}{E^{n+1} + E^n} + \frac{2 - \left(E^{n+1} + E^n\right)}{(\mathbf{N}-i)(E^{n+1} + E^n)} \right] T_i^{n+1} \right.
$$

$$
\left. + \left[\frac{2}{E^{n+1} + E^n + 2} + \frac{-2(E^{n+1} + E^n)}{(\mathbf{N}-i)(E^{n+1} + E^n - 2)} \right] T_{i-1}^{n+1} \right] + T_i^n
$$

$$(4\text{-}3)$$

At the interface the radial length fraction of the increment $\triangle R$ is given by

$$
E^{n+1} = -\frac{\Delta\bar{\bar{\eta}}}{\Delta\bar{R}^2} \left[-\left[\frac{E^{n+1} + E^n + 2}{E^{n+1} + E^n} T_i^{n+1} - \frac{E^{n+1} + E^n}{E^{n+1} + E^n + 2} T_{i-1}^{n+1} \right] \right.
$$

$$
\left. + \frac{k_s}{k_l} \left[-\frac{4 - \left(E^{n+1} + E^n\right)}{2 - \left(E^{n+1} + E^n\right)} T_{i+1}^{n+1} + \frac{2 - \left(E^{n+1} + E^n\right)}{4 - \left(E^{n+1} + E^n\right)} T_{i+2}^{n+1} \right] \right] + E^n
$$

$$(4\text{-}4)$$

57

at point 'i+1'

$$T_{i+1}^{n+1} = \frac{\left[\dfrac{2\Delta\overline{\overline{\eta}}}{STe\cdot\Delta\overline{R}^2}\left(\dfrac{2}{4-\left(E^{n+1}+E^n\right)} + \dfrac{E^{n+1}+E^n-2}{(K-i-1)\left[4-\left(E^{n+1}+E^n\right)\right]}\right)\right]T_{i+2} + T_{i+1}^n}{\left[1.0 + \left[\dfrac{-2\cdot\Delta\overline{\overline{\eta}}}{Ste\cdot\Delta\overline{R}^2}\right]\left[\dfrac{2}{E^{n+1}+E^n-2} + \dfrac{E^{n+1}+E^n}{\left(E^{n+1}+E^n-2\right)(N-i-1)}\right]\right]}$$

$$(4\text{-}5)$$

at point 1

$$T_1 = \frac{-\dfrac{K_p}{K_c}\cdot\dfrac{T_{sur}}{1.39} + 2T_2 - \dfrac{1}{2}T_3}{\dfrac{3}{2} - \dfrac{K_p}{1.39\cdot K_c}}$$

$$(4\text{-}6)$$

at the center

$$T_{i+1} = T_{i-1}$$

at all other points (except points 1, 21, and the point on either side of the phase-change interface)

$$T_i^{n+1} = A_2 T_{i+1}^{n+1} + B_2 T_{i-1}^{n+1} + C_2 T_i^n$$

$$(4\text{-}7)$$

where:

$$A_2 = \frac{\dfrac{\Delta\overline{\overline{\eta}}}{STe\cdot\Delta\overline{R}^2}\left(1 + \dfrac{1}{N-i}\right)}{\left(\dfrac{2\Delta\overline{\overline{\eta}}}{STe\cdot\Delta\overline{R}^2} + 1\right)}$$

$$B_2 = \frac{\dfrac{\Delta\bar{\bar{\eta}}}{STe\cdot\Delta\overline{R}^2}\left(1 - \dfrac{1}{N-i}\right)}{\left(\dfrac{2\Delta\bar{\bar{\eta}}}{STe\cdot\Delta\overline{R}^2} + 1\right)}$$

$$C_2 = 1$$

Case 2: The phase-change lies between point '1' and point '2' (i = 1)

The resulting finite difference equations are:

At the phase-change interface, the radial fraction of / R is

$$E^{n+1} = \frac{\Delta\bar{\bar{\eta}}}{\Delta\overline{R}^2}\left[-\frac{2}{E^{n+1}+E^n}\,T_1 + \frac{K_s}{K_c}\left[\frac{4 - E^{n+1} - E^n}{2 - E^{n+1} - E^n}T_2\right.\right.$$

$$\left.\left. -\frac{2 - E^{n+1} - E^n}{4 - E^{n+1} - E^n}\,T_3\right]\right] + E^n \qquad\qquad (4\text{-}8)$$

The temperature at point '2' is

$$T_2^{n+1} = \frac{\dfrac{2\cdot\Delta\bar{\bar{\eta}}}{STe\cdot\Delta R^2}\left[\left[\dfrac{2}{4 - E^{n+1} - E^n} + \dfrac{1}{(N-2)}\dfrac{E^{n+1}+E^n-2}{4 - E^{n+1} - E^n}\right]T_3^{n+1} + T_2^n\right]}{\left[\left[\dfrac{-2\cdot\Delta\bar{\bar{\eta}}}{STe\cdot\Delta\overline{R}^2}\right]\left[\dfrac{2}{2 - E^{n+1} - E^n} + \dfrac{E^{n+1}+E^n}{(N-2)(2 - E^{n+1} - E^n)}\right] + 1.0\right]}$$

$$(4\text{-}9)$$

and the temperature at the point '1' becomes

$$T_1 = \frac{0.719 \frac{K_p}{K_c} \cdot T_{sur}}{\frac{1}{E} + 0.719 \cdot \frac{K_p}{K_c}} \qquad (4\text{-}10)$$

The temperatures at all other points and at the center of the PCM are the same as those for case 1.

Case 3: The phase-change interface lies between points '2' and '3' (i = 2). The only difference from case 1 is in the equation for the temperature at point '1'. The temperatures at the points on both sides of the phase-change front can be obtained by substituting i = 2 into equations (4-3) and (4-5).

In this case, the temperature at point '1' is given by

$$T_1^{n+1} = \frac{\frac{-(2 + E^{n+1} + E^n)}{E^{n+1} + E} T_2^{n+1} - \frac{K_p}{K_c} \frac{T_p}{1.39}}{\left[\frac{4 + E^{n+1} + E^n}{2 + E^{n+1} + E^n} - \frac{K_p}{K_C} \frac{1}{1.39} \right]} \qquad (4\text{-}11)$$

Case 4: the phase-change interface lies between point '20' and the center of the capsule. At the phase-change interface the radial length fraction of $\triangle R$ is

$$E^{n+1} = \frac{\Delta \overline{\overline{\eta}}}{\Delta \overline{R}^2} \left[-\frac{E^{n+1} + E^n + 2}{E^{n+1} + E^n} T_{20}^{n+1} - \frac{E^{n+1} + E^n}{E^{n+1} + E^n + 2} T_{19}^{n+1} \right]$$

(4-12)

At point '20', the finite difference nodal temperature equation is obtained by substituting ' i=20' into equation (4-3). Finally at the center of the sphere

$$T_{21} \approx 0 .$$

CHAPTER   5

RESULTS AND DISCUSSION

(1) Results for a Sensible Thermal Storage Packed Bed

The results for sensible thermal storage packed beds are shown in figures 5-1 through 5-15. In this case, liquid Freon 113 was used as the energy transporting fluid and glass spheres served as the thermal storage material. The bed length was 1.13 m and the diameter was 0.127 m. The diameter of the glass spheres was 15.87 mm. This bed is identified herein as Bed S.

Figures 5-1 through 5-4 indicate the transient variation of the outlet fluid temperature under typical charging conditions. The computer simulation results are fairly coincident with the experimental data [45], both qualitatively and quantitatively. The agreement between the measured and computed outlet field temperature reveals that the first order model is good enough for this case. As a matter of fact, for these flows the Peclet number is sufficiently high that the second derivative term has a negligible effect on the axial fluid temperature distribution and the temperature at the exit. In these computations, the correlation reported by Ranz [7]. was utilized to compute the heat transfer coefficient between
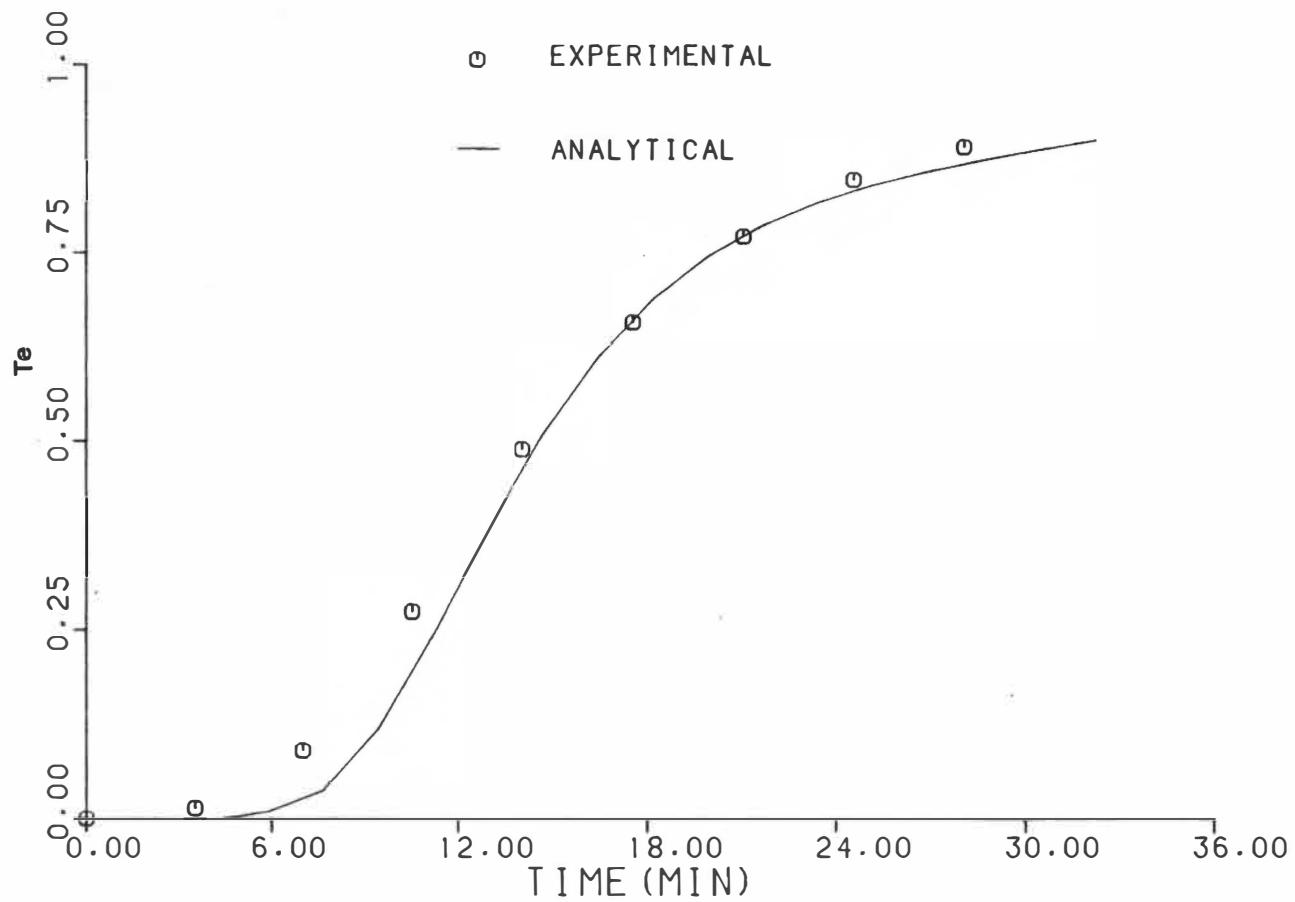
Figure 5-1. Transient Variation of Working Fluid Temperature at Exit
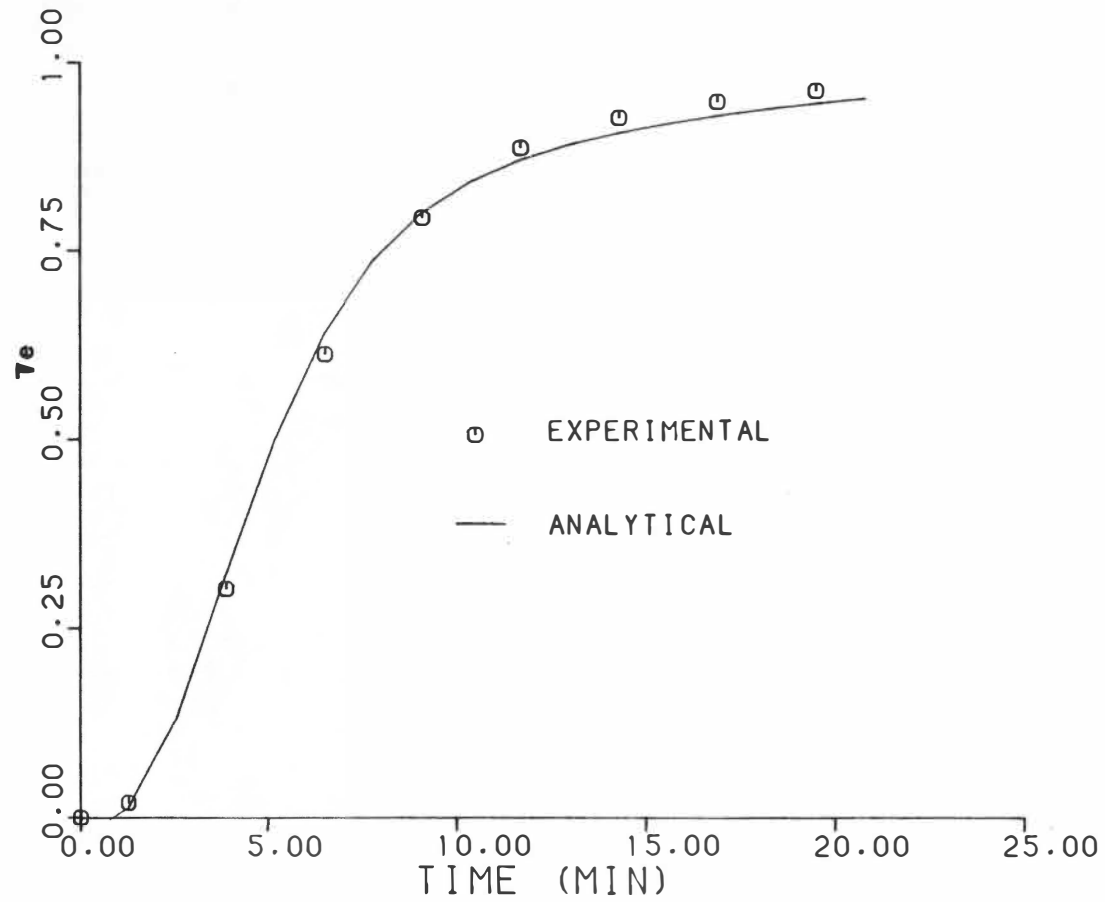for MF=177 Kg/hr (Sensible Heat Storage, First-Order Model)

Figure 5-2. Transient Variation of Working Fluid Temperature at Exit
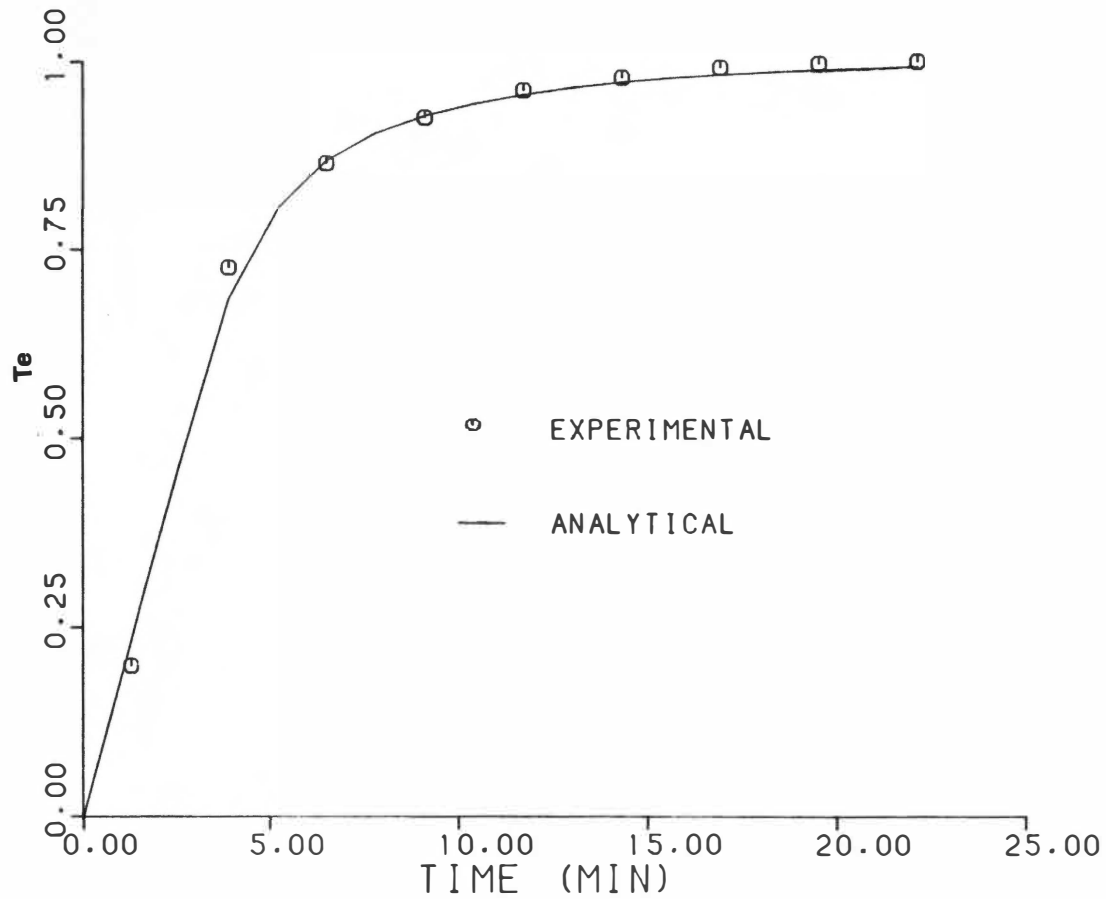for MF=354 Kg/hr (Sensible Heat Storage, First-Order Model)

Figure 5-3. Transient Variation of Working Fluid Temperature at Exit
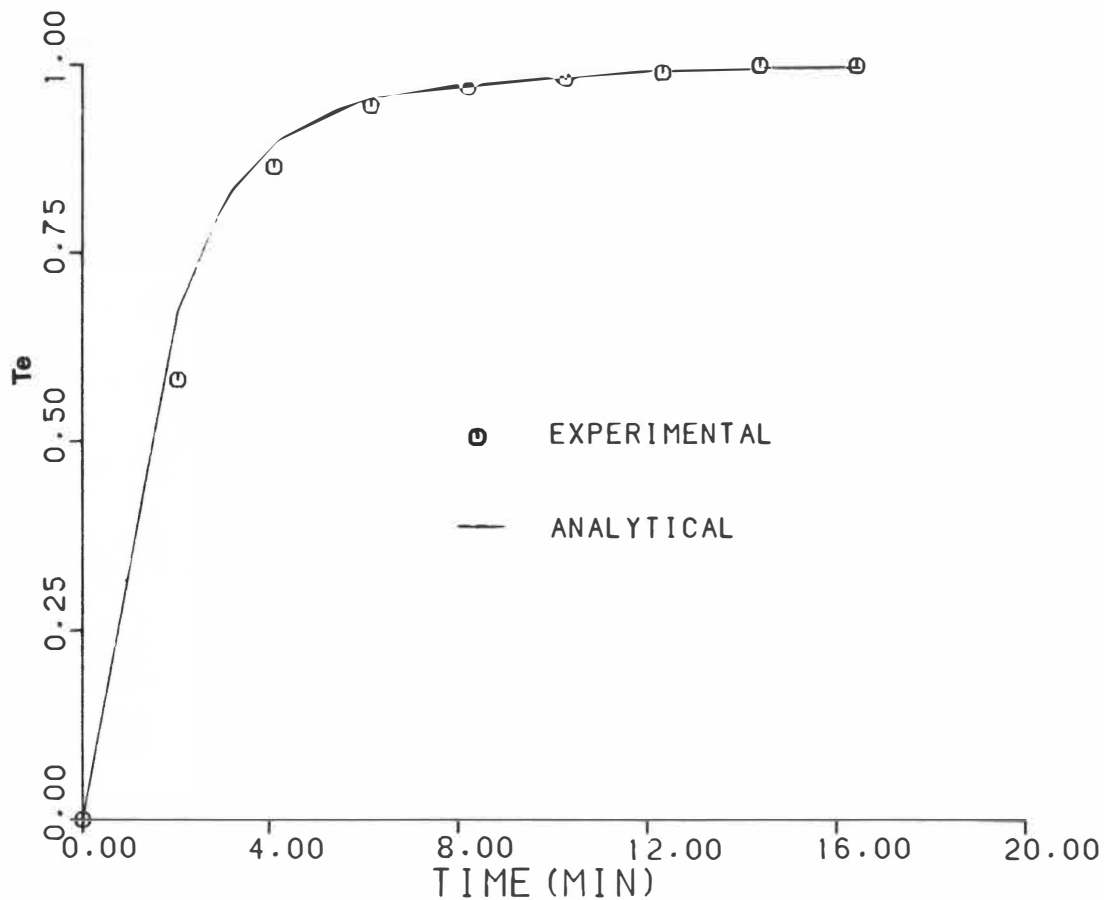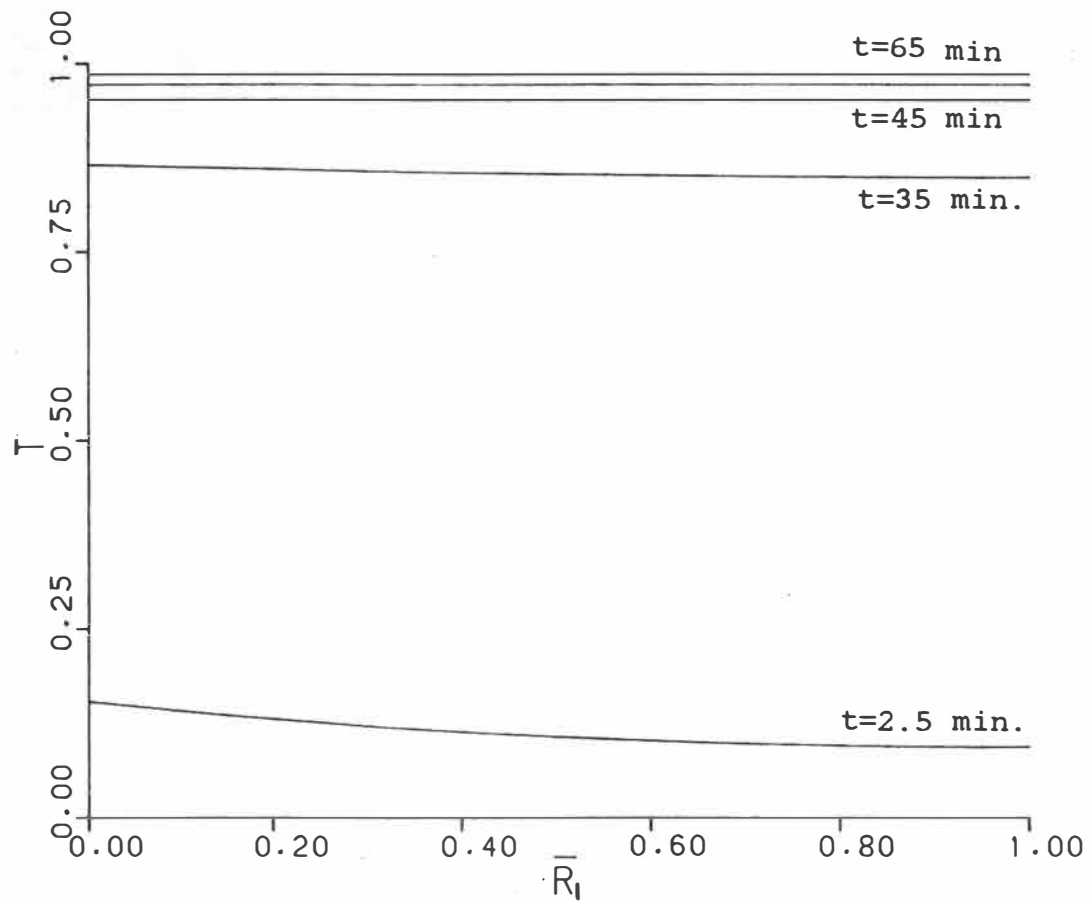for MF=698.89 Kg/hr (Sensible Heat Storage, First-Order Model)

64

Figure 5-4. Transient Variation of Working Fluid Temperature at Exit
for MF=1397.8 Kg/hr (Sensible Heat Storage, First-Order Model)

Figure 5-5. Temperature Distribution Inside Sphere for MF=177 Kg/hr
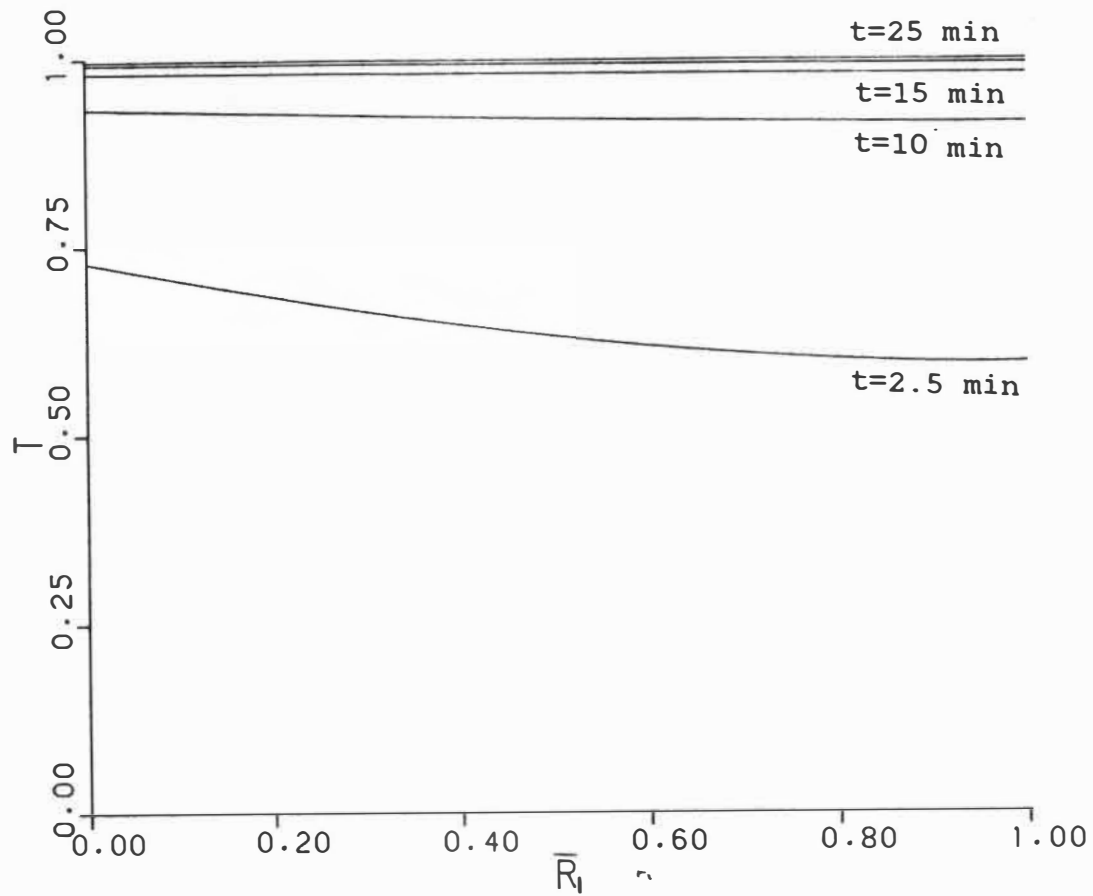(Sensible Heat Storage, First-Order Model)
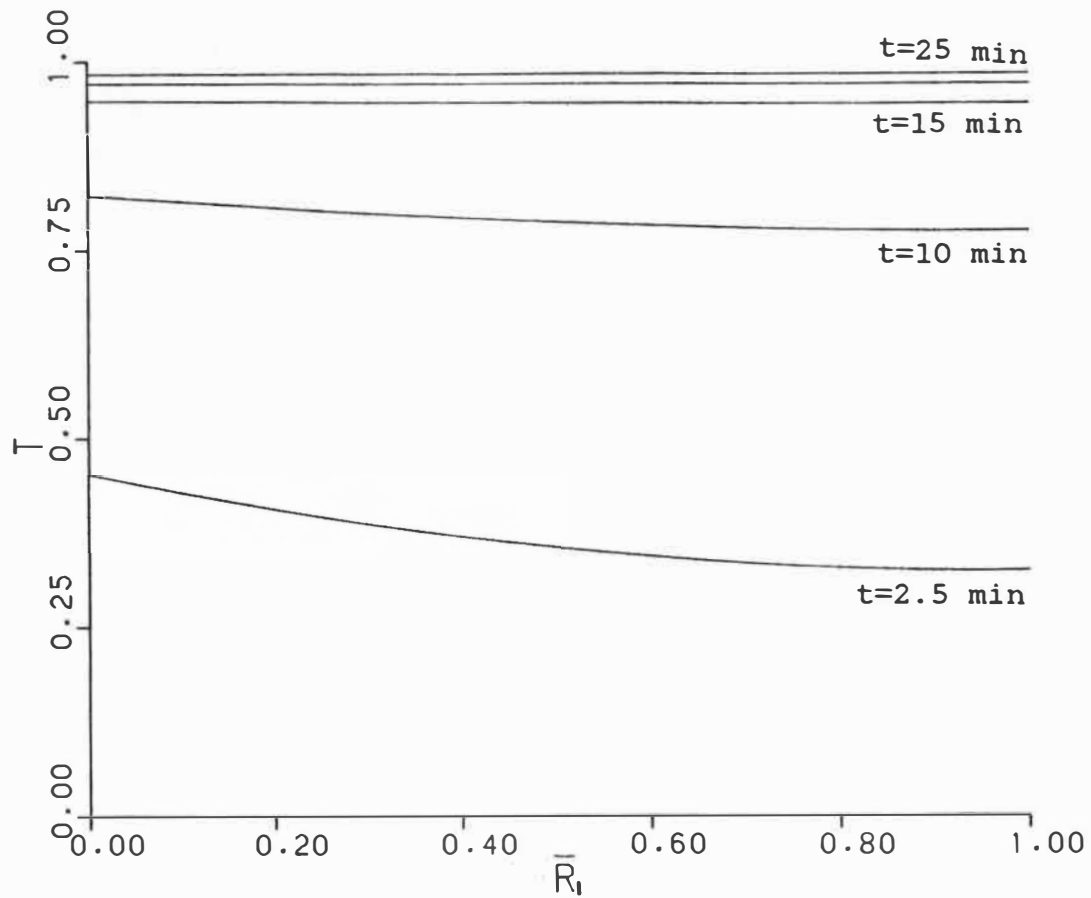
Figure 5-6.   Temperature Distribution Inside Sphere for MF=354 Kg/hr
(Sensible Heat Storage, First-Order Model)

Figure 5-7.   Temperature Distribution Inside Sphere for MF=698.89 Kg/hr
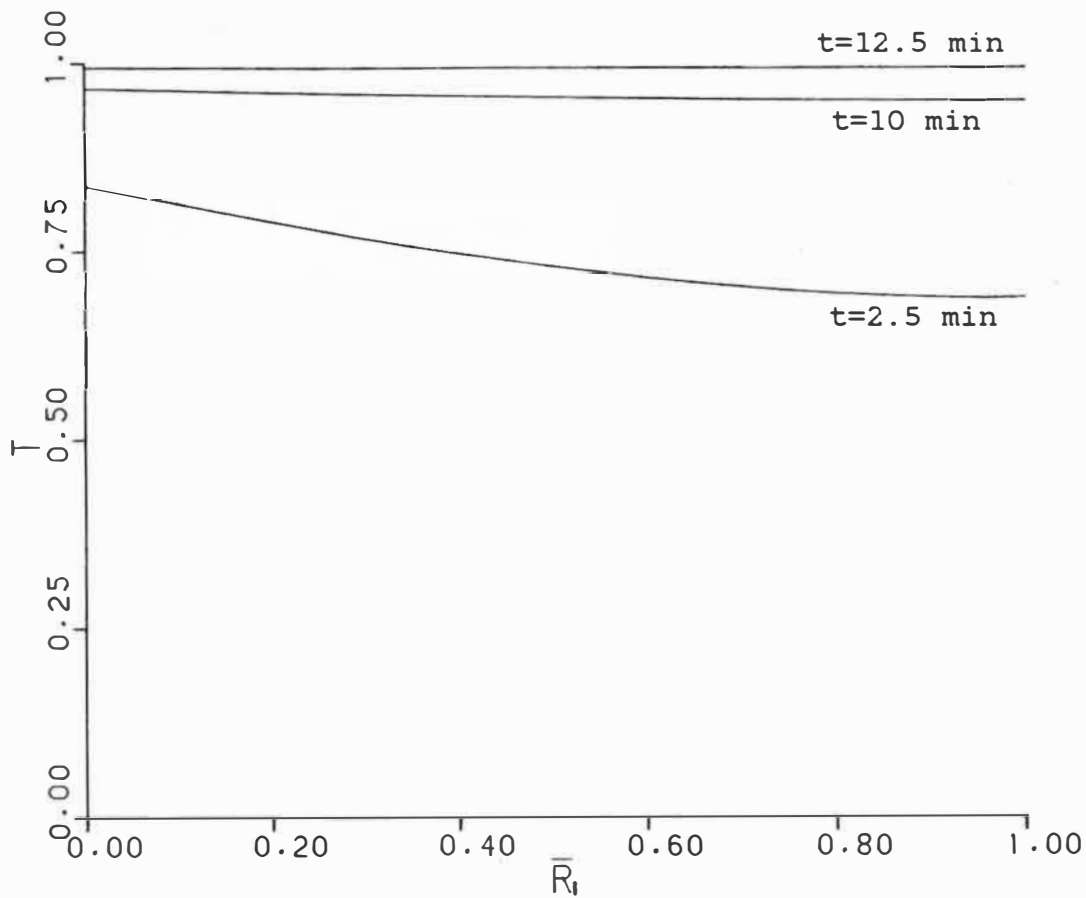(Sensible Heat Storage, First-Order Model)

Figure 5-8.   Temperature Distribution Inside Sphere for MF=1397.8 Kg/hr
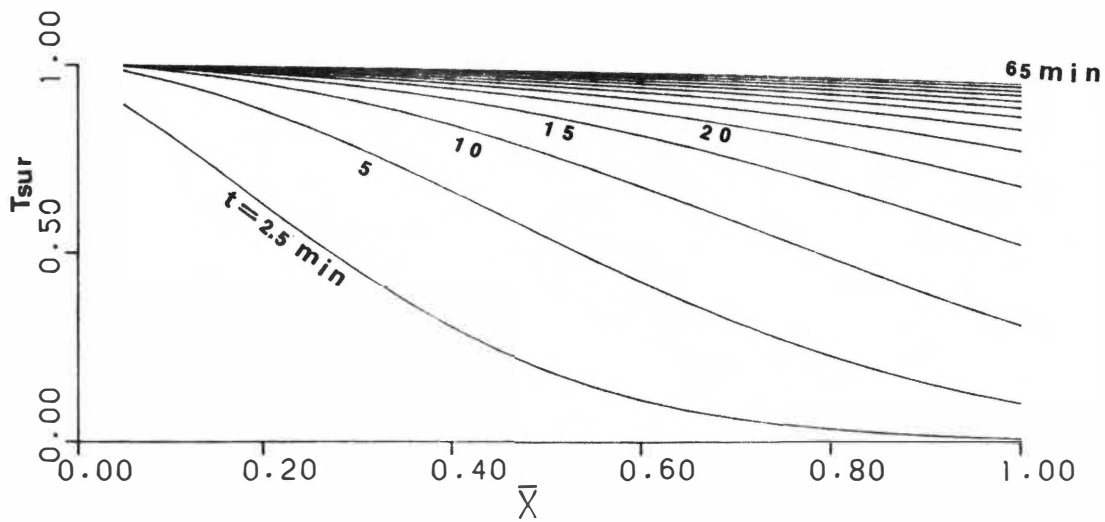   (Sensible Heat Storage, First-Order Model)

Figure 5-9.   Surface Temperature Distribution of Spheres Along Packed Bed
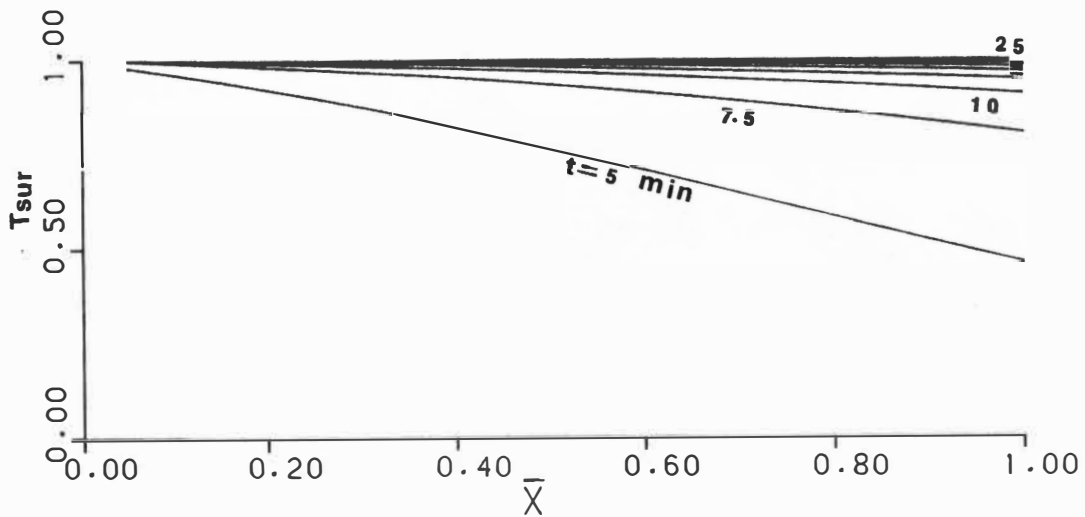for MF=177 Kg/hr (Sensible Heat Storage, First-Order Model)

Figure 5-10.   Surface Temperature Distribution of Spheres Along
Packed Bed for MF=698.89 Kg/hr
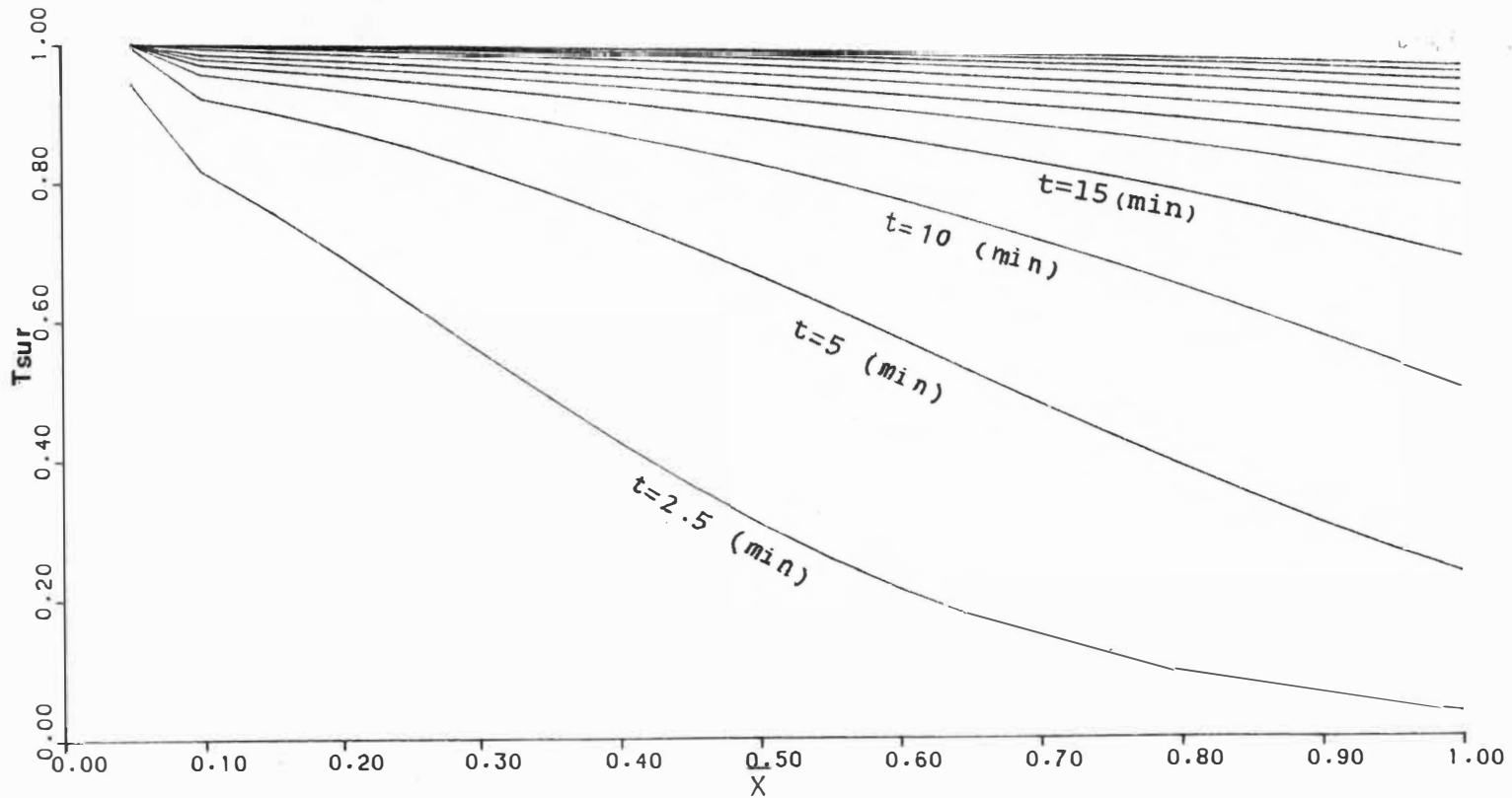(Sensible Heat Storage, First-Order Model)

Figure 5-11. Surface Temperature Distribution of Spheres Along
Packed Bed for MF=354 Kg/hr
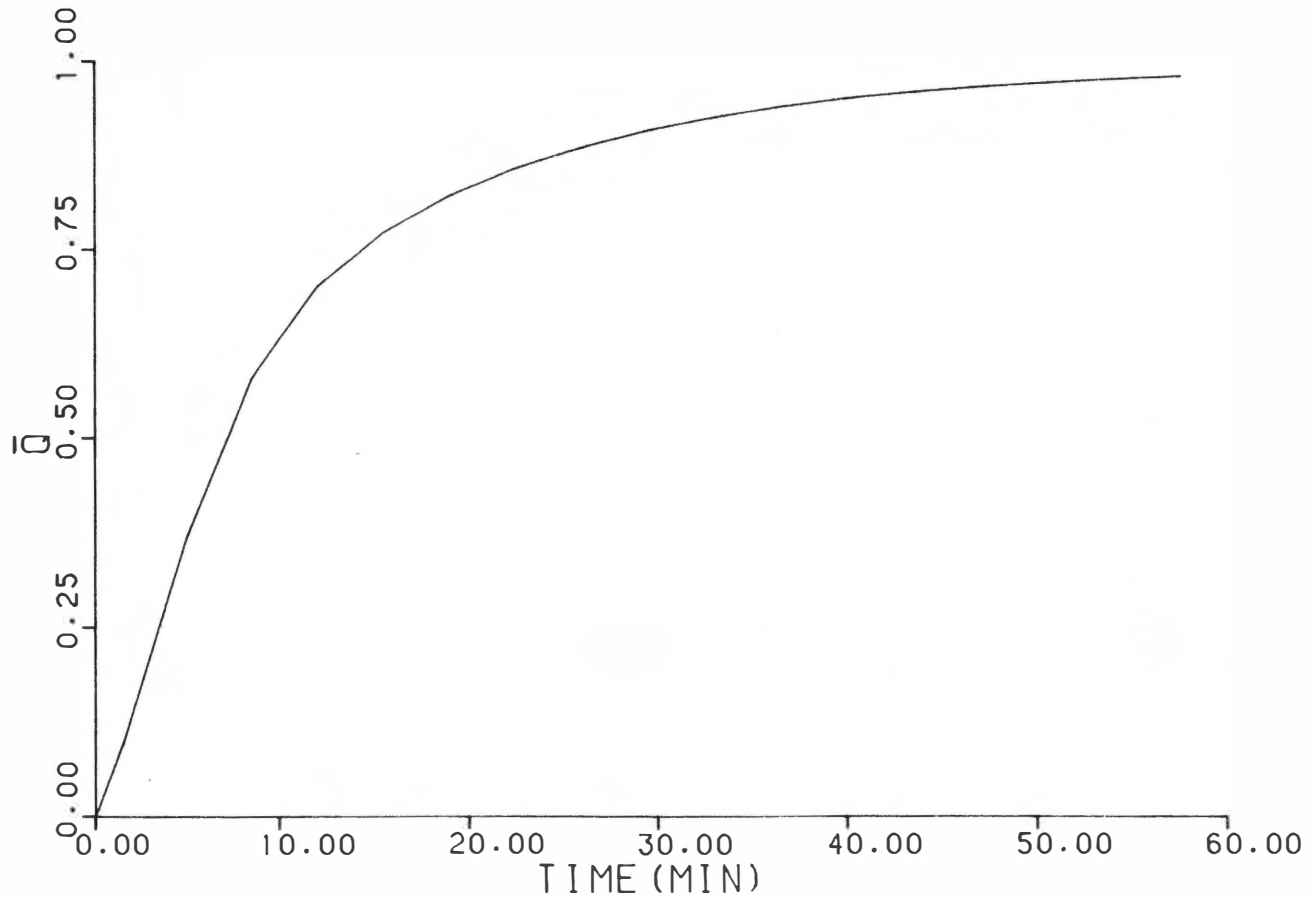(Sensible Heat Storage, First-Order Model)

Figure 5-12. Non-Dimensional Heat Q for Bed S, Mf=177 Kg/hr
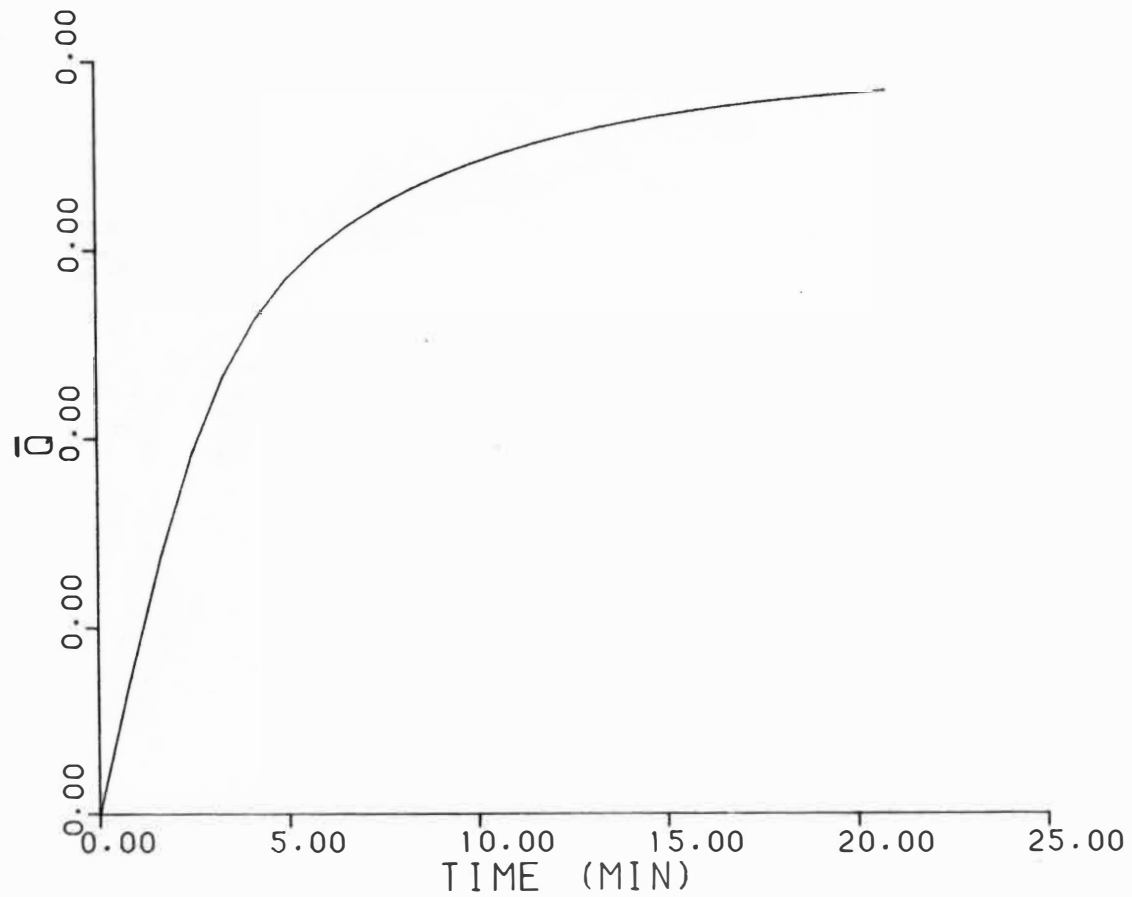(Sensible Heat Storage, First-Order Model)

Figure 5-13. Non-Dimensional Heat Q for Bed S, MF=354 Kg/hr
(Sensible Heat Storage, First-Order Model)

74
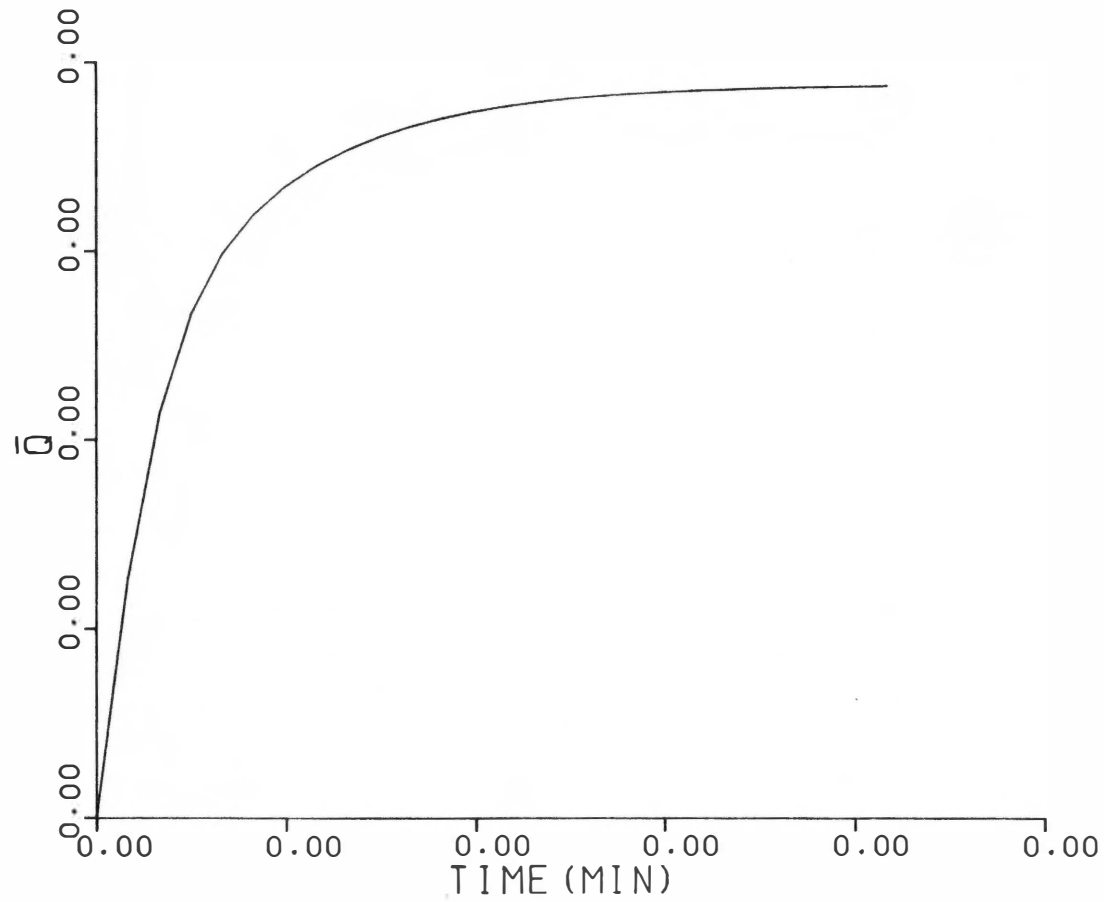
Figure 5-14.   Non-Dimensional Heat Q for Bed S̄, Mf=698.89 Kg/hr
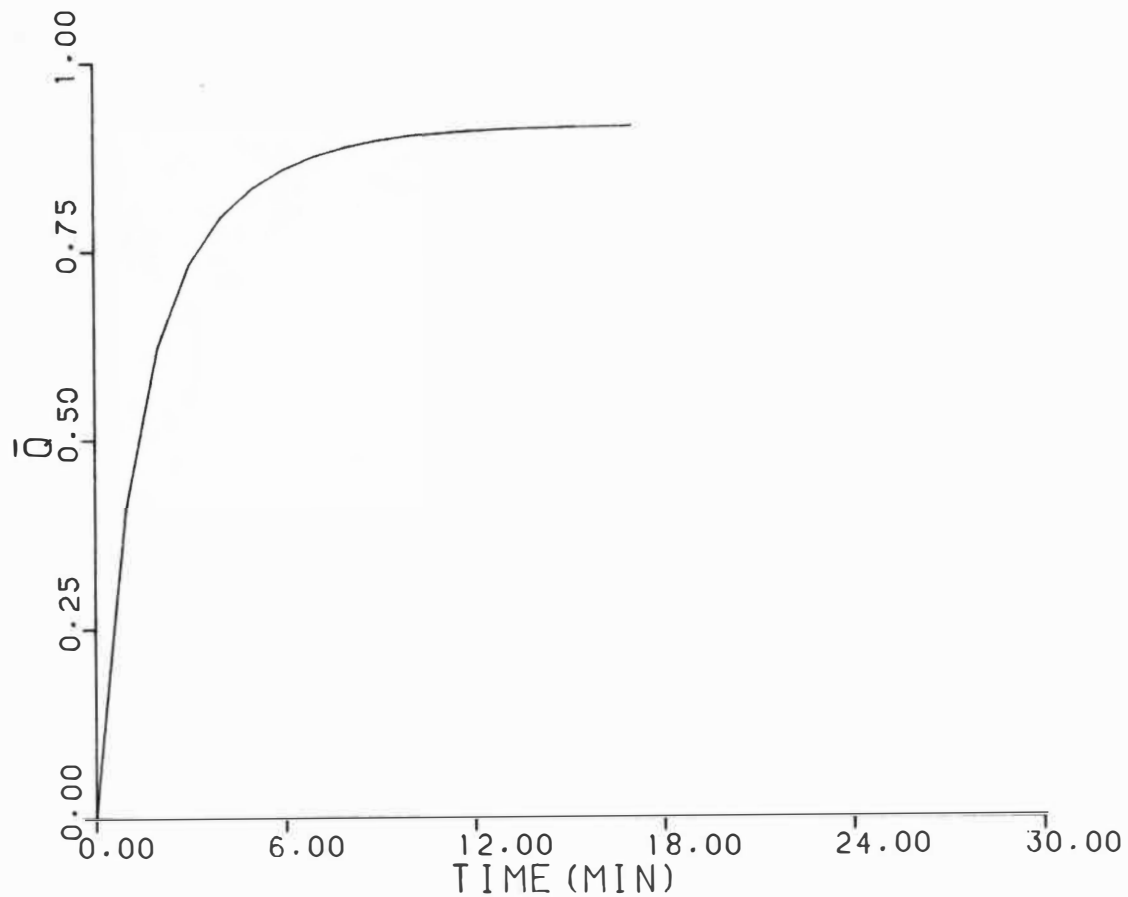(Sensible Heat Storage, First-Order Model)

Figure 5-15.   Non-Dimensional Heat Q for Bed S, MF=1397.8 Kg/hr
(Sensible Heat Storage, First-Order Model)

76

the working fluid and the glass spheres. The heat transfer coefficient between the working fluid and the packed bed wall was from Yagi and Kunii [23]. Figures 5-5 through 5-8 show the non-dimensional temperature distribution inside the spheres. These results indicate that the temperature gradient inside the sphere increases with working fluid flowrate, and, therefore, the uniform temperature assumption for the glass spheres would not be valid, particularly for the situation of high flowrate resulting in a Biot number much larger than 1.0.

Figures 5-9 through 5-11 show surface temperature distributions of the spheres along the packed bed length for different flowrates. After several minutes of bed operation, the sphere surface temperature becomes close to uniform over the bed length. This is a result of the small heat capacity of the sensible heat storage packed bed.

The amount of recoverable energy stored in the packed bed as a function of time of charging operation can be evaluated from figures 5-12 through 5-15.

(2)Results for a Latent Heat Storage Packed Bed

In this section, the experimental data with which the analytical results are compared are taken from Saitoh [39]. The experimental set up was a 1.295 m long and

0.61 m diameter packed bed, well-insulated with fiberglass. This bed is identified hearin as Bed L. The diameter of the bed spherical capsules was 71 mm, and the phase-change material was $NA_2HPO_3 \cdot 12H_2O$. The experimental flowrates were 113.8, 347.4, and 658.6 kg/hr for the melting case, and 119.8, 298.8, and 558.0 kg/hr for the freezing case in their tests.

(2.A)Melting Mode

Figure 5-16 shows the comparison between experimental values of the outlet temperature of the working fluid and results obtained with both the first-order and second-order models. It should be particularly noted here that the melting process in a sphere is predominantly by conduction. Both the first-order and the second-order models are based on the assumption that the heat transmission in the liquid phase inside the capsule is by conduction alone.

From Figure 5-16, it can be seen that the second order results compare very favorably with the experimental data. However, the first-order results deviate significantly from the experimental data at a flowrate of 113.8 kg/hr. This error is a result of neglecting the second derivative term in the governing equation (A-2), and the magnitude of this derivative term depends on the

	MF (Kg/hr)	TI (F)	TS (F)	Experimental
A	113 8	334	289	⊙
B	347.4	324	289	▲
C	658.6	328	289	+

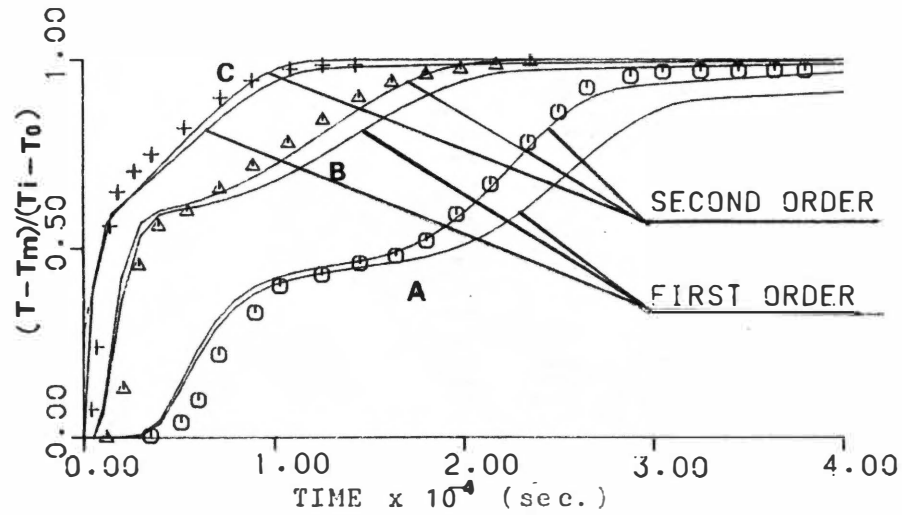(Charging Mode, Bed L)
⟶ Analytical
(Second-Order Model)

Figure 5-16. Comparison of Temperatures at Exit between First-and Second
-Order Models and Experimental Data from Literature

value of the Peclet number (or flowrate).

In Figure 5-16, subcooling also has been taken into account with resulting good agreement between the experimental data and the analysis. Neglecting subcooling will cause a error of approximately 0.5% in total energy storage per degree celsius of subcooling for the material and range of parameters investigated in this study. Because of the added complexity, no previous work has included subcooling in an analysis.

The results given in Figures 5-17 through 5-22 present comparisons between the solutions using the first-order and the second-order models for working fluid temperature and surface temperature of the capsules as a function of non-dimensional distance. All of these results are as expected and give an additional confirmation of the consistency of the mathematical models and the computational scheme of the present study.

Figure 5-23 shows the comparison of corresponding outlet temperatures between the experimental and the analytical results for a prescribed, time-depedent inlet temperature. Here again, good agreement between the experimental results and the second-order analytical model was obtained.
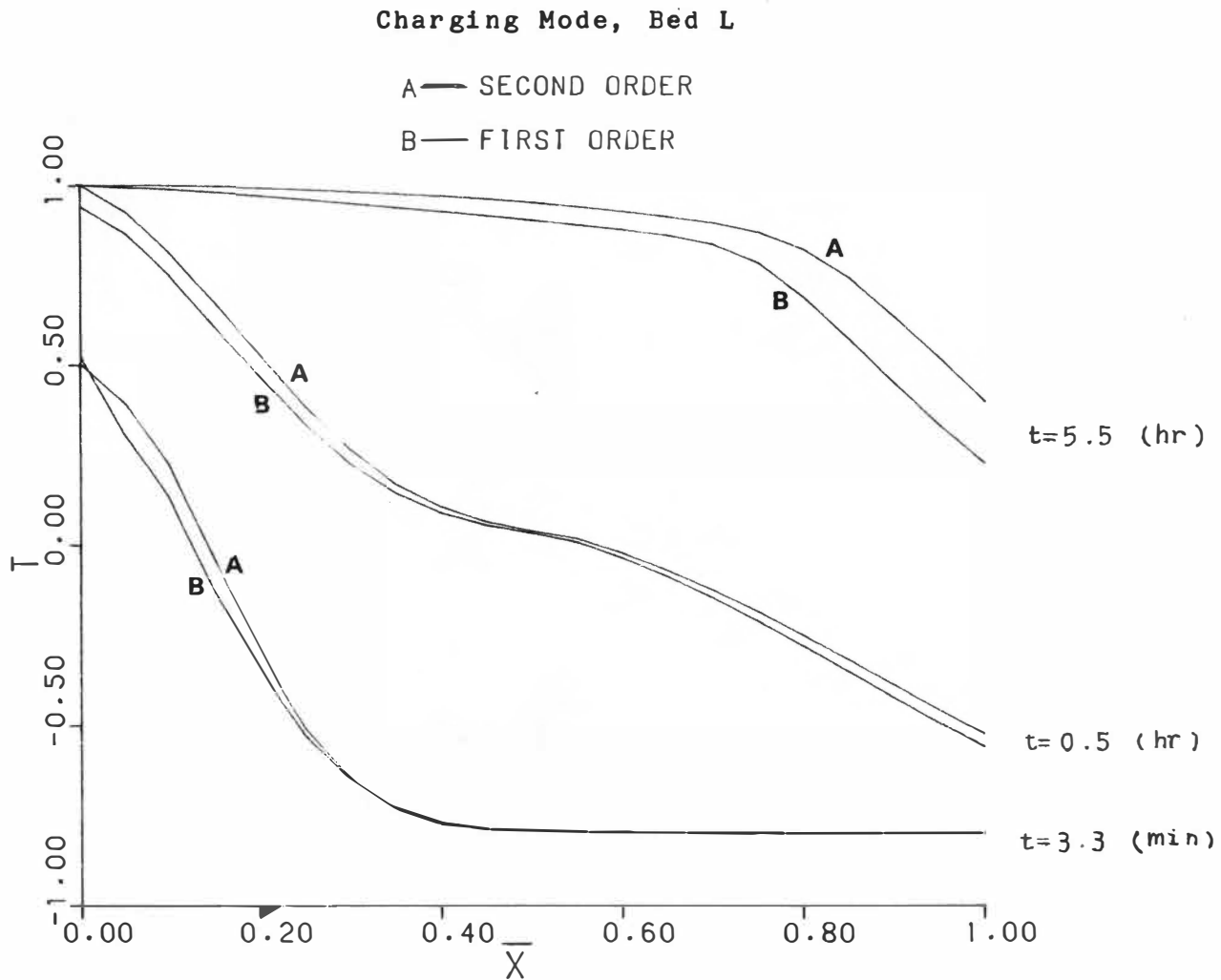
Figure 5-17.   Comparison of Surface Temperature of Spherical Capsules
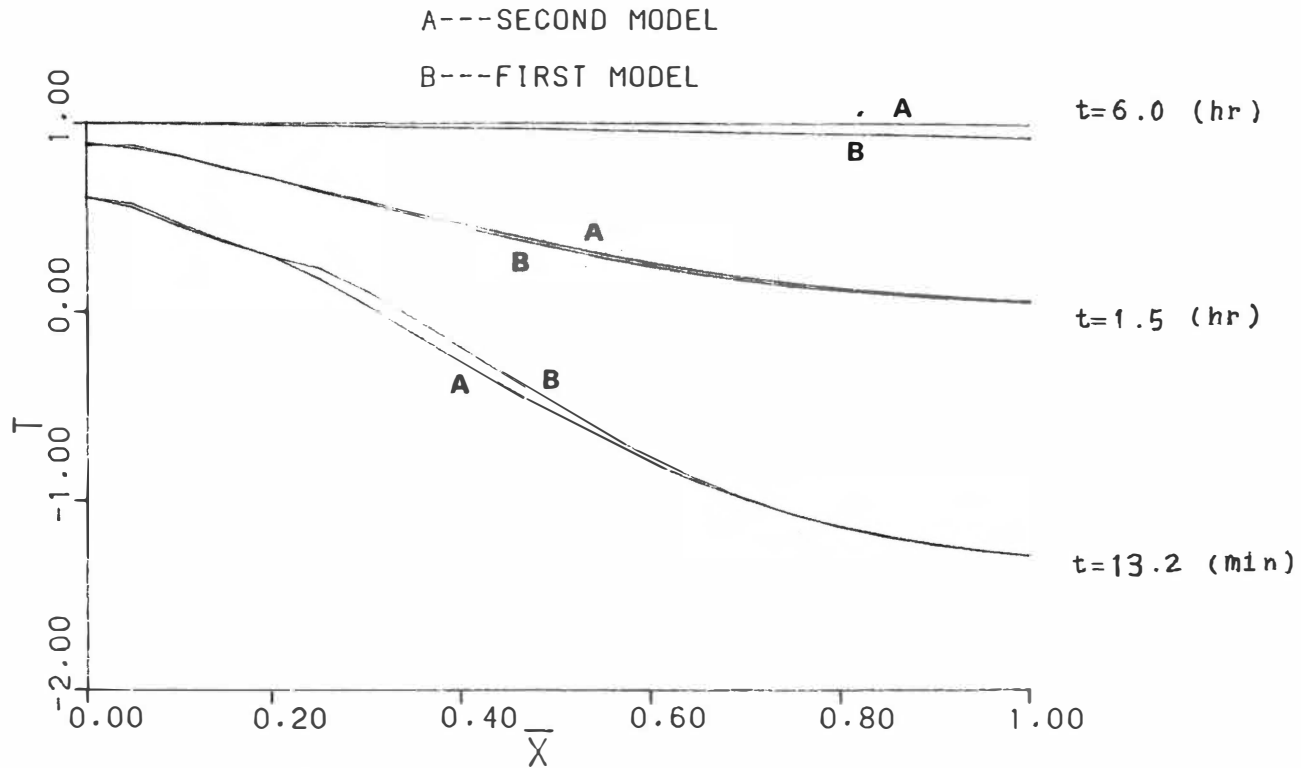between First- and Second-Order Models, MF=113.8 Kg/hr

Charging Mode, Bed L

A---SECOND MODEL

B---FIRST MODEL

t=6.0 (hr)

t=1.5 (hr)

t=13.2 (min)

$\overline{X}$

T

82

Figure 5-18. Comparison of Surface Temperature of Spherical Capsules
between First- and Second-Order Models, MF=347.4 Kg/hr
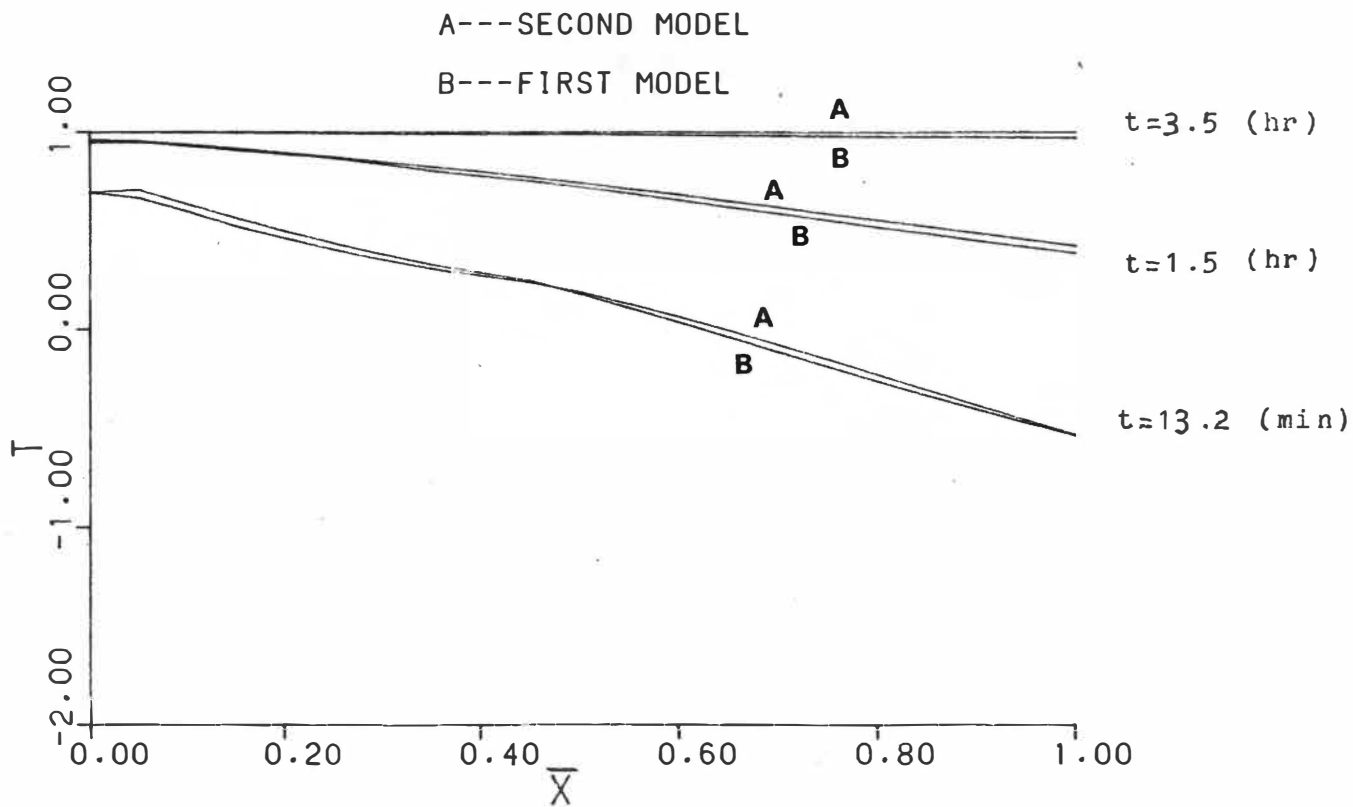
Figure 5-19. Comparison of Surface Temperature of Spherical Capsules between First- and Second-Order Models, MF=658.6 Kg/hr
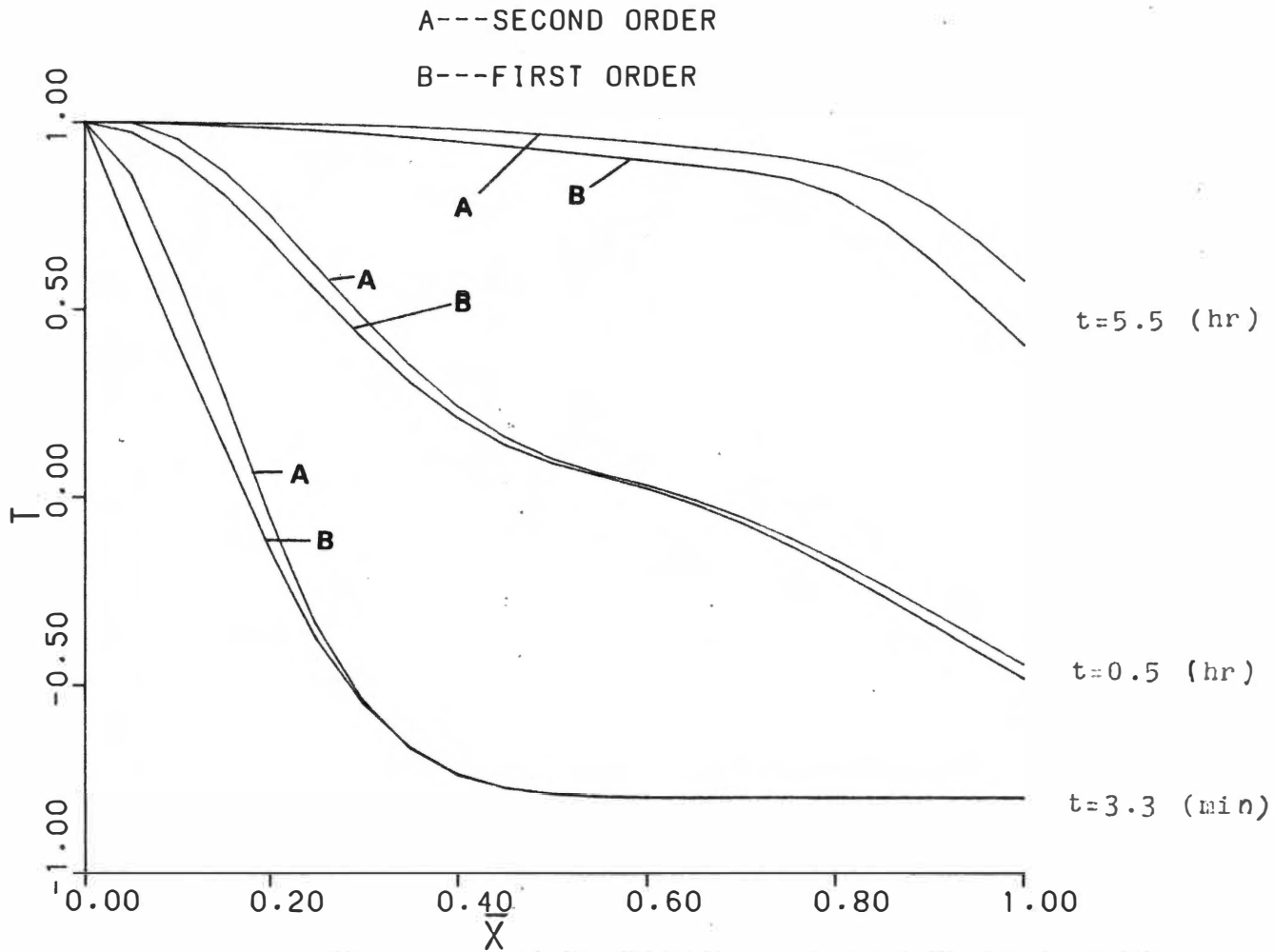
Figure 5-20.   Comparison of Temperature Of Working Fluid between
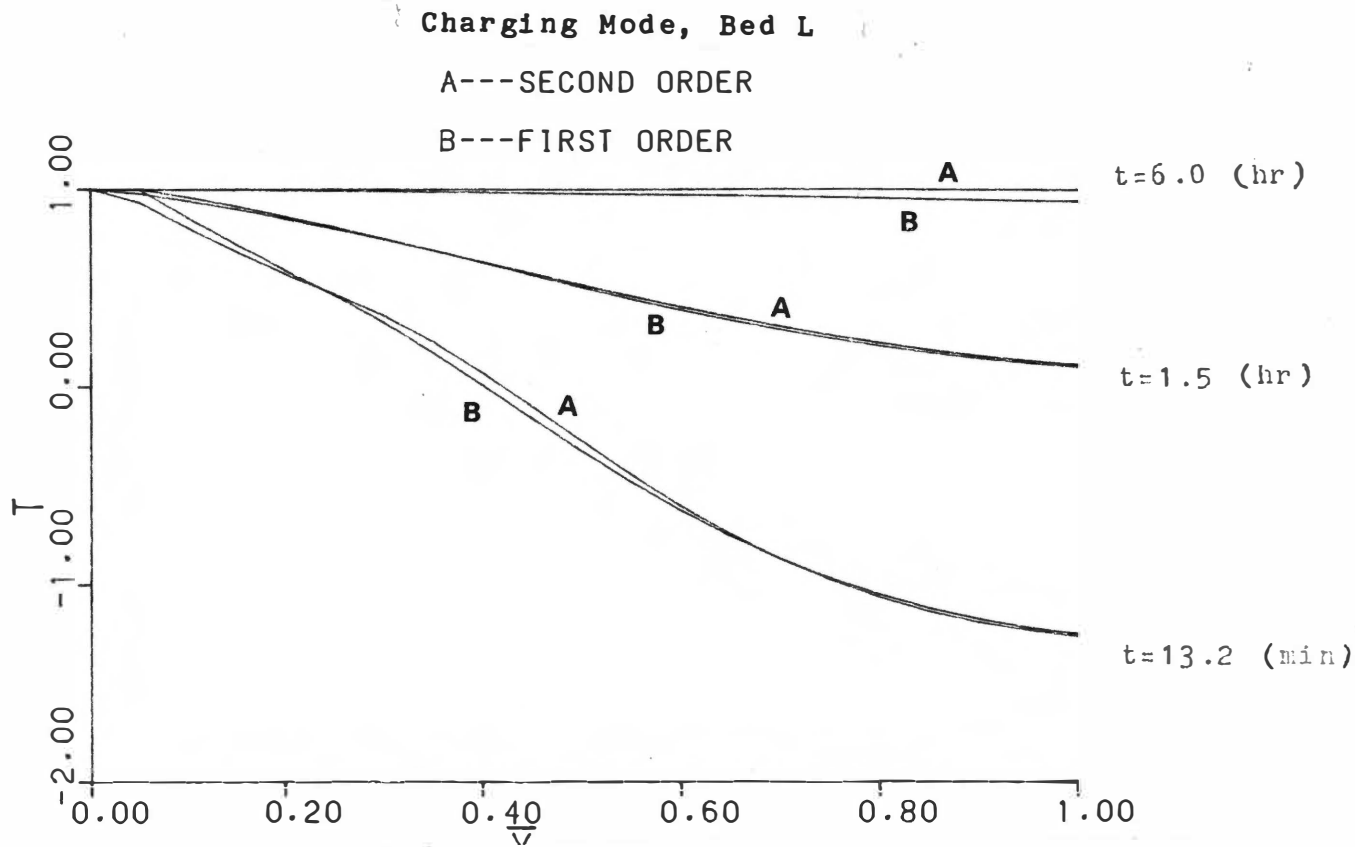First-I and Second-Order Models, MF=113.8 Kg/hr

Figure 5-21. Comparison of Temperature Of Working Fluid between
First- and Second-Order Models, MF=347.4 Kg/hr
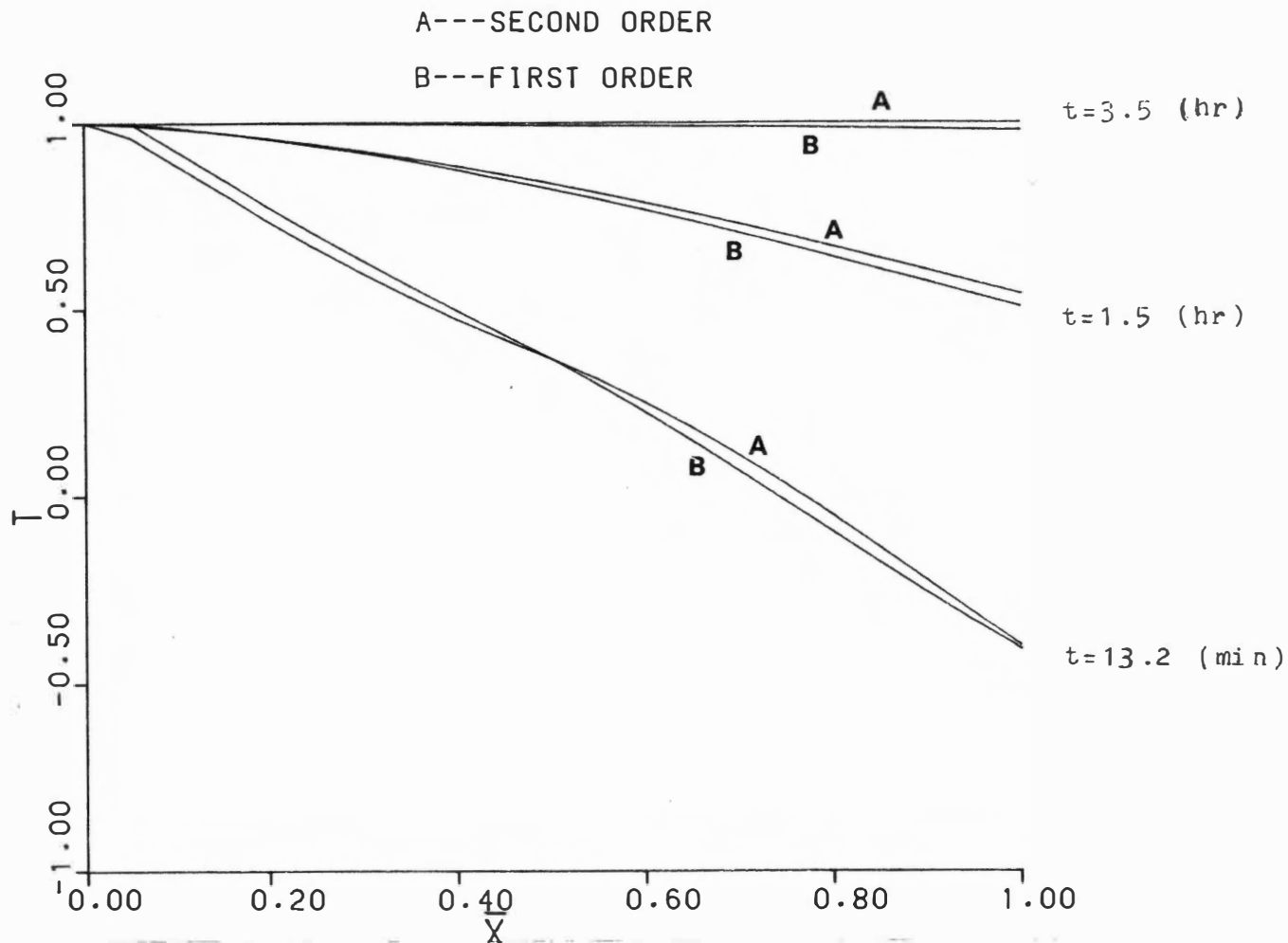
(Charging Mode, Bed L ;

A---SECOND ORDER

B---FIRST ORDER

Figure 5-22.   Comparison of Temperature Of Working Fluid between
First- and Second-Order Models, Mf=658.6 Kg/hr
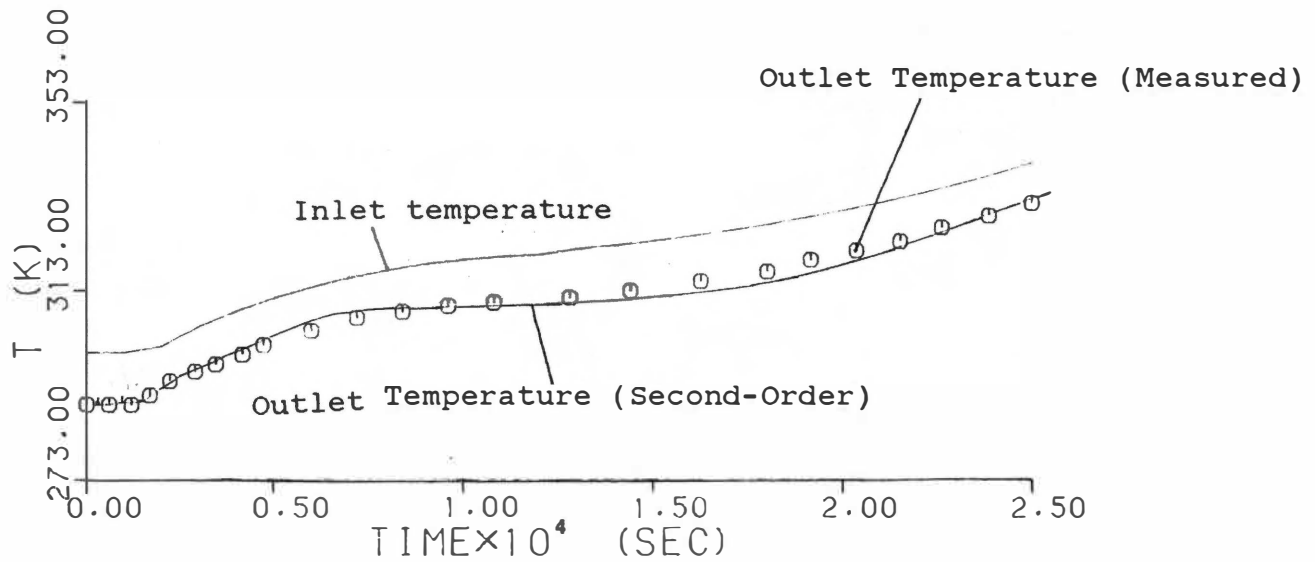
Figure 5-23.   Transient Variation of Outlet Temperature for a Prescribed
              Inlet Temperature (MF=347.4 Kg/hr, Latent Heat Storage,
              Second-Order Model, Exp.Data from Saitoh [37])

Figures 5-24 through 5-29 show the transient variation of the non-dimensional working fluid temperature along the length of the packed bed obtained with the two models. The general trends of the curves for the different models are similar to each other. The subcooling region and phase change region exist distinctly in these plots. The release of the heat of fusion of the PCM produces some inflexion points on the boundary between the two regions.

Figures 5-30 through 5-35 show the surface temperature variation of the capsules in the axial direction. Compared with Figures 5-9 through 5-11, more time is needed for the PCM to reach the working fluid entrance temperature.

Figures 5-36 through 5-41 indicate the transient temperature gradient inside the spheres as a function of bed length location along the axial center of the packed bed. Three separate regions, subcooling, phase-change, and superheating, can be seen in these figures. It is clear from the figures that the area 'A' of non-dimensional temperature below the zero value represents subcooling where no melting appears. The top area 'C' represents the superheating. In this region, all the PCM is in liquid phase. The phase change region, area

Figure 5-24.   Transient Variation of Working Fluid Temperature
              (MF=113.8 Kg/hr, Latent Heat Storage, First-Order Model)

Charging Mode, Bed L)

Figure 5-25.   Transient Variation of Working Fluid Temperature
              (MF=347.4 Kg/hr., Latent Heat Storage, First-Order Model)

Figure 5-26. Transient Variation of Working Fluid Temperature
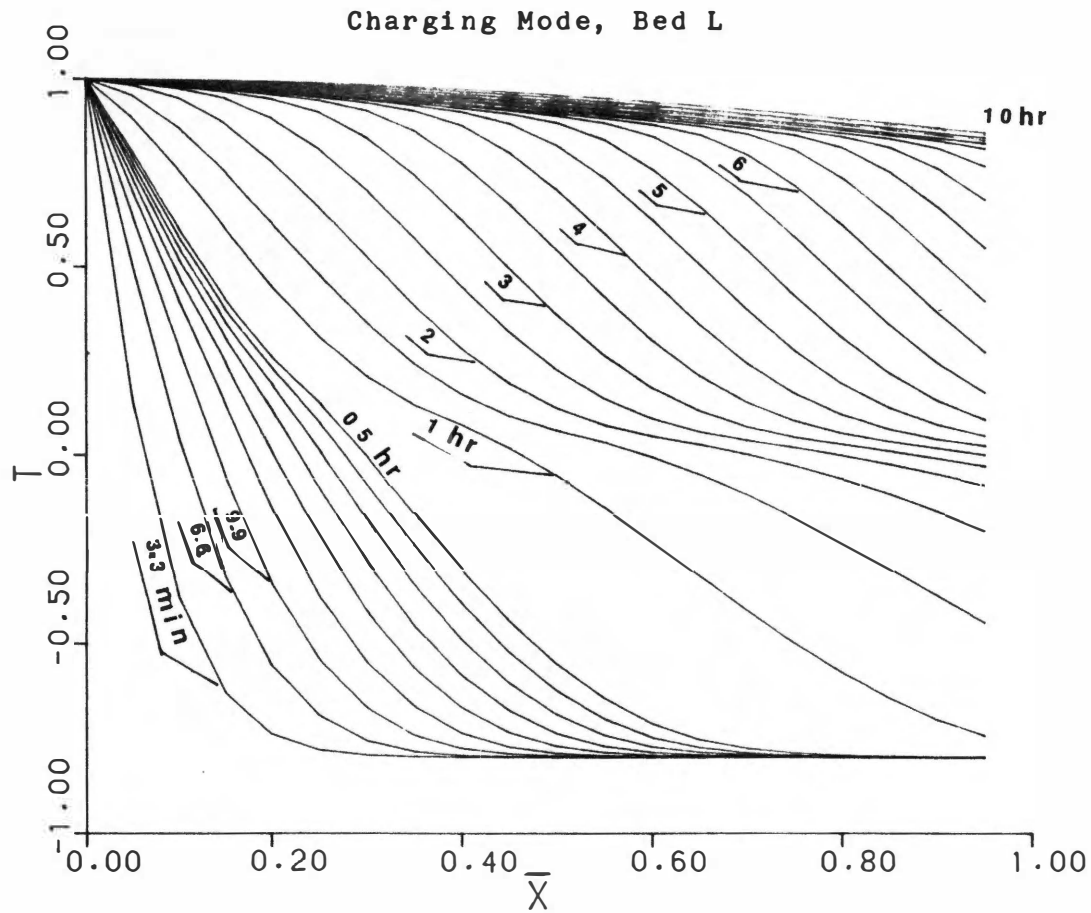(MF=658.6 Kg/hr, Latent Heat Storage, First-Order Model)
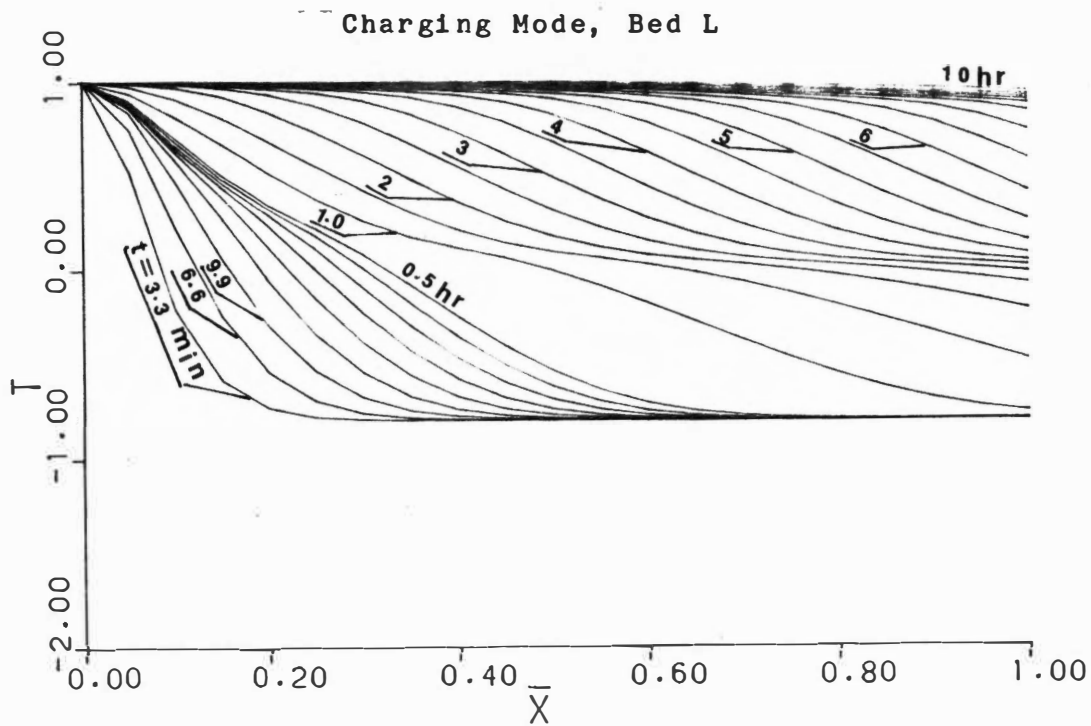
Figure 5-27. Transient Variation of Working Fluid Temperature
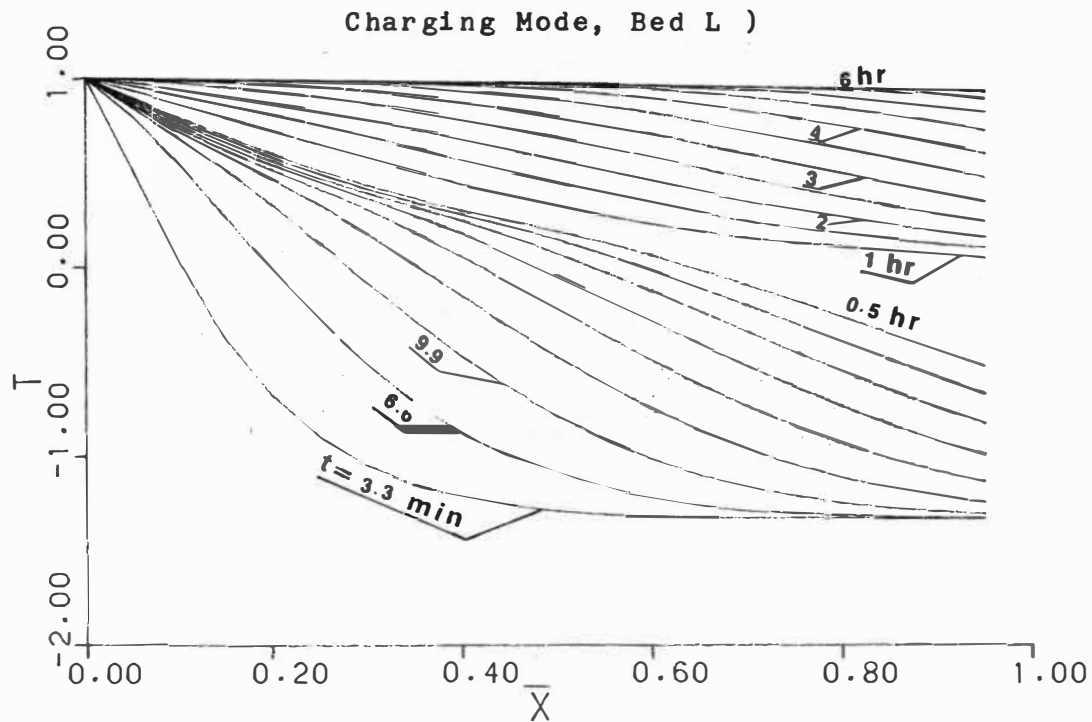(MF=113.8 Kg/hr, Latent Heat Storage, Second-Order Model)
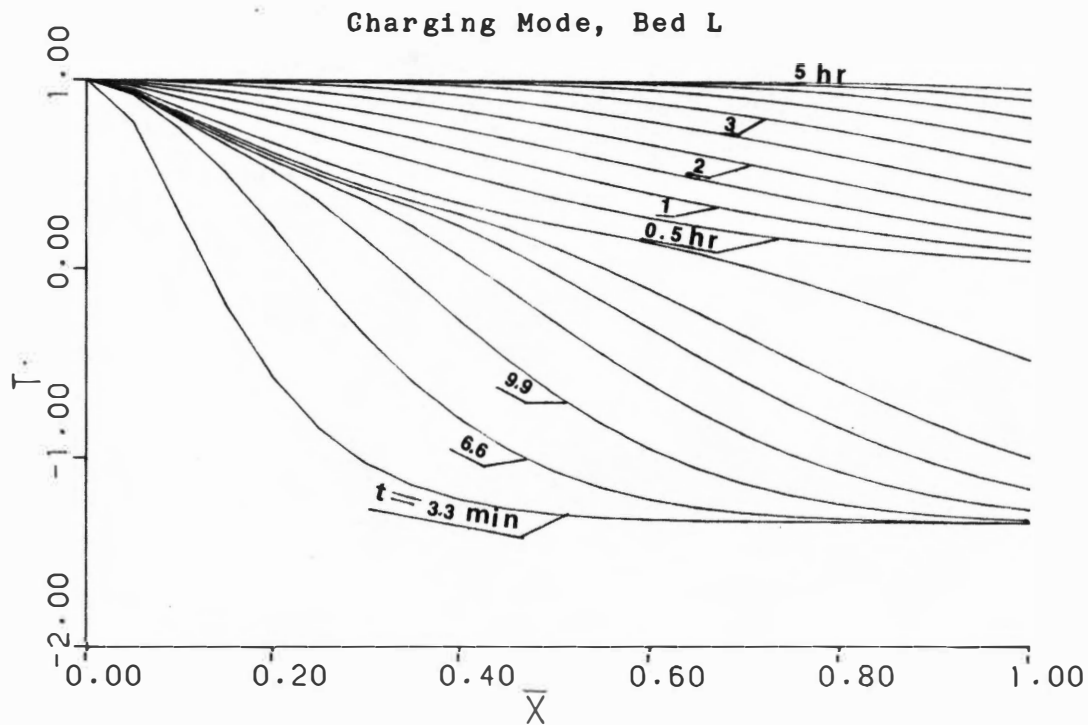
Figure 5-28. Transient Variation of Working Fluid Temperature
(MF=347.4 Kg/hr, Latent Heat Storage, Second-Order Model)
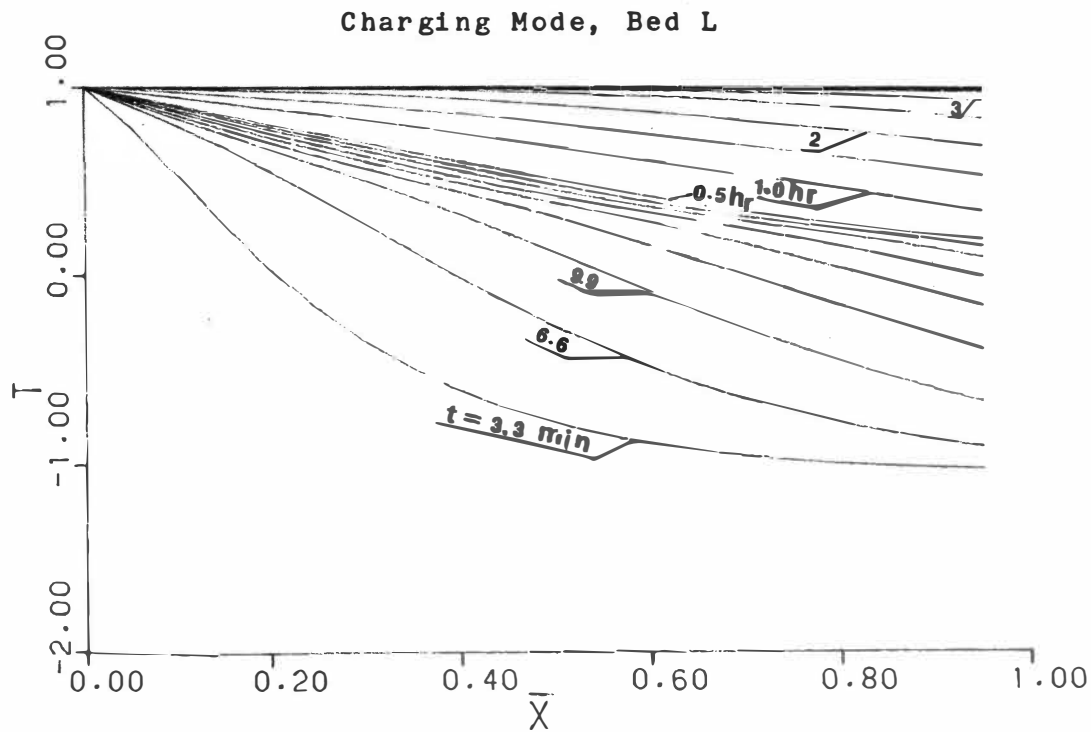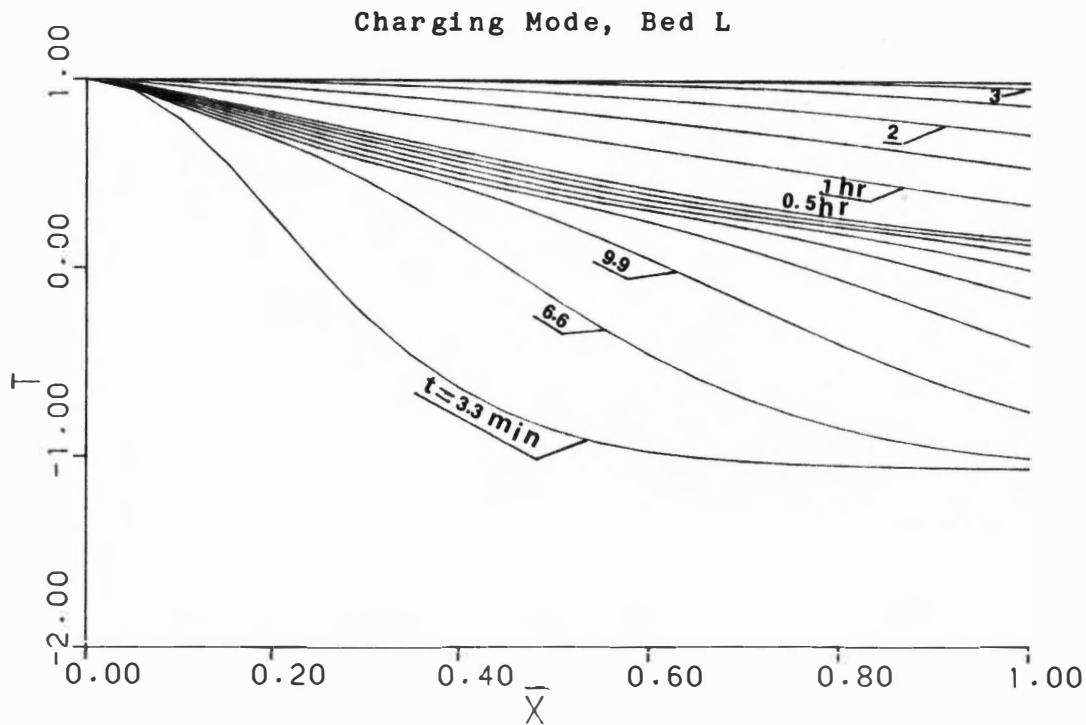
Figure 5-29   Transient Variation of Working Fluid Temperature
(MF=658.6 Kg/hr, Latent Heat Storage, Second-Order Model)

94
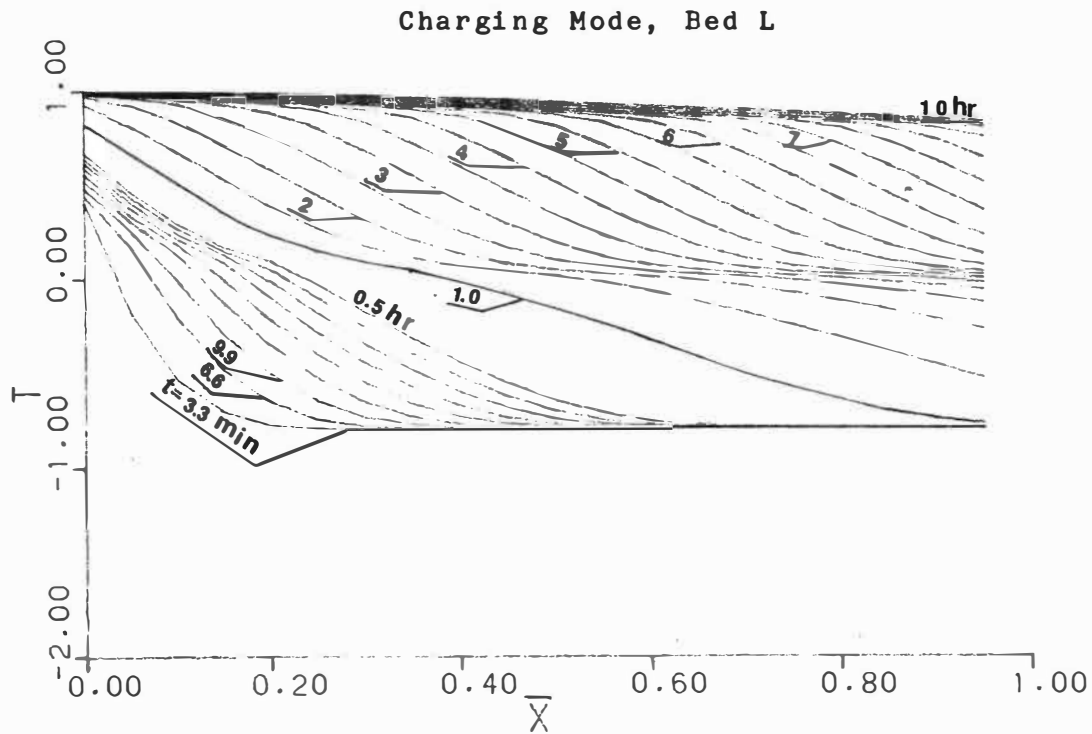
Figure 5-30. Surface Temperature of Capsule Along Packed Bed
(MF=113.8 Kg/hr, Latent Heat Storage, First-Order Model)
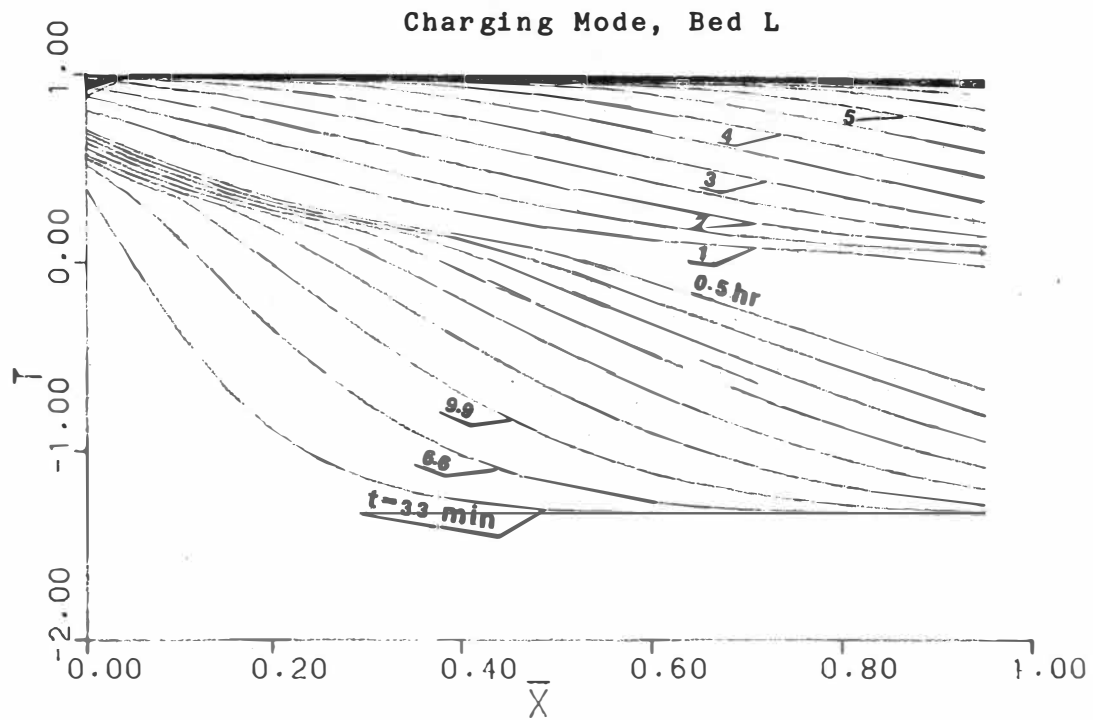
Figure 5-31.   Surface Temperature of Capsule Along Packed Bed
                (MF=347.4 Kg/hr, Latent Heat Storage, First-Order Model)
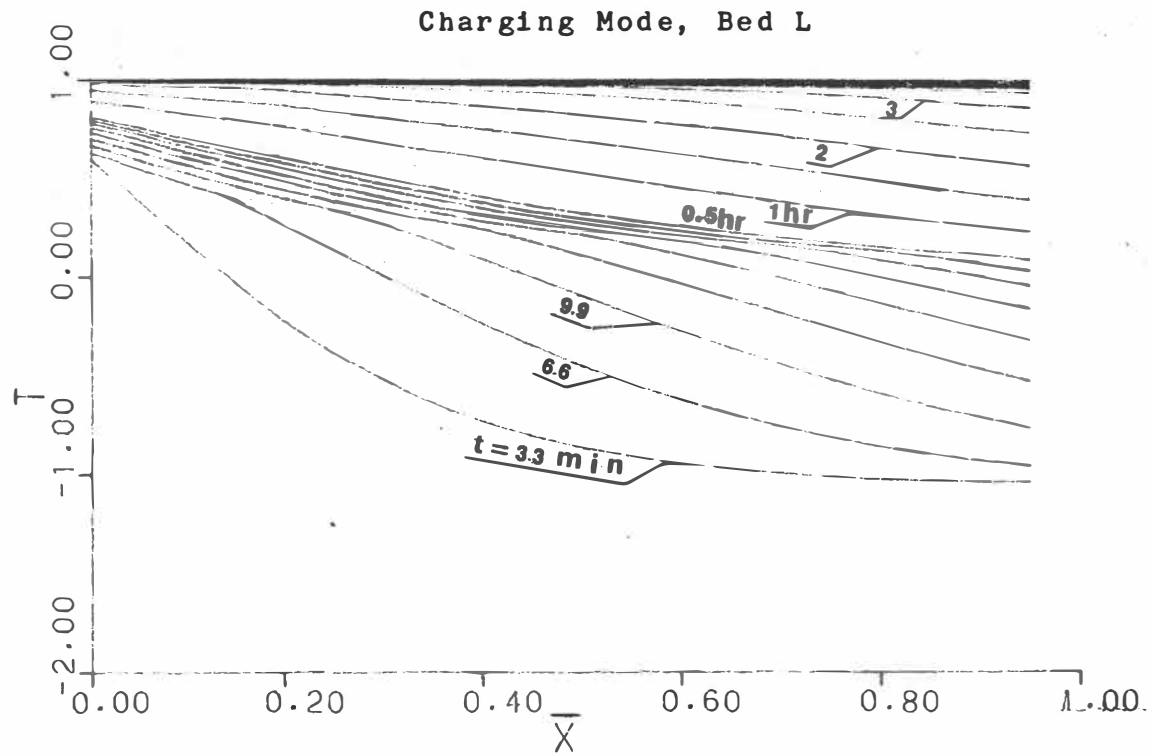
Figure 5-32.   Surface Temperature of Capsule Along Packed Bed
                (MF=658.6 Kg/hr, Latent Heat Storage, First-Order Model)

Charging Mode, Bed L

98
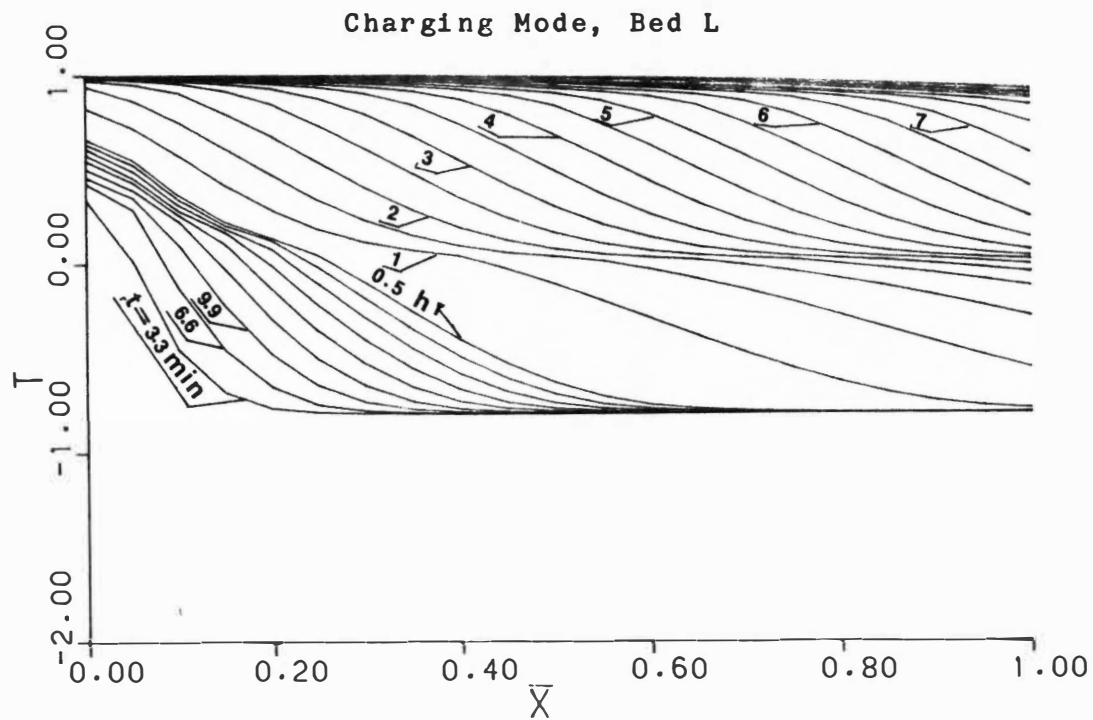
Figure 5-33.   Surface Temperature of Capsule Along Packed Bed
(MF=113.8 Kg/hr, Latent Heat Storage, Second-Order Model)
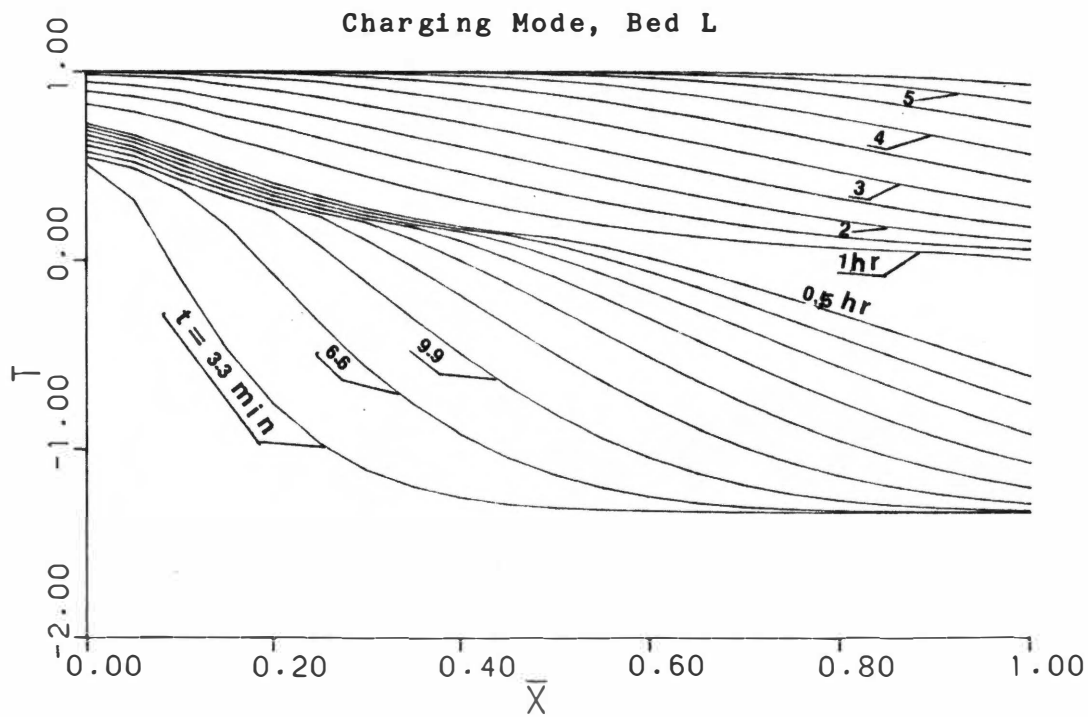
Figure 5-34. Surface Temperature of Capsule Along Packed Bed
(MF=347.4 Kg/hr, Latent Heat Storage, Second-Order Model)
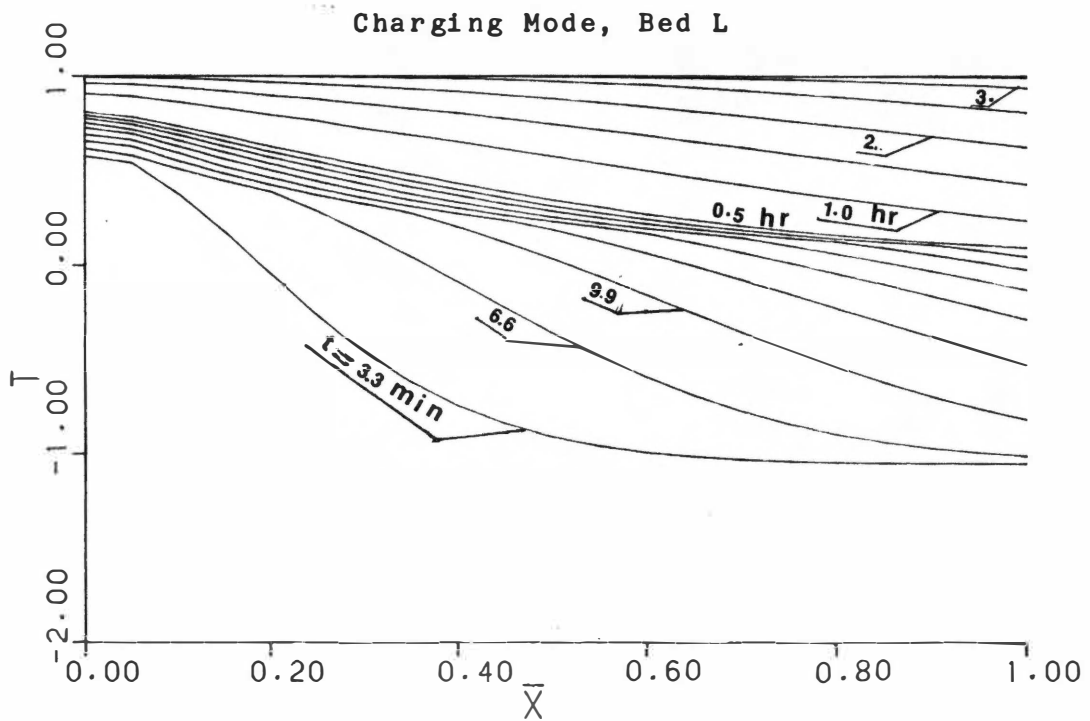
Figure 5-35.   Surface Temperature of Capsule Along Packed Bed
                (MF=658.6 Kg/hr, Latent Heat Storage, Second-Order Model)
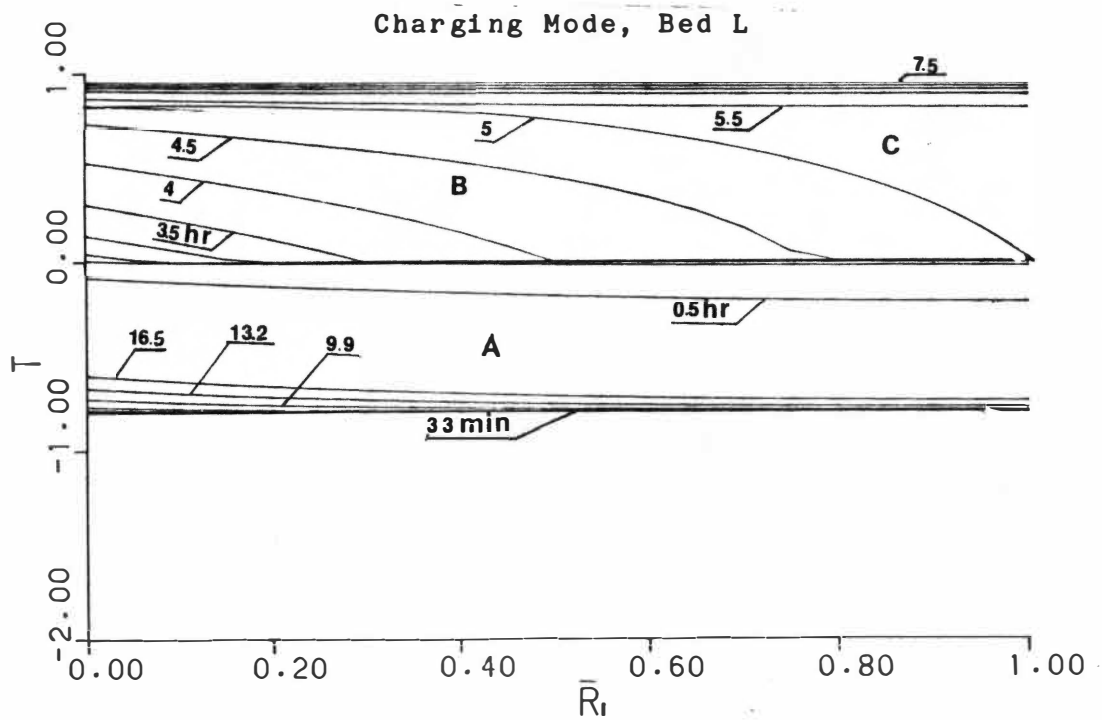
Figure 5-36. Temperature Distribution Inside Sphere
(MF=113.8 Kg/hr, Latent Heat Storage, First-Order Model)
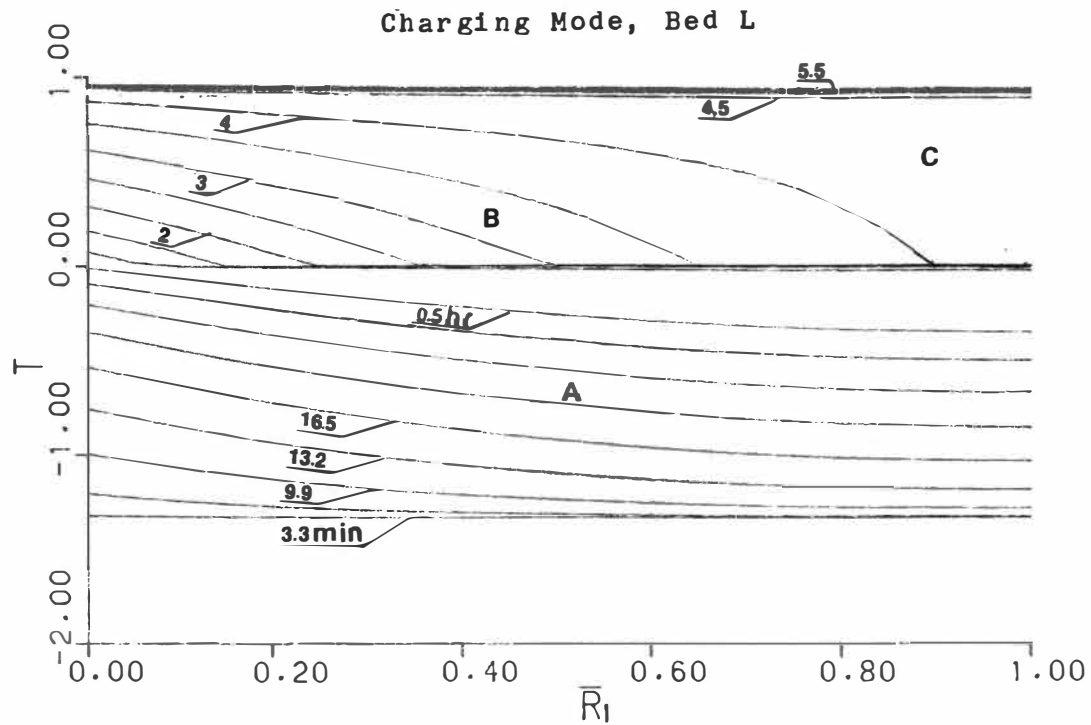
Figure 5-37. Temperature Distribution Inside Sphere
(MF=347.4 Kg/hr, Latent Heat Storage, First-Order Model)

(Charging Mode, Bed L)
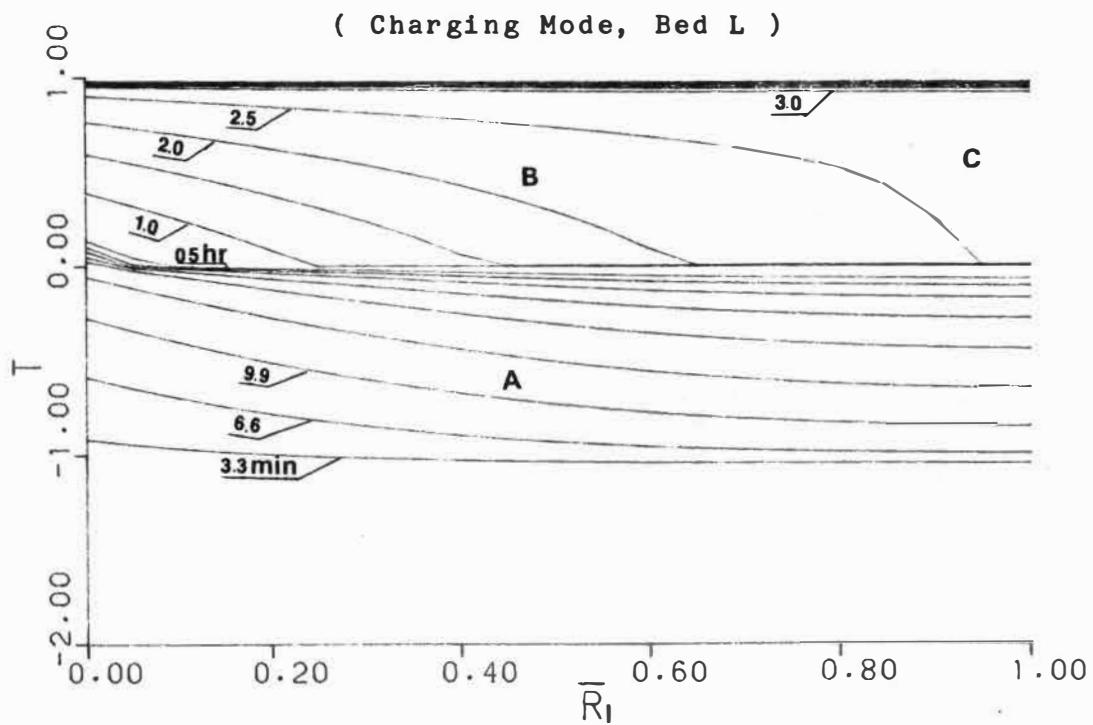
Figure 5-38. Temperature Distribution Inside Sphere
(MF=658.6 Kg/hr, Latent Heat Storage, First-Order Model)
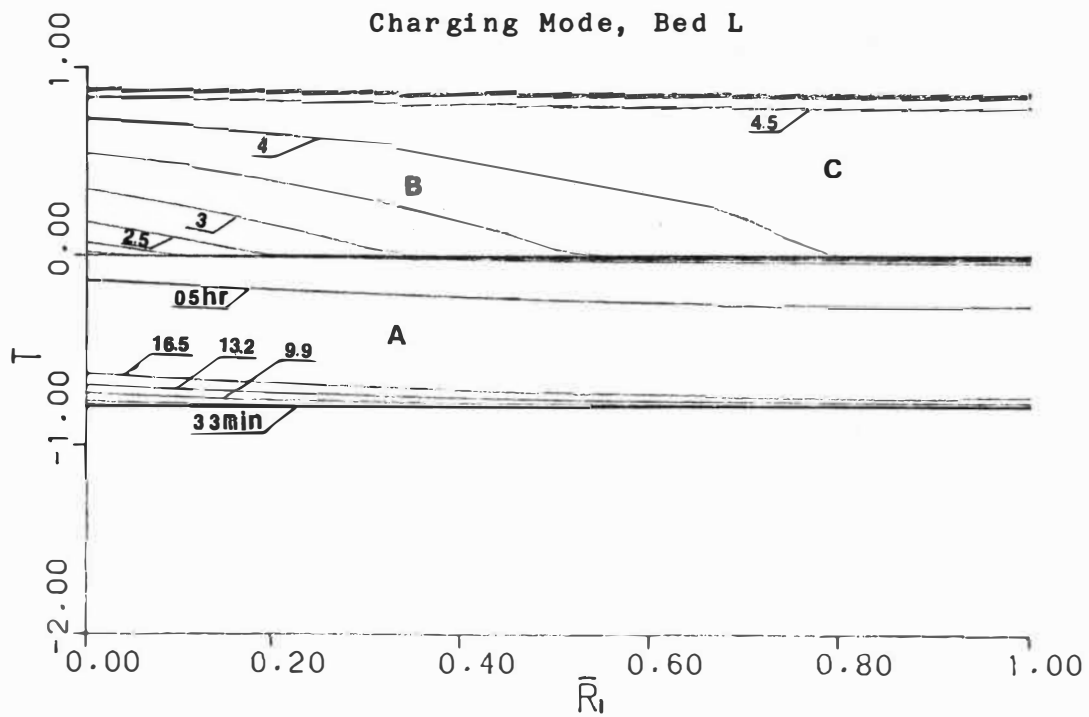
Figure 5-39. Temperature Distribution Inside Sphere
(MF=113.8 Kg/hr, Latent Heat Storage, Second-Order Model)
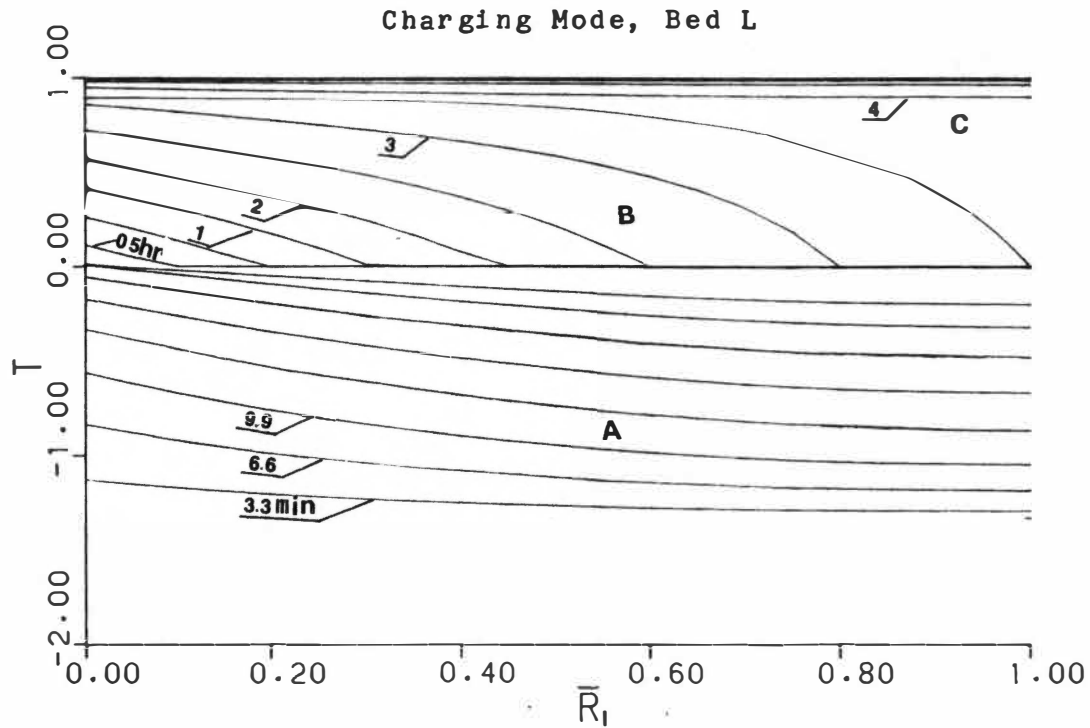
Figure 5-40. Temperature Distribution Inside Sphere
(MF=347.4 Kg/hr, Latent Heat Storage, Second-Order Model)
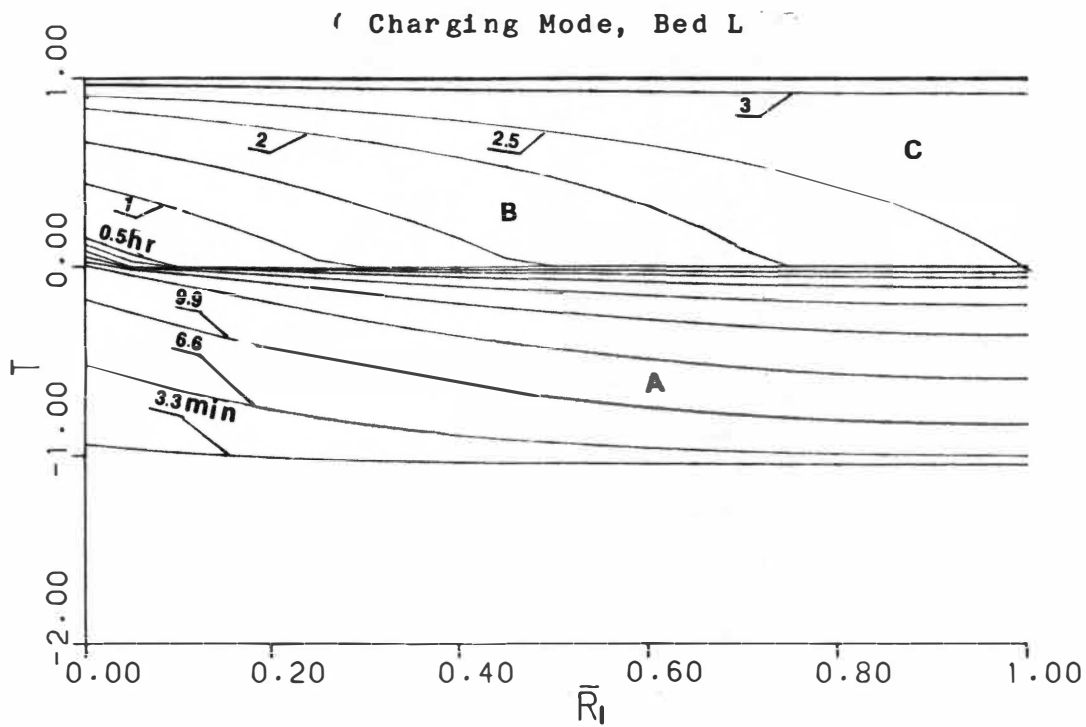
Figure 5-41. Temperature Distribution Inside Sphere
(MF=658.6 Kg/hr, Latent Heat Storage, Second-Order Model)

'B' where both liquid phase and solid phase co-exist, lies between the above two. the temperature gradient inside the sphere is not equal to zero (except at the center of the sphere), particularly in the phase change region. The lumped model, therefore, is not suitable for a PCM.

Figures 5-42 through 5-47 indicate the so-called "melting gradient" lines. These figures give the total melting time, the melted fraction at any specific time, and the location of the melting front. This information is essential for the designer to make the best choices of parameters in a latent heat, packed bed design.

Finally the non-dimensional heat storage 'Q' for different flowrates is shown in Figures 5-48 through 5-51.

(2.B) Freezing Mode

Figure 5-52 is an example of the working fluid temperature at the exit as a function of time for discharging. After the working fluid flows through the packed bed, the outlet temperature promptly drops to a point below the melting temperature due to supercooling, then remains temporarily constant, and finally experiences a temperature jump at the end of the flat segment. Following the jump, the outlet temperature gradually falls to the entrance temperature. The 'jump' phenomena was experimentally observed by Graves' [45]. In the
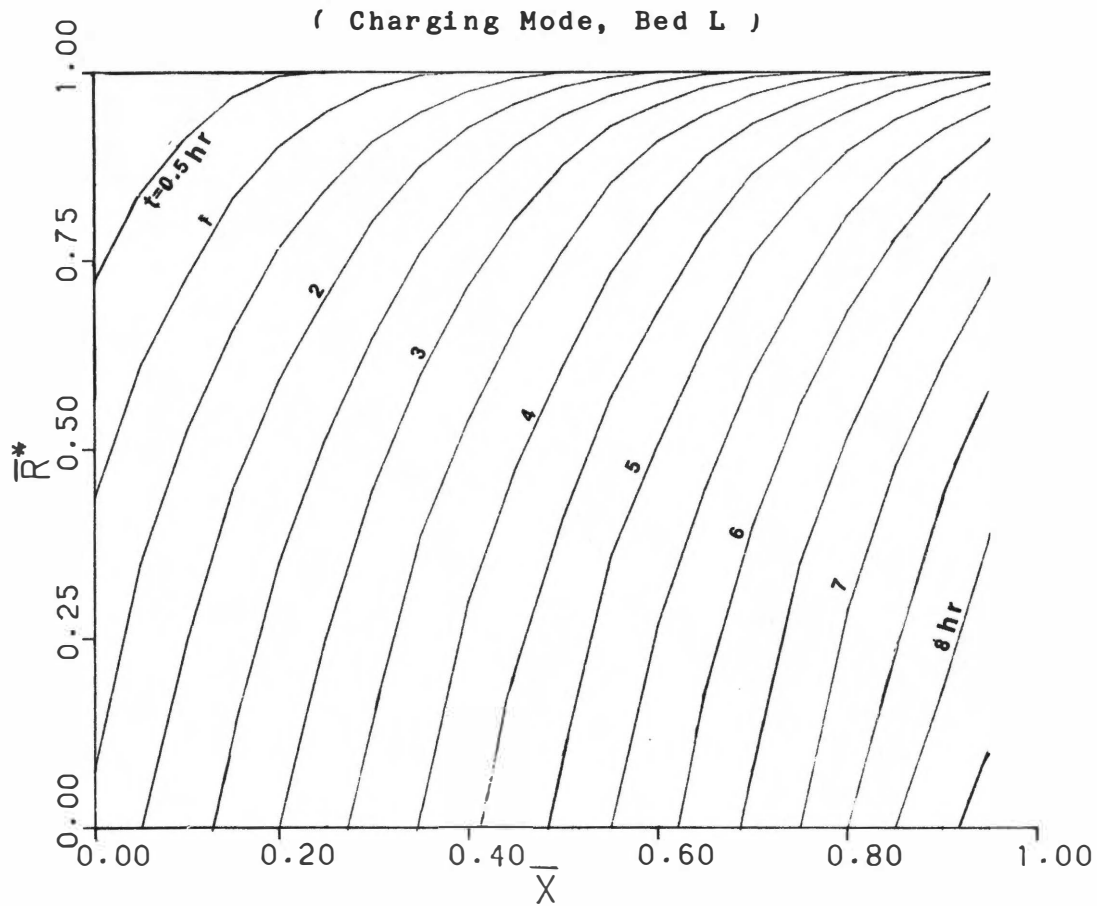
Figure 5-42.   Transient Variation of Melting Front Radius
               (MF=113.8 Kg/hr, First-Order Model, Melting Case)
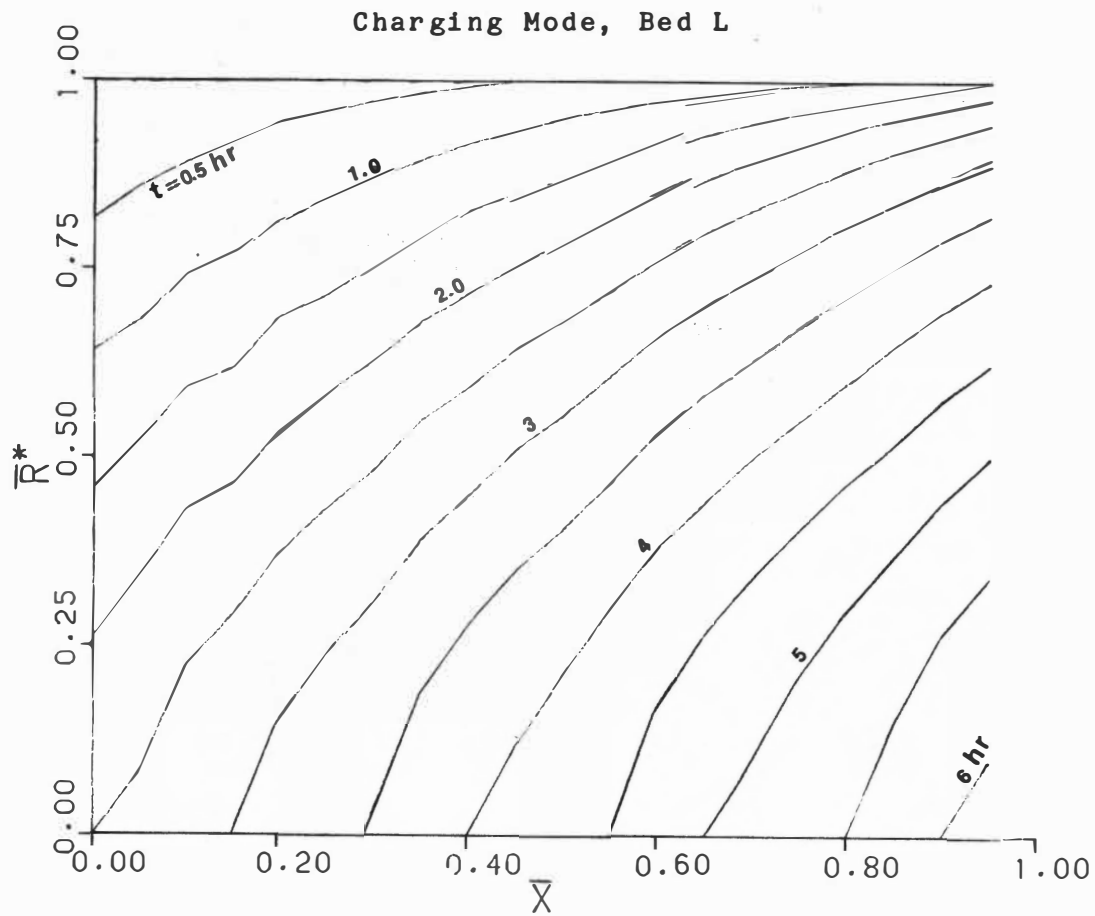
Figure 5-43.   Transient Variation of Melting Front Radius
(MF=347.4 Kg/hr, First-Order Model, Melting Case)
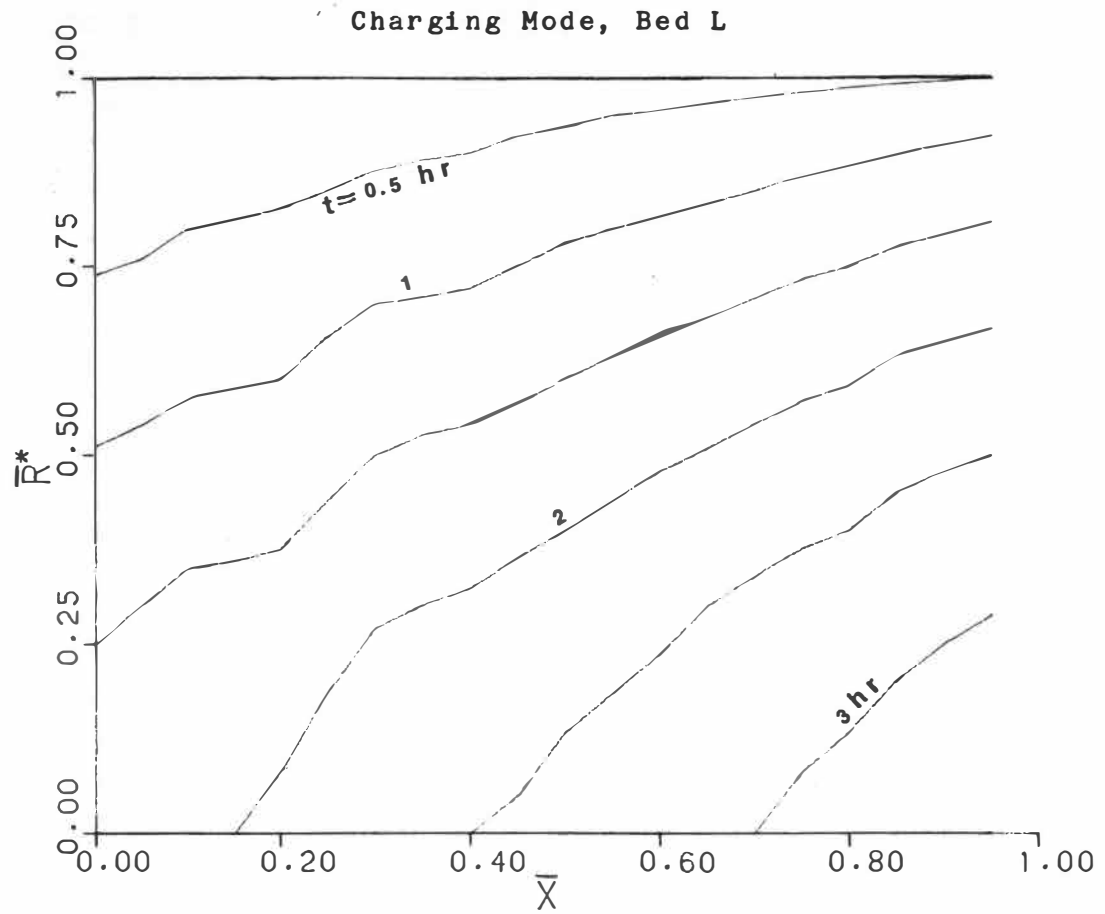
Figure 5-44. Transient Variation of Melting Front Radius
(MF=658.6 Kg/hr, First-Order Model, Melting Case)
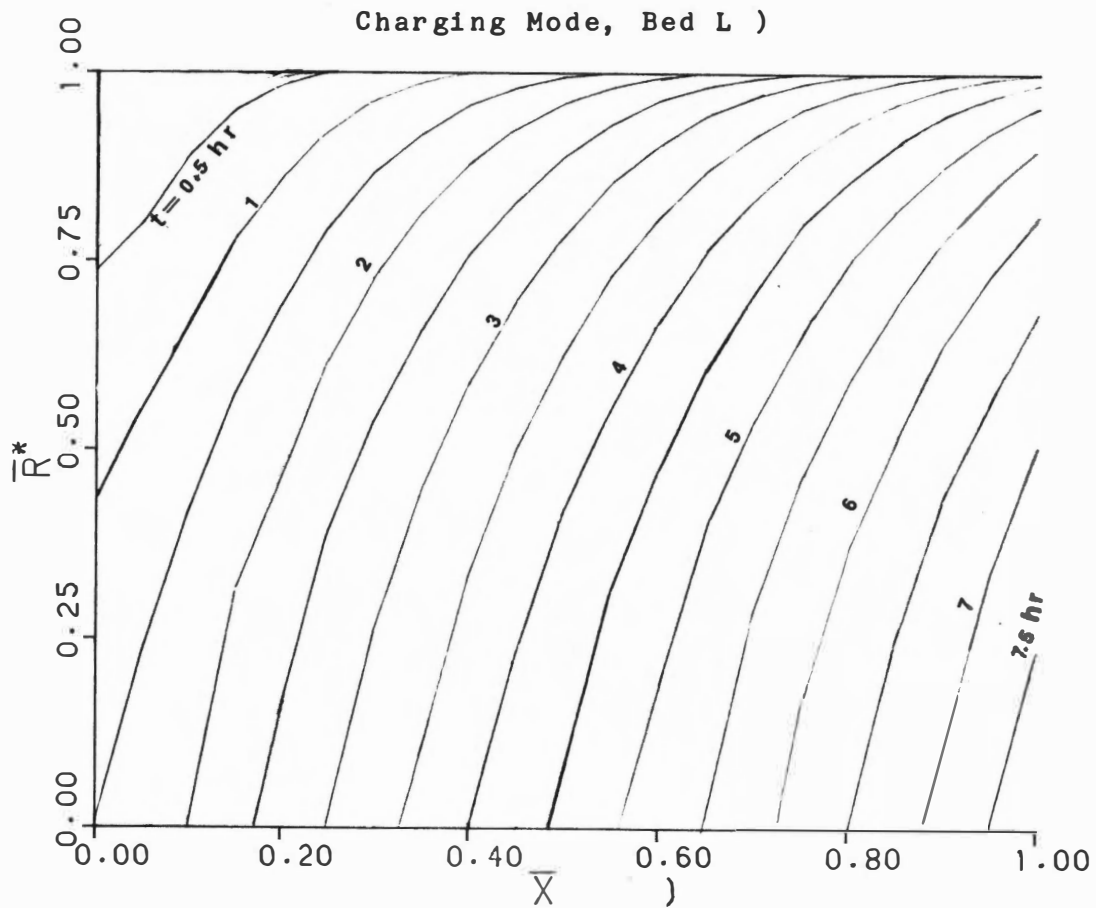
Figure 5-45.   Transient Variation of Melting Front Radius
(MF=113.8 Kg/hr, Second-Order Model, Melting Case)

111
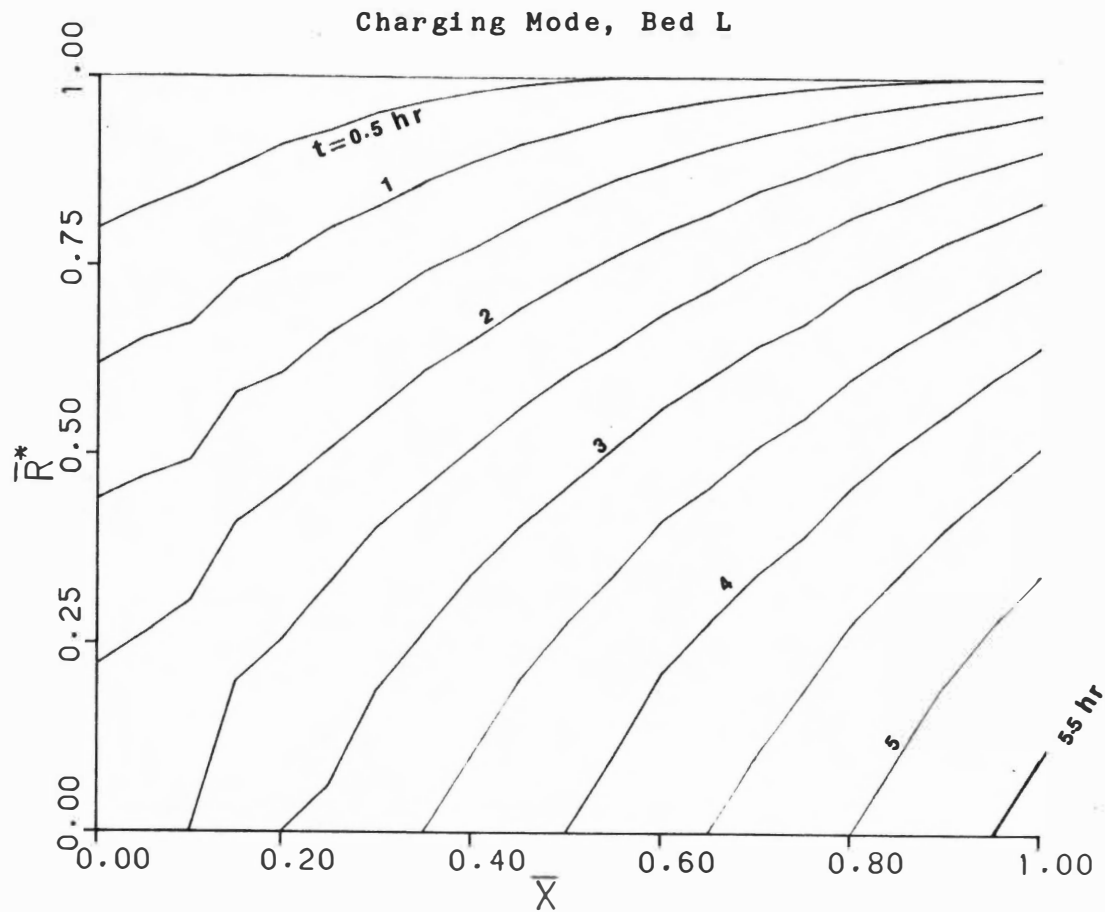
Figure 5-46. Transient Variation of Melting Front Radius
(MF=347.4 Kg/hr, Second-Order Model, Melting Case)
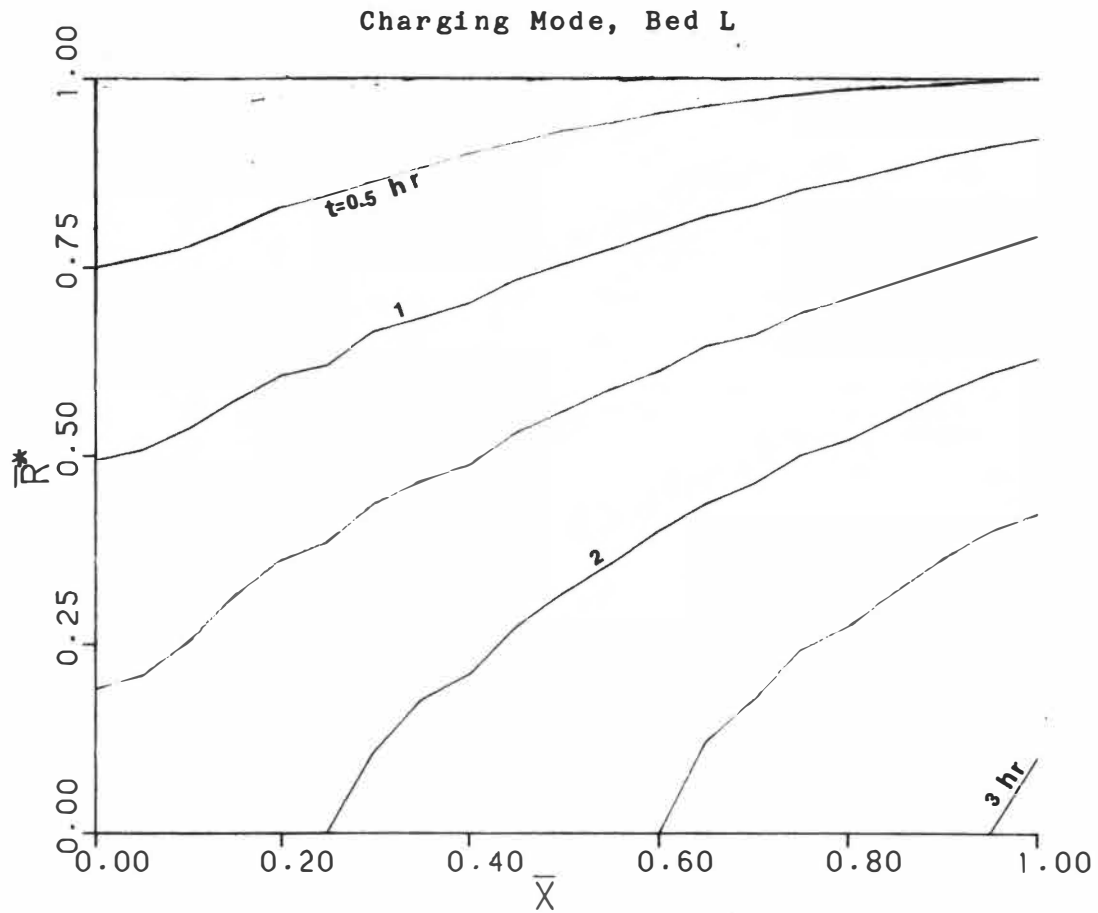
Figure 5-47. Transient Variation of Melting Front Radius
(MF=658.6 Kg/hr, Second-Order Model, Melting Case)
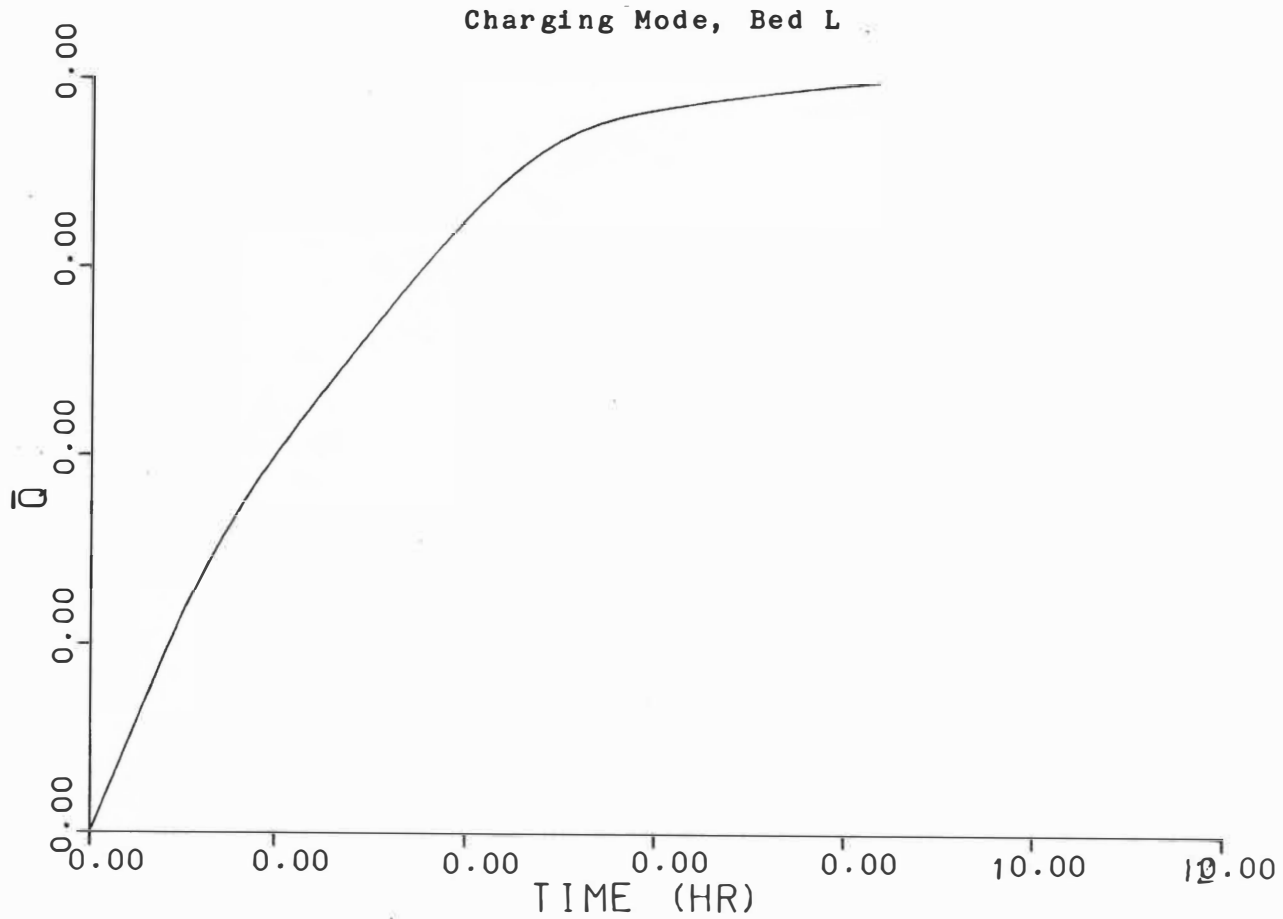
Figure 5-48.   Non-dimensional Heat Q for MF=113.8 Kg/hr
(Latent Heat Storage, Second-Order Model)

114

Charging Mode, Bed L

$\bar{Q}$

TIME (HR)
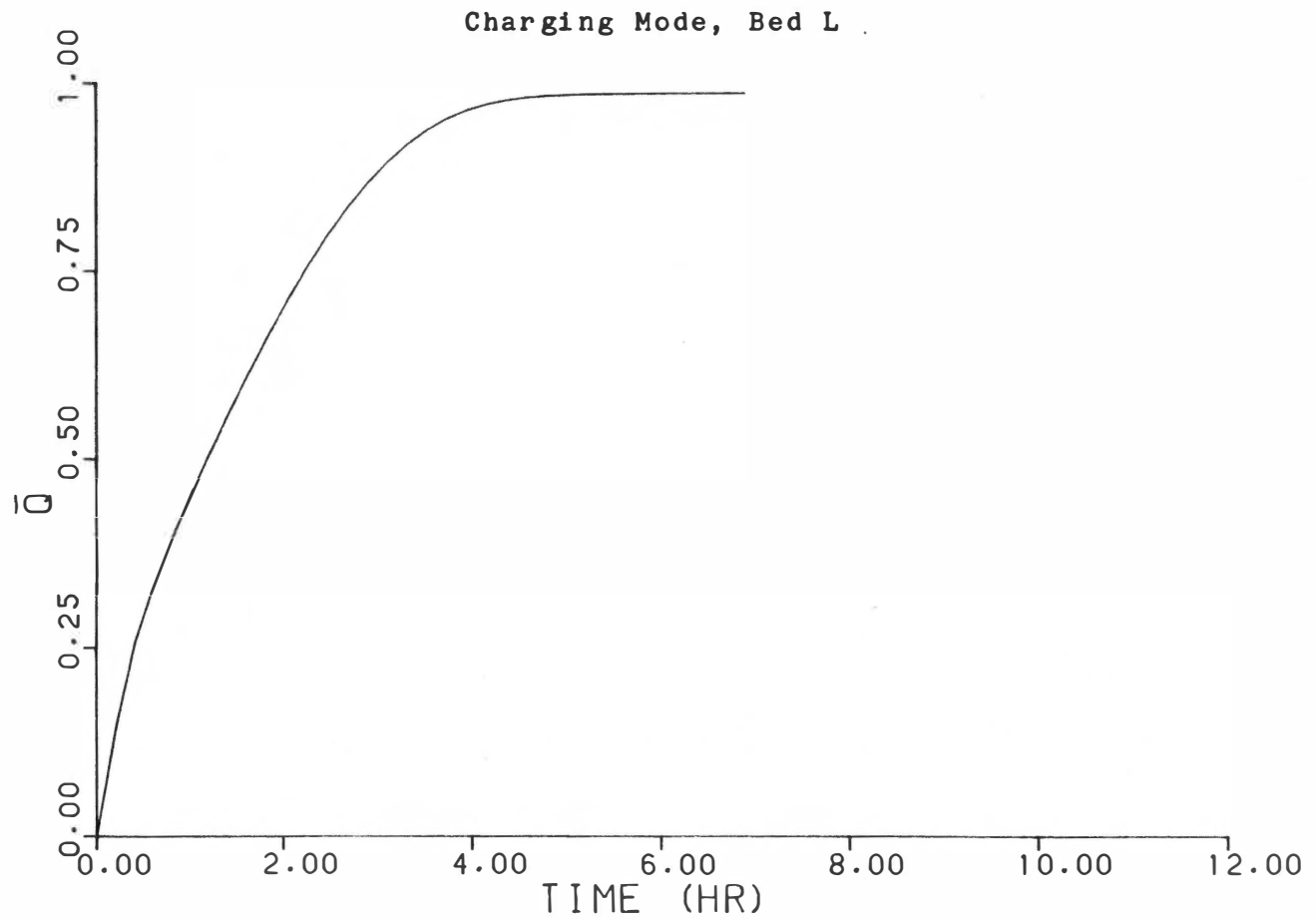
Figure 5-49. Non-dimensional Heat Q for MF=347.4 Kg/hr
(Latent Heat Storage, Second-Order Model)
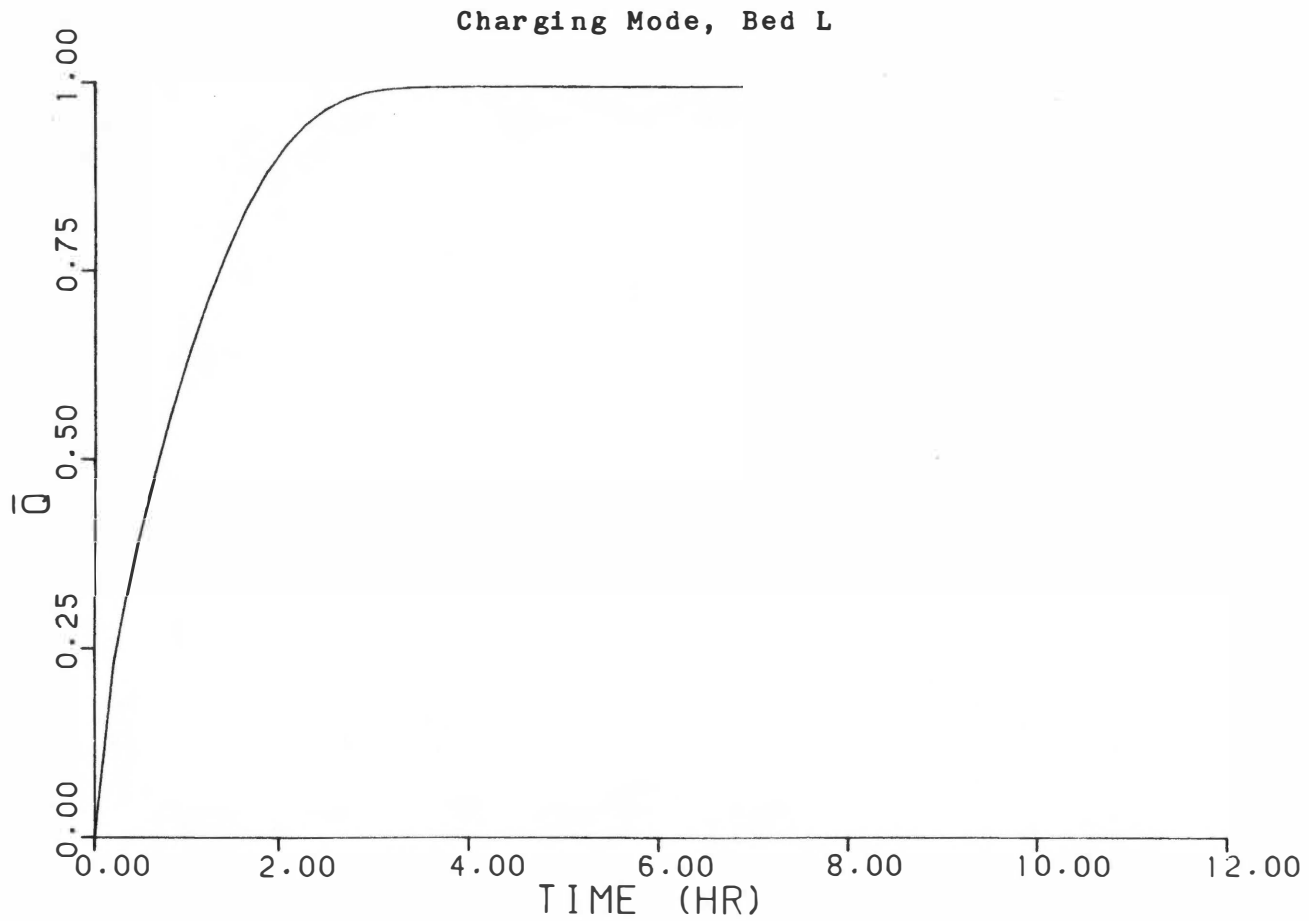
Figure 5-50. Non-dimensional Heat Q for MF=658.6 Kg/hr
(Latent Heat Storage, Second-Order Model)
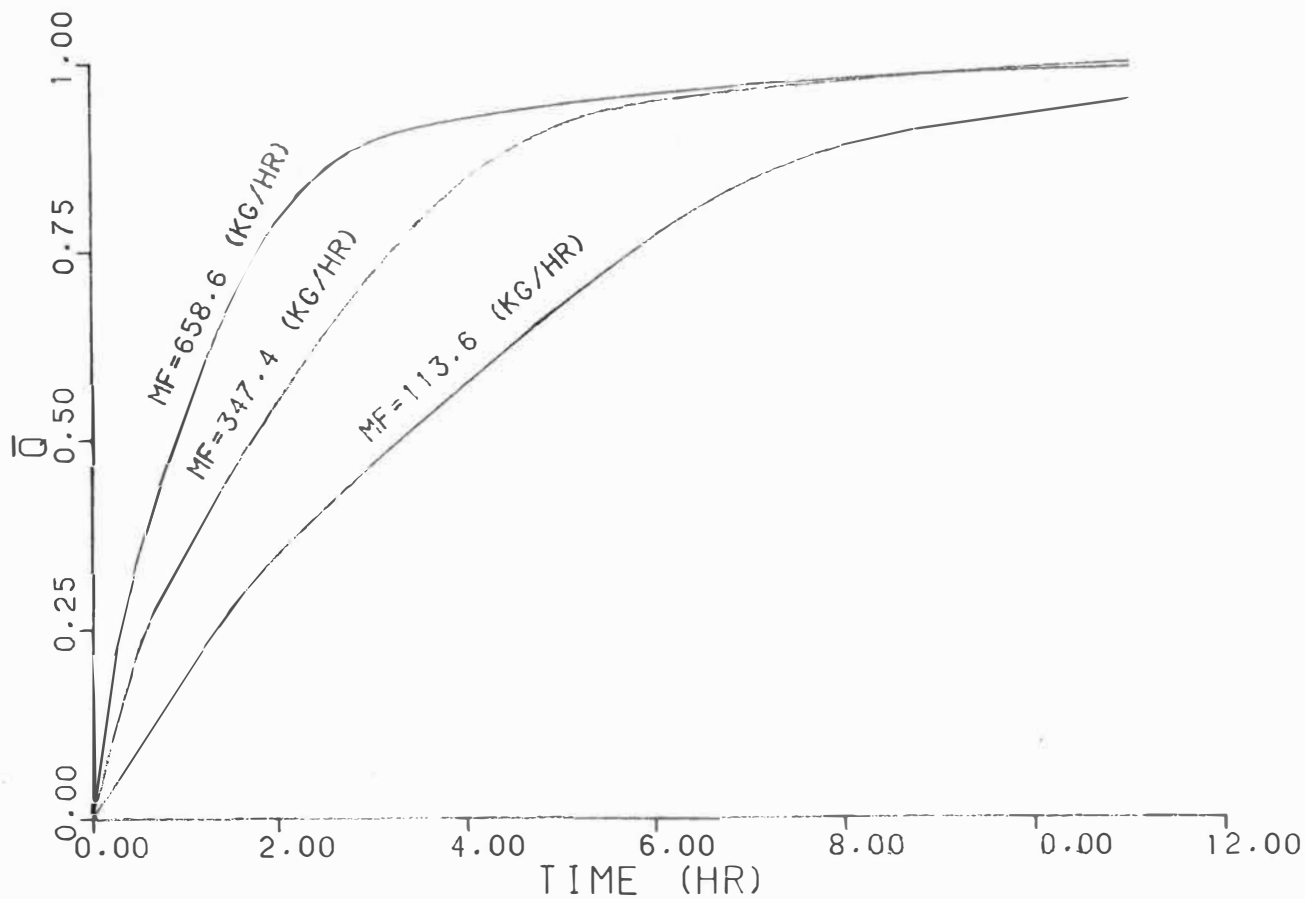
Figure 5-51. Non-Dimensional Heat Q for Different Mass Flowrates
(Latent Heat Storage, First-Order Model)

	MF (Kg/hr)	TI (F)	TS (F)	Experimental
A	119.9	289	326.5	☉
B	298.8	289	325.5	△
C	558.0	289	327.5	+

(Discharging Mode, Bed L)
———-- Analytical
(Second-Order Model)
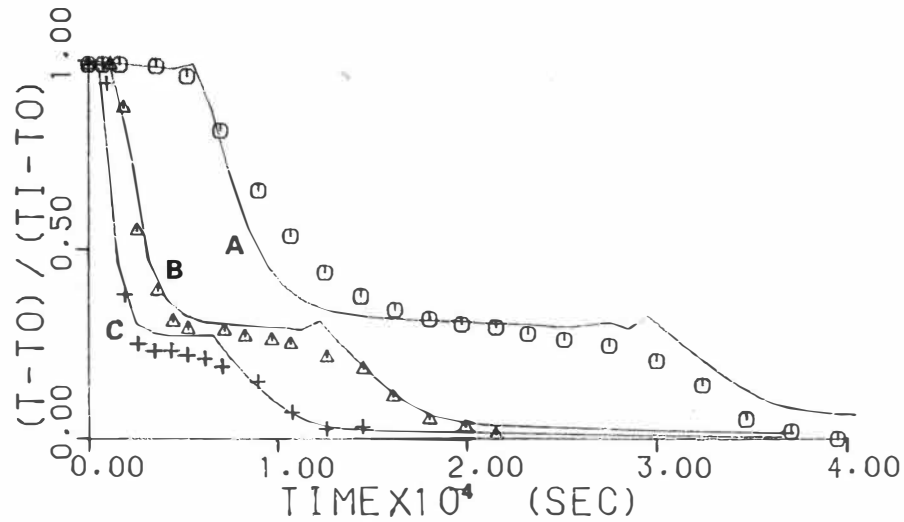
Figure 5-52. Variation of the Outlet Temperature History Curve with
Flowrate (with Supercooling)

charging process, the outlet temperature gradually rises even while the phase change is proceding. In the discharging process, the latent heat released by the PCM per unit time is almost constant while solidification is proceeding. The temperature 'jump' is the result of suddenly and appreciably raising the capsule's surface temperature during the solidification at the downstream end of the packed bed.

In Figure 5-53, an example of analytical results without considering supercooling is shown. Compared with the results with supercooling shown in Figure 5-52, the curves exhibit no plateau and no temperature jump. If we invert the curves , they are seen to be very similar to the curves for the melting process shown in Figure 5-16. Figures 5-54 through 5-56 show the working fluid temperature variation along the axial direction. A unique characteristic of this set of figures is that an intersection appears among some curves; this is caused by supercooling. The superheating and phase-change regions are separated naturally in these figures.

The variation of surface temperature of spherical capsules with distance and time is shown in Figures 5-57 through 5-59. Because the surface temperature is strongly influenced by the supercooling, some zig-zag temperature

	MF (Kg/hr)	TI (F)	TS (F)	Experimental
A	119.9	289	326.5	⊕
B	298.8	289	325.5	△
C	558.0	289	327.5	+

(Discharging Mode, Bed L)
——— Analytical
(Second-Order Model)
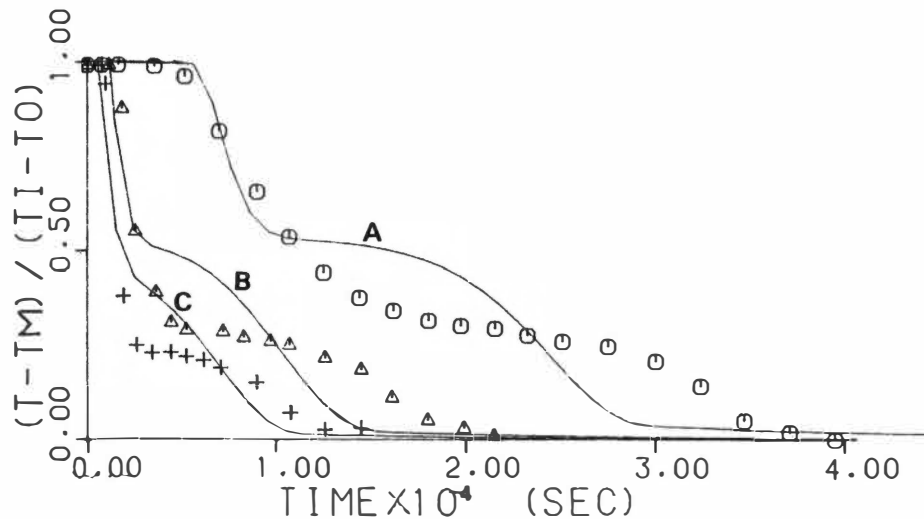
Figure 5-53. Variation of the Outlet Temperature History Curve with Flowrate (without Supercooling)
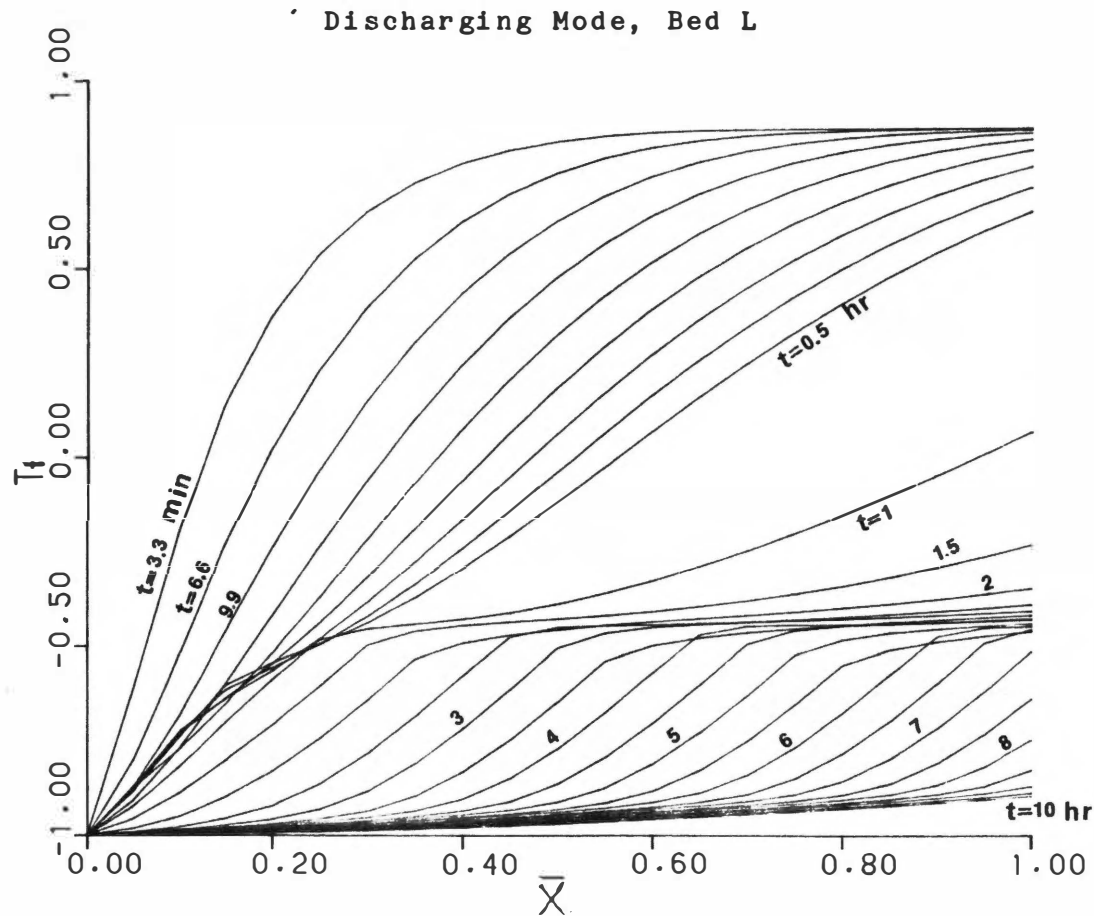
Figure 5-54. Variation of Working Fluid Temperature with Distance and Time (with Supercooling); Mf=119.9 Kg/hr
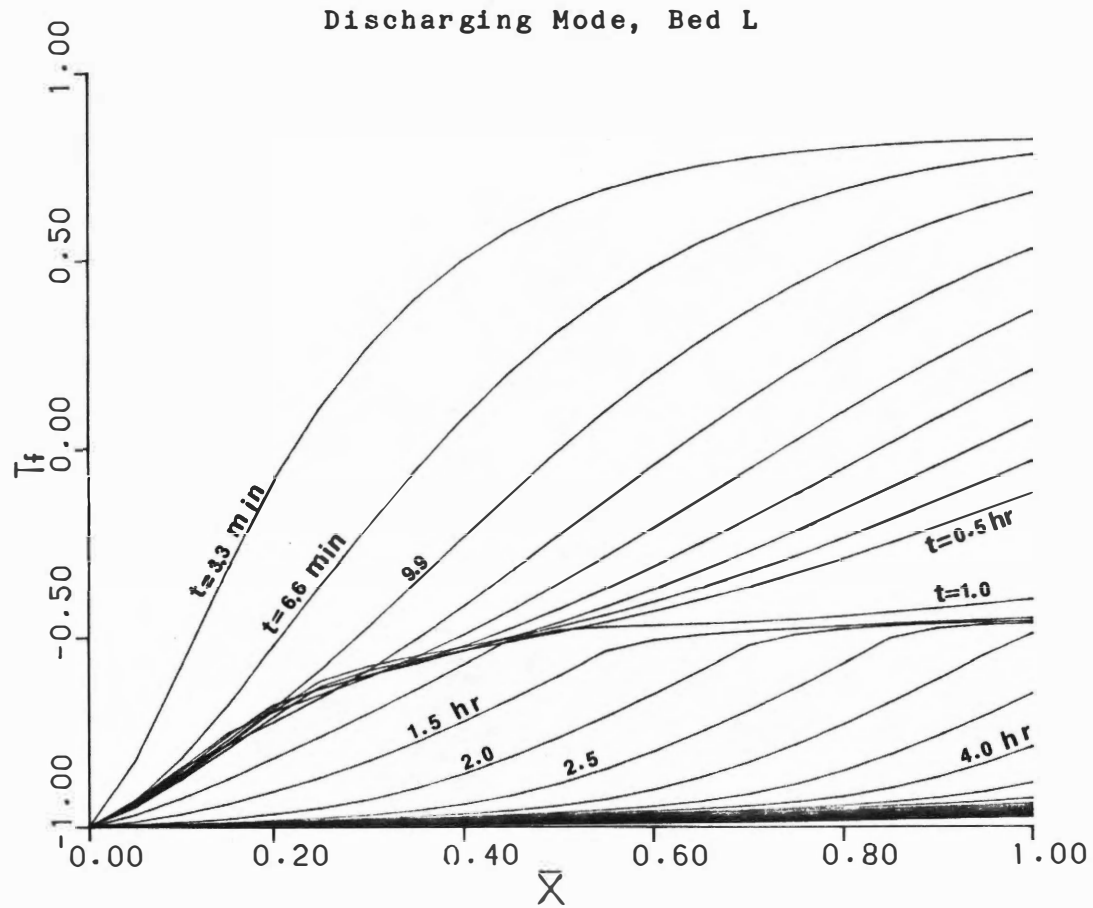
Figure 5-55.   Variation of Working Fluid Temperature with Distance
and Time (with Supercooling); MF=298.8 Kg/hr
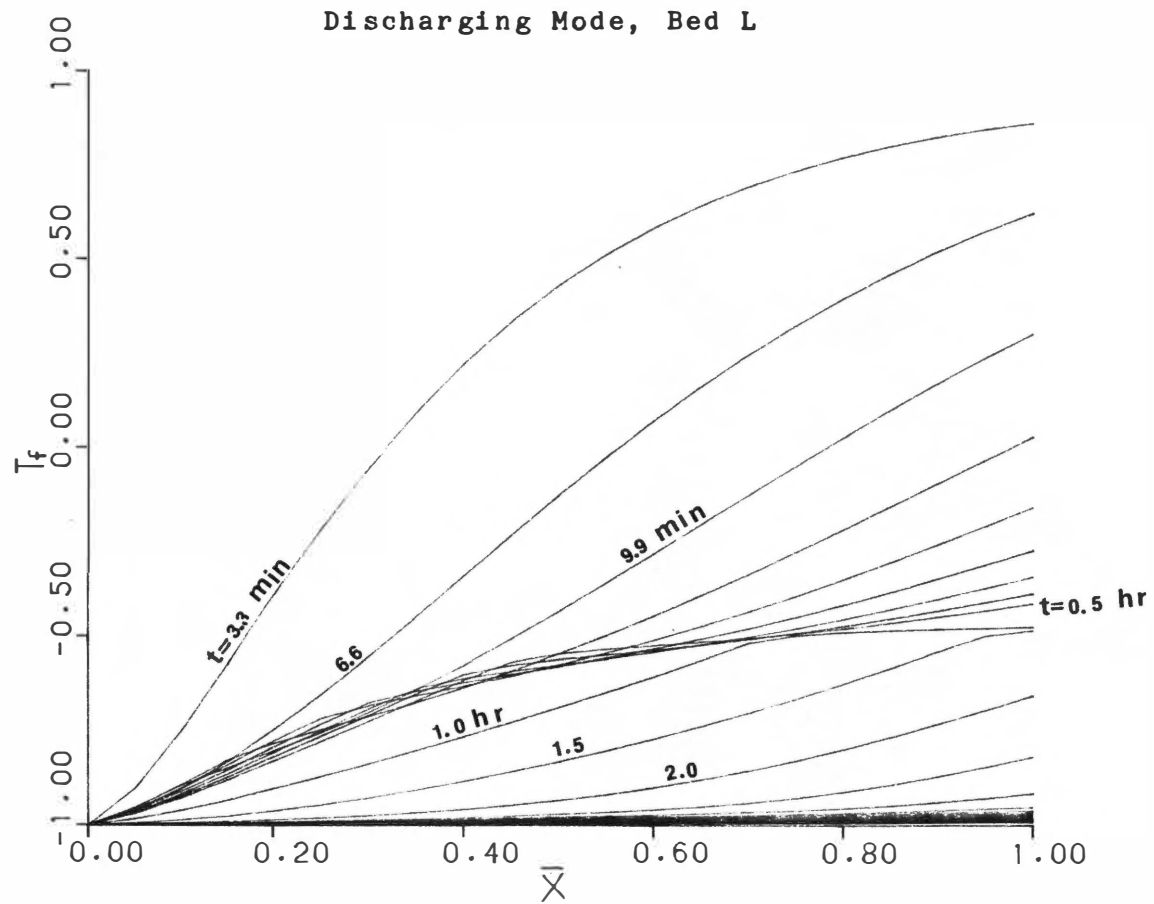
Figure 5-56.   Variation of Working Fluid Temperature with Distance
and Time (with Supercooling); MF=558 Kg/hr

123
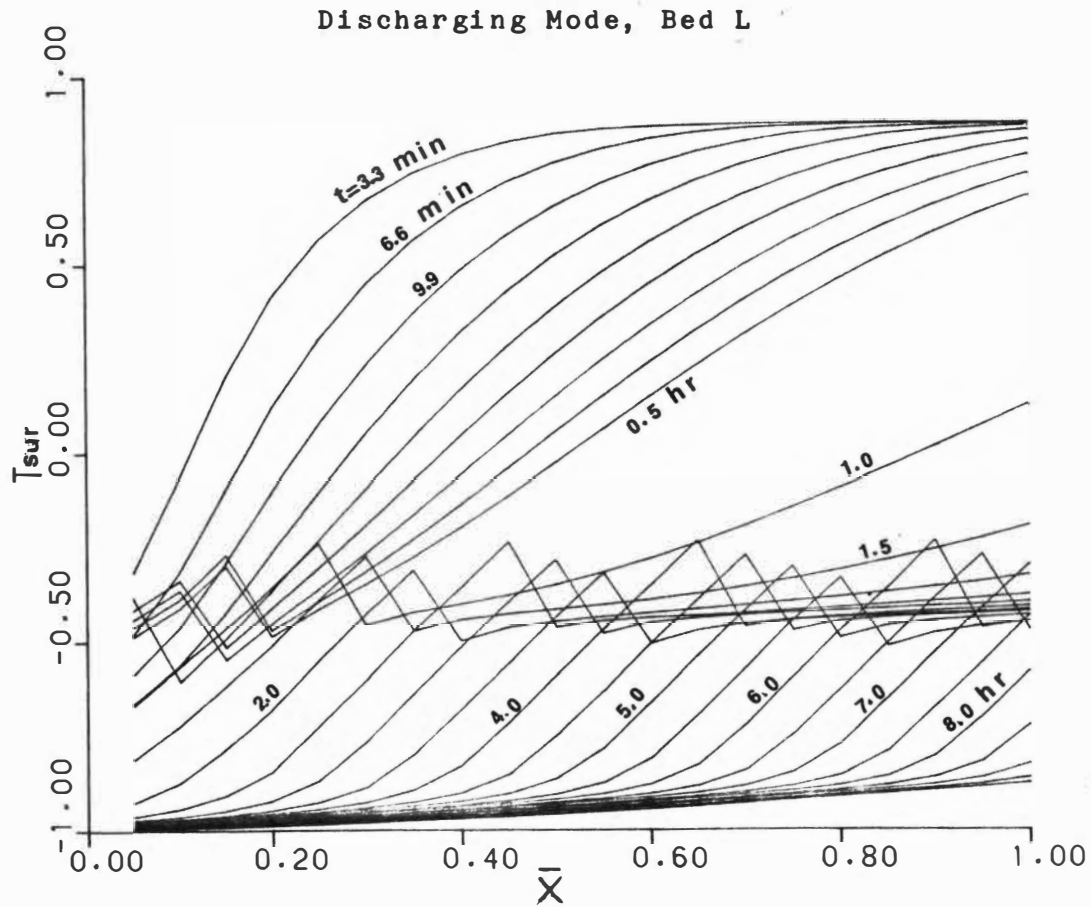
Figure 5-57. Variation of Surface Temperature of Spherical Capsule
with Distance and Time (with Supercooling); MF=119.9 Kg/hr
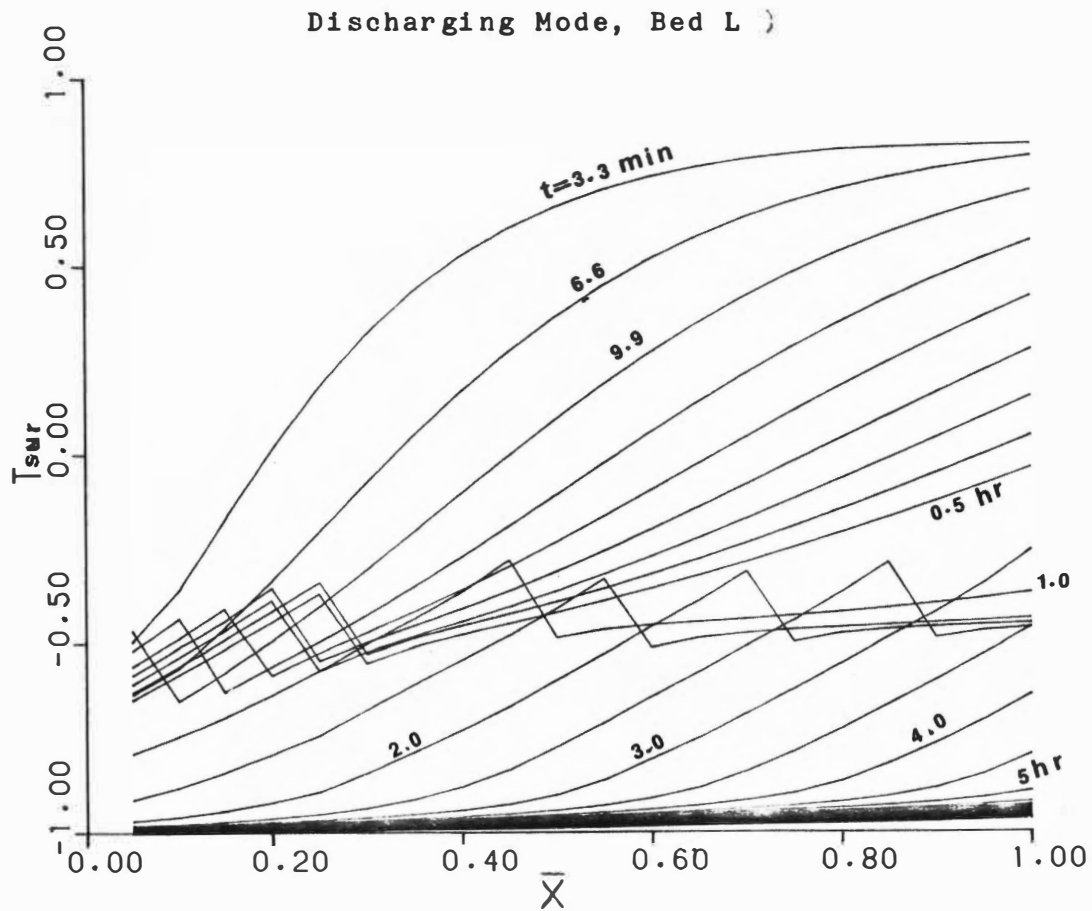
Figure 5-58. Variation of Surface Temperature of Spherical Capsule with Distance and Time (with Supercooling); MF=298.8 Kg/hr
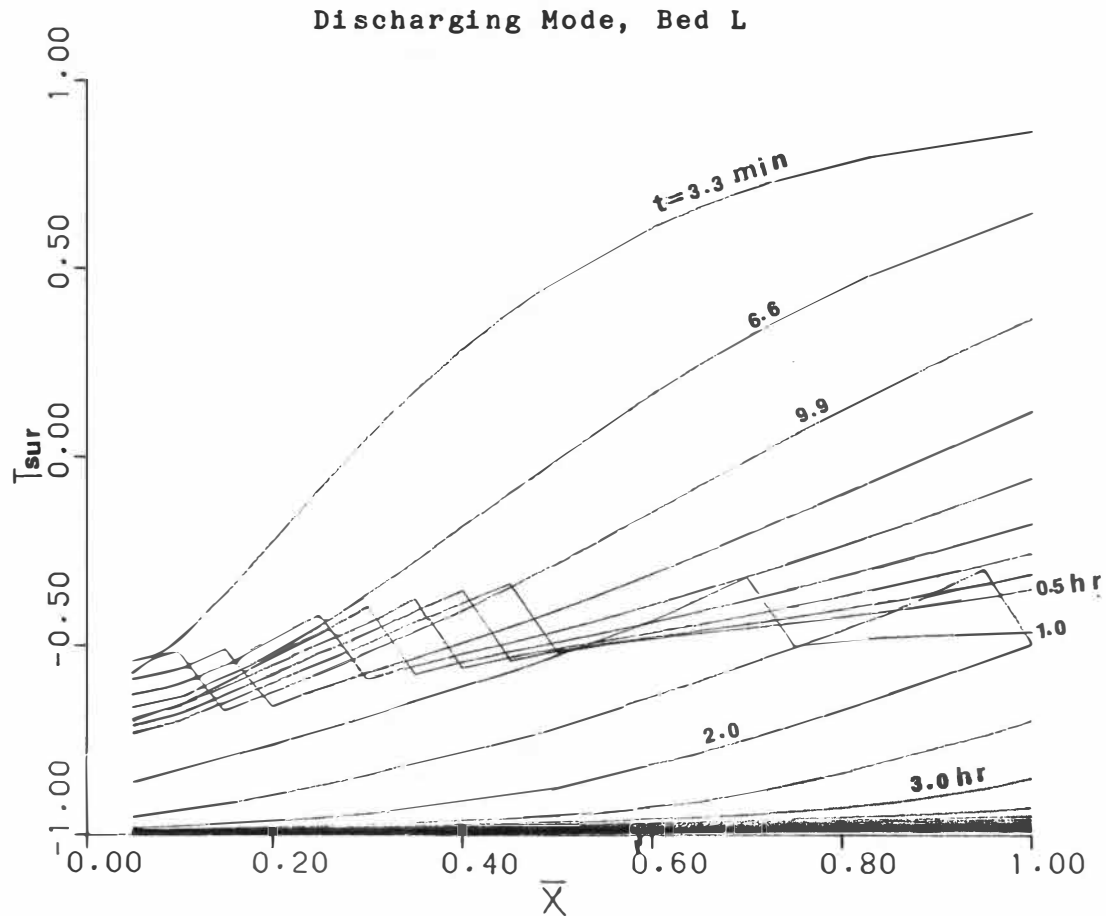
Figure 5-59. Variation of Surface Temperature of Spherical Capsule with Distance and Time (with Supercooling); MF=558 Kg/hr

gradient discontinuities are produced when the solidification is proceeding. The initial solidification occurs very rapidly and is probably associated with a rapid return to the equilibrium temperature after an initial supercooling. The solidification proceeds until the phase change interface reaches the center of the capsule, and the surface temperature decreases steadily until it reaches the entrance temperature.

In Figures 5-60 through 5-63 the measured and predicted temperatures at the center of capsules are compared. Good agreement is seen to exist between the analytical and the experimental data. The non-dimensional temperature jump due to supercooling varies with position in the packed bed. The bed axial length was divided into 20 equal distances for defining bed length locations. Thus, the point"2" is 2/20 or 10 percent of the bed length,etc. At the position "2", the jump was so slight that there seems to be no jump at all. The jump gets larger with increasing axial distance. This is considered to be due to the different rates of cooling at different positions, since the PCM has poor conductivity and it takes a significant amount of time to cool down the center point of the capsule. As soon as the initial solidification occurs, the latent heat released at the
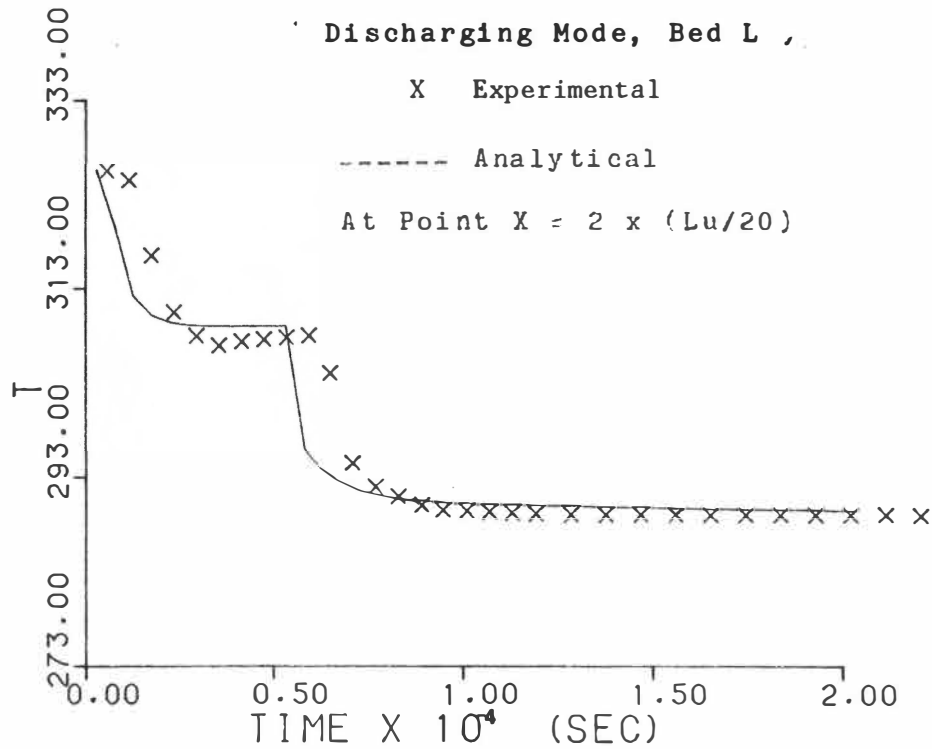
Figure 5-60. Transient Variation of Temperature at Center of Spherical
Capsule (Freezing Case); X=0.1 of Bed Length; MF=298.8 Kg/hr
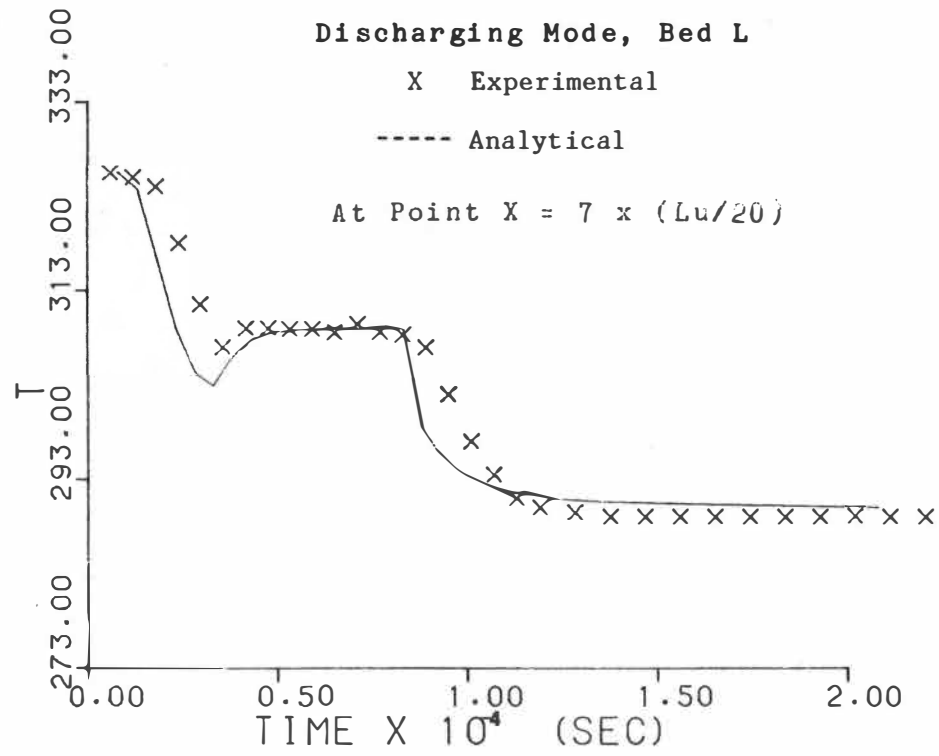
Figure 5-61. Transient Variation of Temperature at Center of Spherical Capsule (Freezing Case); X=7/20 of Bed Length; MF=298.8 Kg/hr
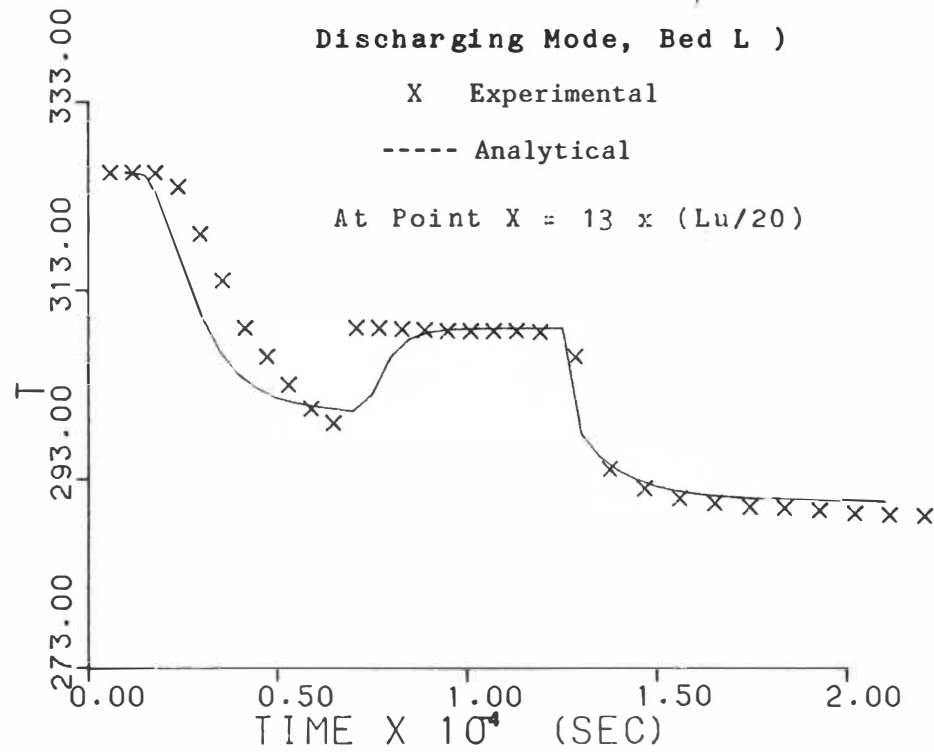
Figure 5-62. Transient Variation of Temperature at Center of Spherical
Capsule (Freezing Case); X=13/20 of Bed Length; Mf=298.8 Kg/hr
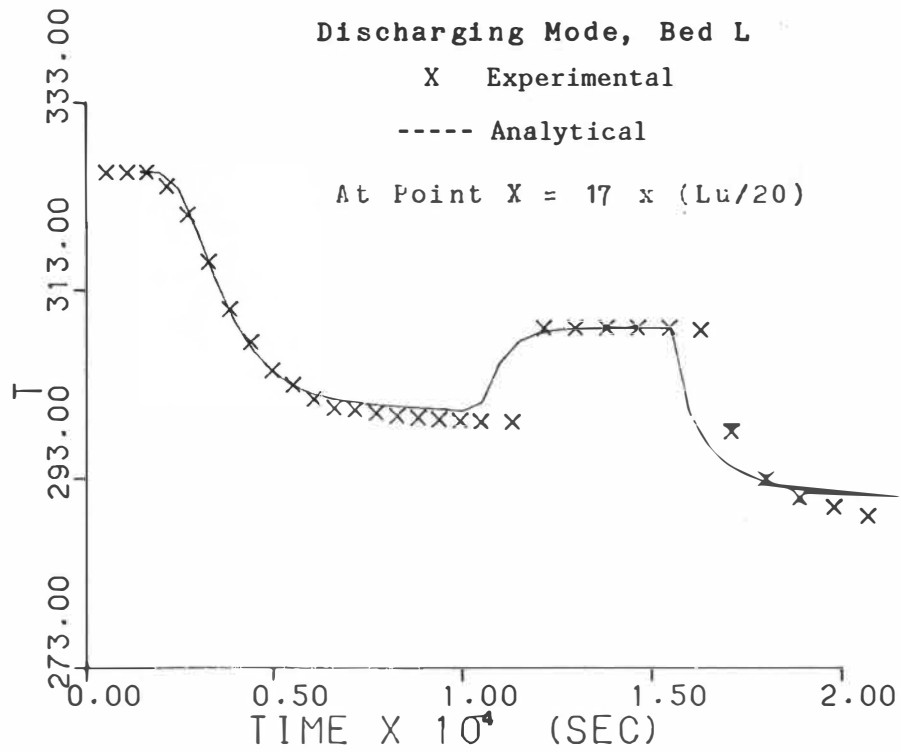
Figure 5-63. Transient Variation of Temperature at Center of Spherical Capsule (Freezing Case); X=17/20 of Bed Length; MF=298.8 Kg/hr

phase-change interface will be transferred not only to the working fluid but also to the inner part of the capsules. The temperature at the center will rise until the melting temperature is reached.

Figure 5-64 shows the transient variation of the predicted temperature at the capsule center for a flowrate of 558.0 kg/hr. The time variation of the location of the freezing front is given in Figures 5-65 through 5-67 where the non-dimensional freezing front radius is plotted against non-dimensionalized axial location. All of these curves follow trajectories similar to those of the same type in the melting mode.

It is understandable that the total solidifying time of the packed bed varies with the flowrate; viz., approximately 9 hours for a flowrate of 119.9 kg/hr, 5 hours for 298.8 kg/hr, and three hours for 559.0 kg/hr.

The prediction of the transient response of the outlet temperature, subject to a time-varying inlet temperature, is shown in Figure 5-68. It can be seen from this figure that the predicted transient characteristics of the packed bed at the exit closely resemble the measured characteristics at the exit.
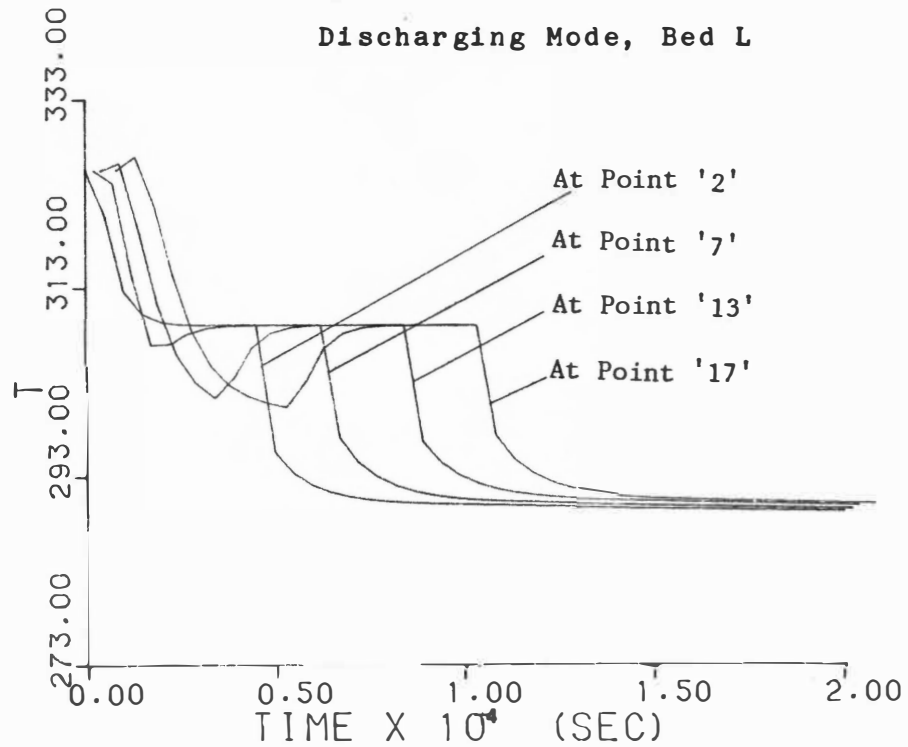
Figure 5-64. Transient Variation of Temperature at Center of Spherical Capsule (Analytical, Freezing Case), MF=558 Kg/hr
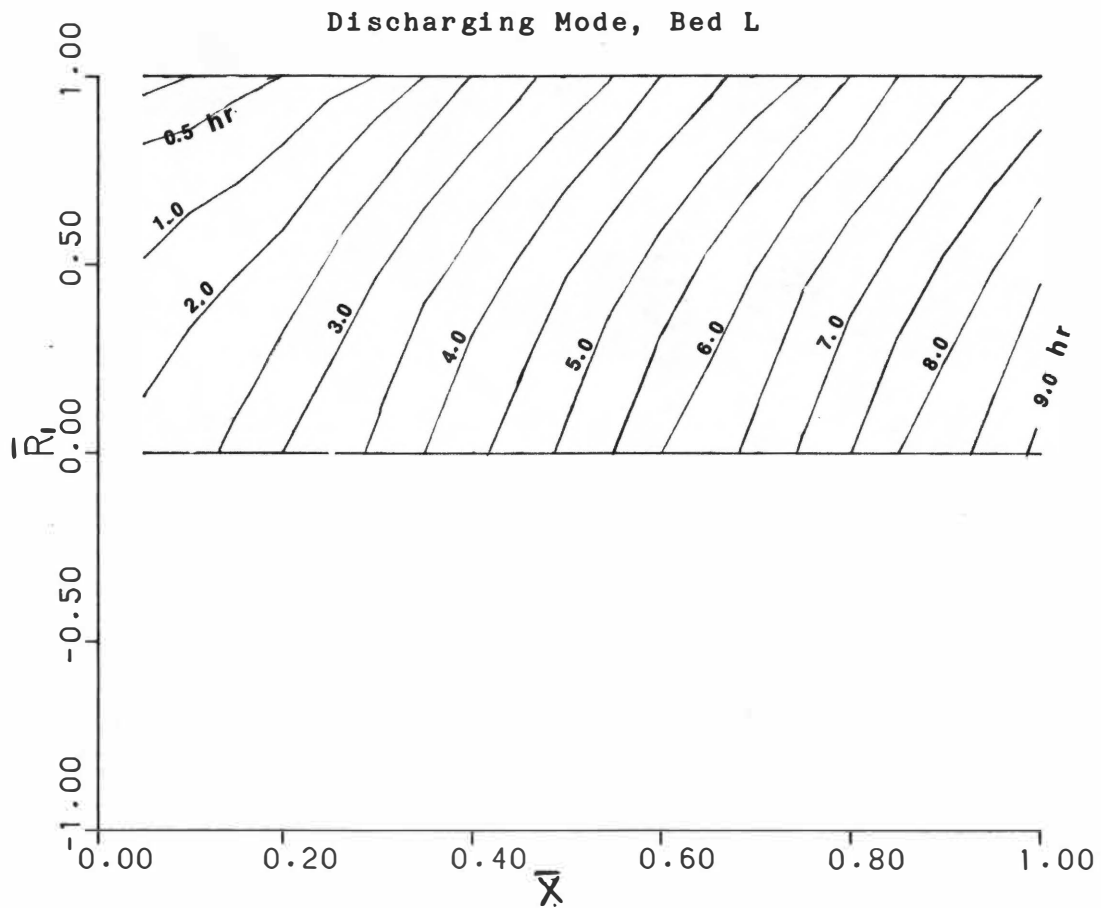
Figure 5-65. Variation of Location of Freezing Front with Distance
and Time, MF=119.9 Kg/hr

134
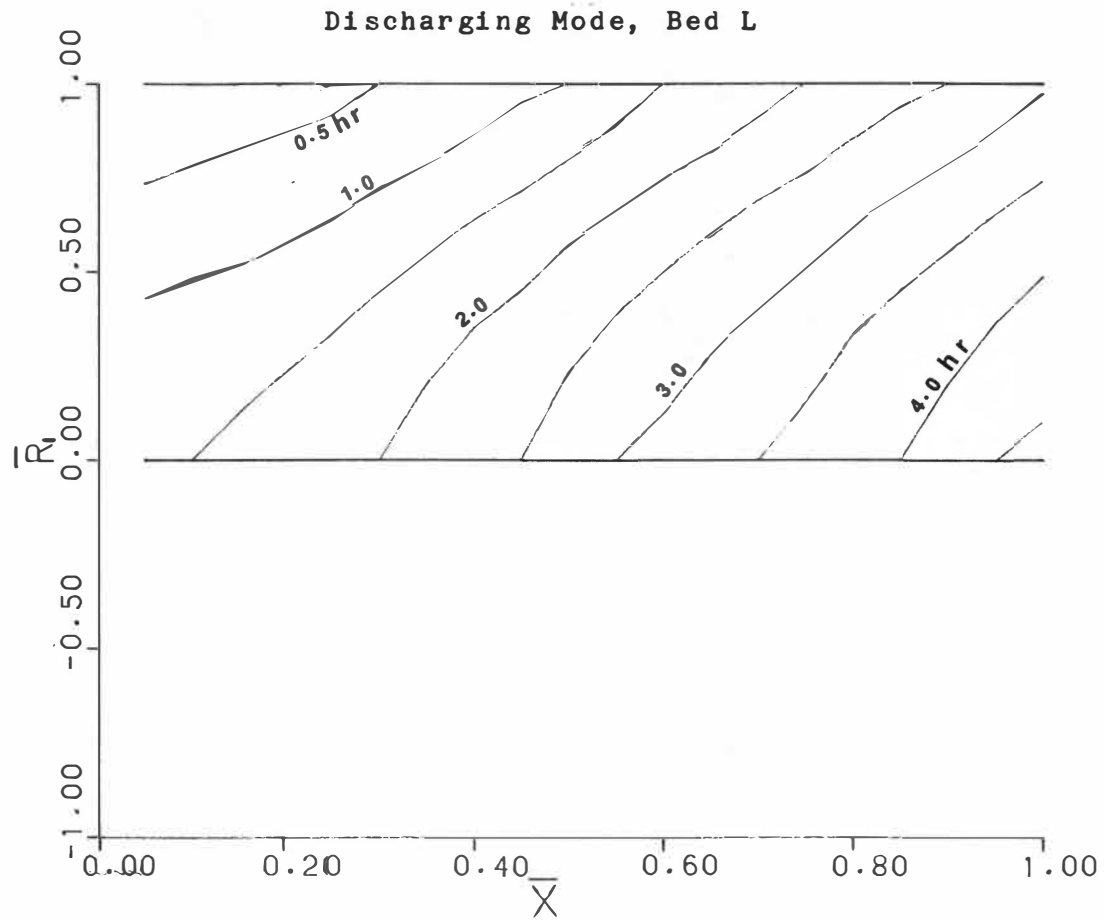
Figure 5-66. Variation of Location of Freezing Front with Distance and Time, MF=298.8 Kg/hr
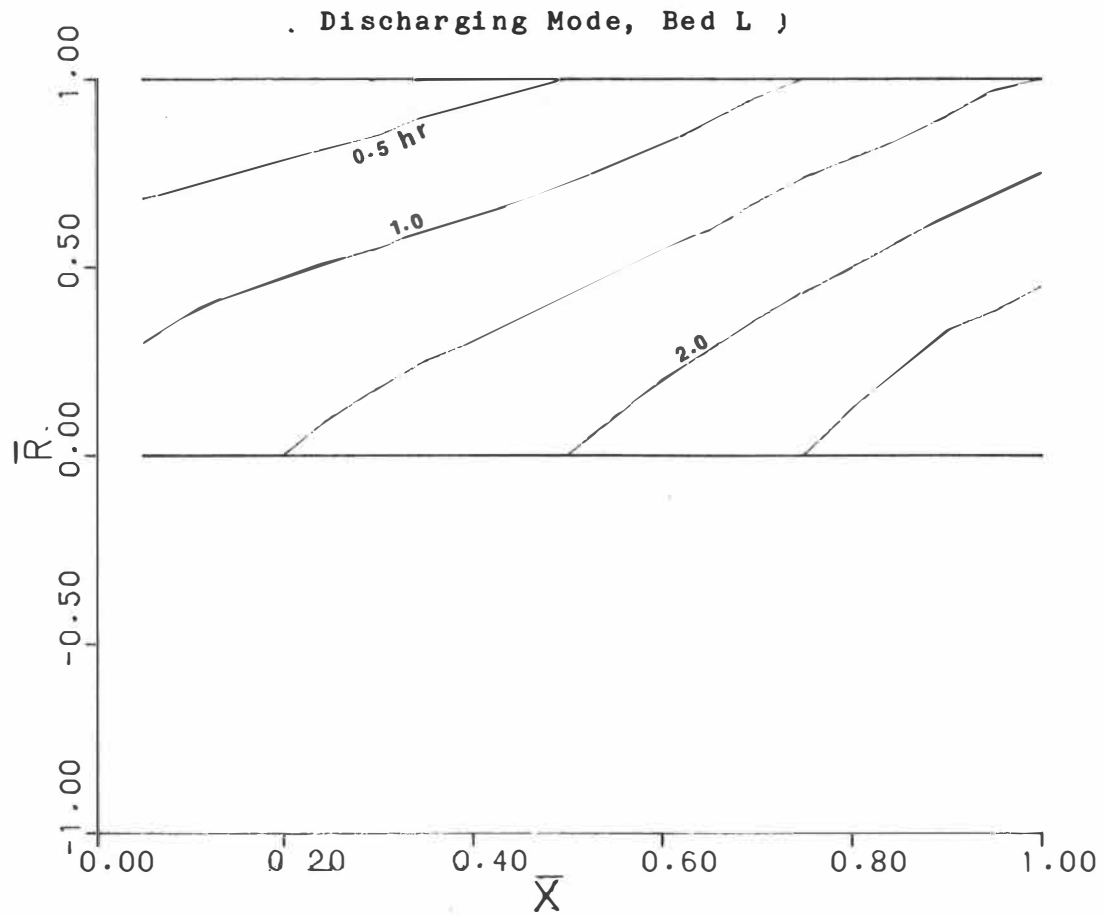
Figure 5-67.   Variation of Location of Freezing Front with Distance
and Time, MF=558 Kg/hr

Discharging Mode, Bed L
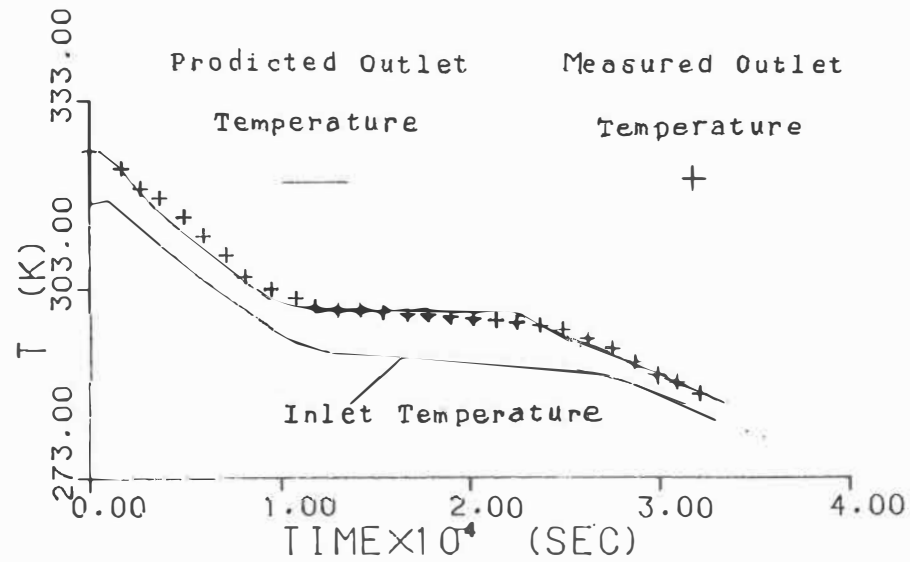
Figure 5-68. Variation of Inlet and Outlet Temperature History
(Freezing Case), MF=396 Kg/hr

(3) Results for the Packed Bed with the Working Fluid undergoing Phase Change

Figure 5-69 shows the relationship of the heat transfer coefficient between the two-phase working fluid and the thermal energy storage material to the thermodynamic quality based on Graves' experimental data for a 'bed S' configuration. The constants A and n of equation 3-13 were determined by using the least square curve fitting method and are equal to 14.687 and -0.184, respectively.

Figure 5-70 indicates the transient variation of thermodynamic quality of the two-phase working fluid with a Glauber salt as the thermal energy storage material. Figure 5-71 shows the location of the solidification front. Because the heat transfer coefficient between the working fluid and the capsules is very large, the solidification front moves rapidly. The curves in figure 5-71 are somewhat rough because of this relatively high speed.
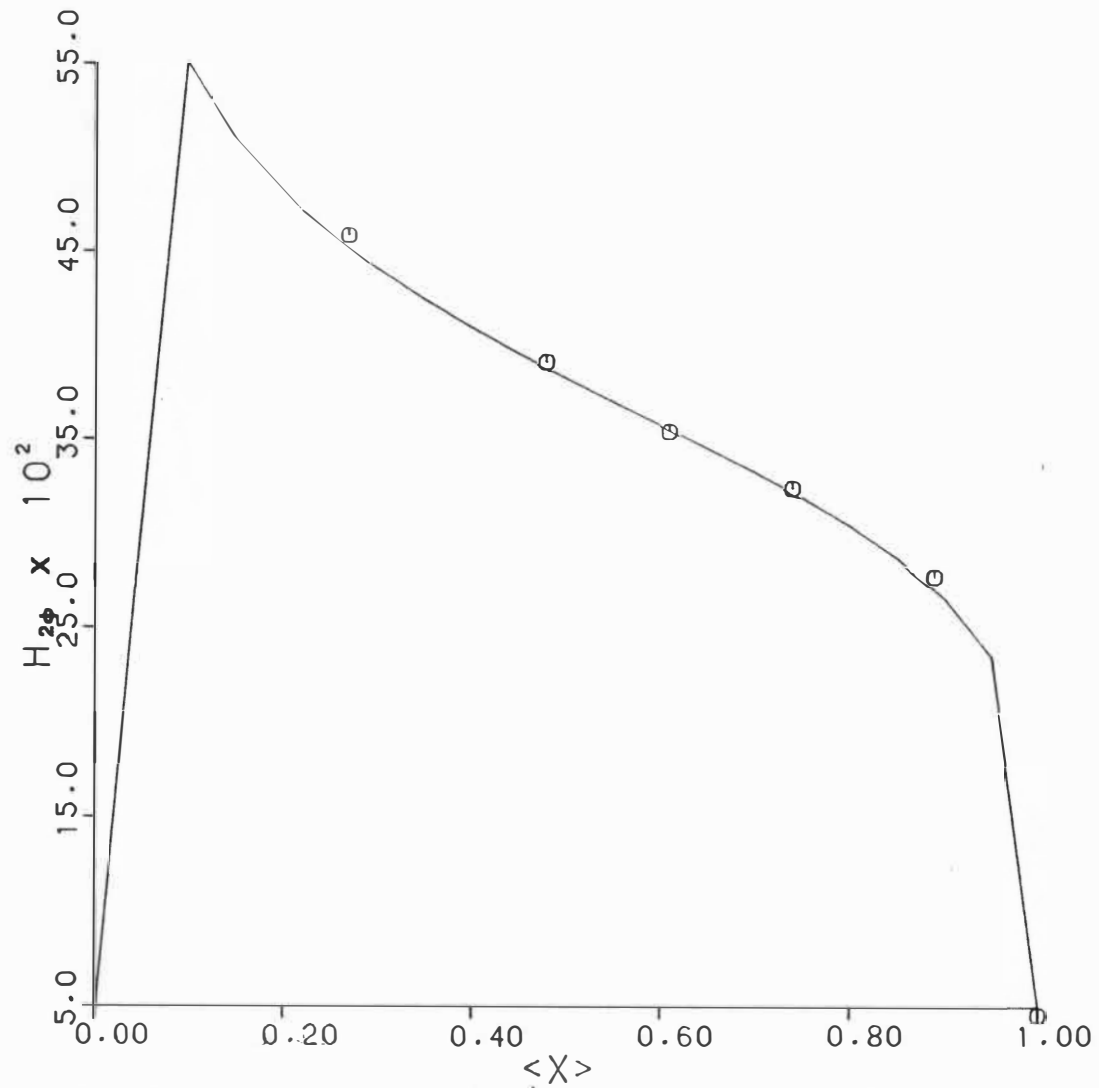
5-69 Heat Transfer Coefficient between Two-Phase
Working Fluid and Heat Storage Material versus
Thermodynamic Quality of Working Fluid(Boiling Case)
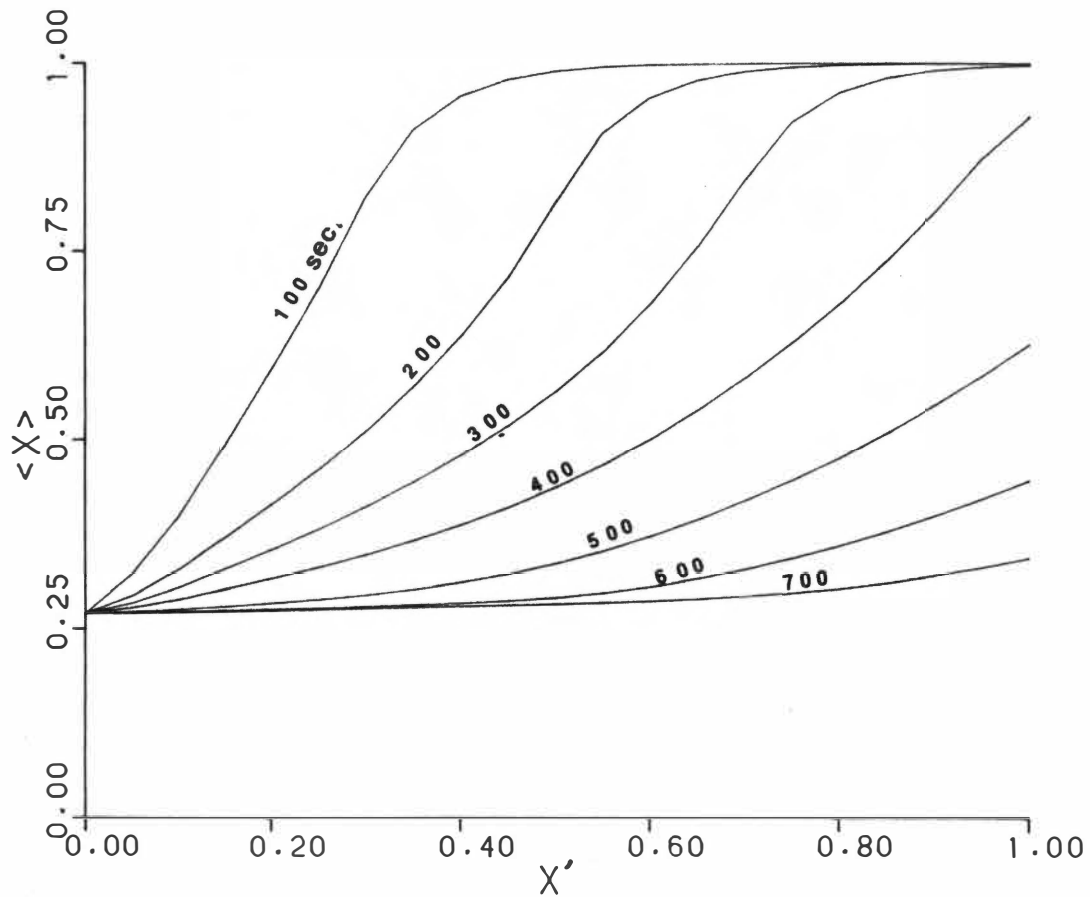
Figure 5-70. The Transient Variation of Thermodynamical Quality
of Two-Phase Working Fluid in Packed Bed.
(Latent Heat Storage, Boiling Case), MF=88.72 Kg/hr
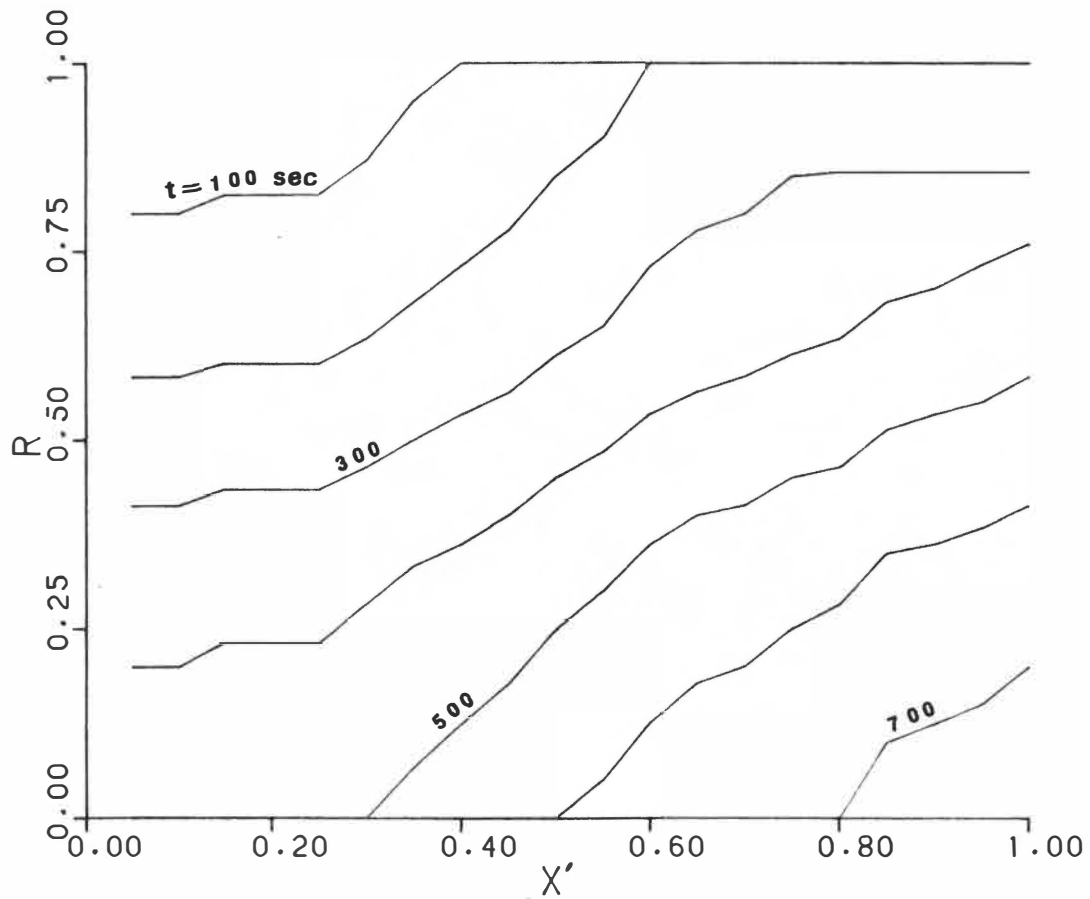
Figure 5-71.   The Location of Solidification Front in Packed Bed
(Latent Heat Storage, Boiling Case),MF=88.72 Kg/hr

CHAPTER   6

CONCLUSIONS

In order to predict the thermal performance of sensible heat and latent heat storage packed beds, two models designated as second-order and first-order were developed in this study. Both of the models take the intraparticle conduction into consideration, but the effect of the dispersion in the fluid in the axial direction is considered only in the second-order model. It has been shown that the second-order model is in good agreement with published experimental data by Saitoh and Kirose [37], and in fact, is significantly better than results of previous analyses reported in the literature. In addition, an improved exiting fluid temperature boundary condition used in the present work provides a more physically meaningful description of the exit condition for the bed.

Compared with the second-order model, the major advantage of the first order model is simplicity, but this model gives less accurate results, particularly at low Peclet number. For Peclet number larger than 200, however, the outlet working fluid non-dimensional temperature difference between the first and second-order

models is less than 10% for the beds and operating parameters considered in the present study. For Peclet number larger than 1000, the results from the first-order model gave a very good coincidence with the unpublished data of sensible heat storage previously obtained by researchers at the University of Tennessee.

The effects of subcooling, superheating, and supercooling of the PCM has been included in the computer simulation of this study, and good agreement between the results of the computer simulation and the experimental data has been found where these effects are existant.

An outstanding new feature of the present numerical method lies in tracking the entire bed phase change interface for both the charging and discharging modes. As a natural result of this method, the so-called "melting/freezing gradient" lines were determined. These results are helpful in the design of a latent heat storage packed bed, particularly with regard to estimating the energy stored or withdrawn from the bed. Specifically, these results are useful in making compromise design choices of parameters such as flowrate, size of the bed, heat storage materials, etc.

Typical computations of thermal performance of the packed bed with a phase-change working fluid have been carried out. The very high heat transfer coefficient between the two-phase working fluid and the thermal energy storage material results in short charging and discharging times of the packed bed. In order to make full use of the latent heat of the two-phase working fluid, the packed bed should either have a large heat capacity or utilize a very small flowrate of the two-phase working fluid.

LIST OF REFERENCES

146

LIST OF REFERENCES

[1] Schmidt, F.W., Willmott, A. J., "Thermal Energy Storage and Regeneration," Hemisphere, New York, 1981.

[2] Beghi, G., "Thermal Energy Storage," D. Reidel Publishing Company, 1981.

[3] Steemers,T.C., "A Review on The R and D on Heat Storage in The European Solar Energy Programme," International Conference on Energy Storage, Brighton, UK, April 29-May 1, 1981.

[4] MacCracken, C.D., "PCM Bulk Storage," International Conference on Energy Storage, Brighton, UK, April 29-May 1, 1981.

[5] Ergun, Sabri, "Fluid Flow Through Packed Bed Columns," Chemical engineering Progress, Vol.48,No.2, 1952, pp 89.

[6] MacDonald,I.F., El-Sayed,M.S., Mow,K., and Dullien,F.A.L., "Flow Through Porous Media - The Ergun Equation Revisited," Ind.Engng. Chem.Fundam.,18,No.3, 1979, pp 199.

[7] Ranz,W.E., "Friction and Transfer Coefficients for Single Particles and Packed Beds," Chem. Engng Prog., No.5, 1952, PP46.

[8] Kusik,C.L., and Happel,J., "Boundary Layer Mass Transport with eterogeneous Catalysis," AIChE J.,8, 163 (1962).

[9] Galloway, T.R. and Sage, B.H., "A model of the Mechanism of Transport in Packed Distended and Fluidized Beds," Chem.Engng Sci., 25, 1970, pp 495.

[10] Gauvin, W.H. and Katta, S., "Momentum Transfer Through Packed Beds of Various Particles in the Turbulent Flow Regime," AIChE J., Vol.19, No.4, July, 1973, pp 775.

[11] King,R. and Burns,A.P., "Sensible Heat Storage in Packed Beds," International Conference on Energy Storage, Brighton, UK, April 29-May 1.1981.

[12] Stanek, V. and Szekely, J., "The Effect of Non-Uniform Porosity in Causing Flow Maldistributions in Isothermal Packed Beds," Can. J. Chem. Engng, 50,1972, pp 9.

[13] Stanek, V. and Szekely, J., "Flow Maldistribution in Two Dimensional Packed Beds--- Part II: The Behavior of non-Isothermal Systems," Can. J. Engng, 51, 1973, pp 22.

[14] Stanek, V. and Szekely, J., "Three-Dimensional Flow of Fluids Through Non-Uniform Packed Beds," AIChE J., 27, No.5, 1981, pp 705.

[15] Barker, J.J., "Heat Transfer in Packed Beds," Ind.Engng Chem., 57,No.4, 1965, pp 43.

[16] Mickley, H.S. and Smith, K.A., "Fluid Flow in Packed Beds," Chem. Engng Sci. 20,1965, pp 237.

[17] Handley, D. and Heggs, P.J., "Momentum and Heat Transfer Mechaniisms in Regular Packings," Trans. Instn Chem. Engrs, 46, 1968.

[18] Schumann, T.E.W., "Heat Transfer: A Liquid Flowing Through A Porous Prism," J. Franklin Inst., 208, 1928, pp 405.

[19] Beasley, D.E. and Clark, J.A., "Transient Response of A Packed Bed for Thermal Energy Storage," ASME Paper 83-WA-SOL-4, 1983.

[20] Kulakowski, B.T. and Schmidt, F.W., "Design of A Packed Bed Thermal Storage Unit for A Solar System," J. Solar Energy Engng, 104, 1982, pp 223.

[21] Dunkle, R.V. and Ellul, W.M.J., "Ramdomly-Packed Particulate Bed Regenerators and Evaporative coolers," Mech. Chem. Engng Transactions, Nov. 1972.

[22] Zabrodsky, S.S., "Hydrodynamics and Heat Transfer in Fluidized Beds," M.I.T. Cambridge, Massachusetts and London, England. pp 180.

[23] Yagi,S. and Kunii,D., "Studies on Heat Transfer Near Wall Surface in Packed Beds," AIChE J., 6, No.1,1960, pp 97.

[24] Benenati, R.F. and Brosilow, C.B., "Void Fraction Distribution in Beds of Spheres," AIChE J., 8,No.3, 1962, pp 359.

[25] Longwell, P.A., "A Graphical Method for Solution of Freezing Problems," AIChE J., Vol.4, NO.1, 1958, PP53.

[26] Murry, W.D. and Landis, F., "Numerical and Machine Solutions of Transient Heat-Conduction Problems Involving Melting or Freezing. Part 1- Method of Analysis and Sample Solutions," Transactions of ASME, May, 1959, PP108.

[27] Sunderland, J.E. and Grosh, R.J., "Transient Temperature in a Melting Solid," Transaction of ASME,, Nov. 1961, PP410.

[28] Hsiao, J.S., "An Efficient Algorithm for Finite Difference Analyses of Heat Transfer with Melting and Solidification," ASME paper 84-WA/HT-42.

[29] Tao, L.C., "Generalized Numerical Solutions of Freezing a Saturated Liquid in Cylinders and Spheres," AIChE J. 13, No.1, 1967, pp 165.

[30] Siegel, R., "Solidification of Low Conductivity Material Containing Dispersed High Conductivity Particles," Int.J. HeatMass Transfer, 20, 1977, pp 1087.

[31] Solomon, A.D., "On the Melting Time of a Simple Body with a Convection Boundary Conduction," Letters in Heat Mass Transfer, 7, 1980, pp 183.

[32] Ku, J.Y. and Chan S.H., "A Systematic Approach to the Exact Solutions of Some Phase-change Problems," ASME paper 84-HT-1.

[33] Marianowski, L.G. and Maru, H.C., "Latent heat Thermal Energy Storage Systems above 450 C," 12th IECEC 779090, pp 555.

[34] Lou, D.Y.S., "Solidification Process in a Glauber Salt Mixture," Solar Energy, 30, No.2, 1983, pp 115.

[35] Abe, Y., Takahashi, Y., Sakamoto,R., Kalari, K., and Ozawa, T., "Charge and discharge Characteristics of a Direct Contact Latent Thermal Energy Storage Unit Using Form-Stable High Density Polyethylene," ASME-JSME Thermal Engineering Joint Conference Proceedings, Honolulu, Hawaii, March, 1983, PP20-24.

[36] Wood, R.J., Gladwell, S.D., O'Callaghan, P.W., and Probert, S.D., "Low Temperature thermal Energy Storage Using Packed Beds of Encapsulated Phase-change Materials," International Conference on Energy Storage, Brighton, UK, April 29-May 1, 1981.

[37] Saitoh, T. and Kirose,K., "High-Performance Phase-Change Thermal Energy Storage Using Spherical Capsules," ASME Paper 84-HT-8.

[38] Lahey, R.T. and Moody, F.J., "The Thermal-Hydraulics of a Boiling Water Nuclear Reactor," Publishd by The American Nuclear Society, Hinsdale, Illinois 60521,USA.

[39] Collier, J.G., "Convective Boiling Condensation," McGraW-Hill Book Company, 1972.

[40] Beyer, W. H., "Standard Mathematical Tables", 25th Edition, CRC Press.

[41]Yang,J.W.,"Laminar Film Condensation on a Sphere," J. Heat Transfer, May 1973,PP 174.

[42] Kutateladze, S.S., Gogonin,N.I., Dorokhov, A.R., and Sosunov, V.I., " Film Condensation of Flowing Vapor on a Bundle of Plain Horizontal TUbes," Thermal Engng, 26 (5),1979.

[43]Rubenstein, L.I.,"The Stefan Problem" Vol.27, Translations of Mathematical Monographs, Vol.27, American Mathematical Sociaty.

[44]Ozisik, M.N., "Heat Conduction" John Wiley and Sons Inc.

[45]Graves, A.G., "Transient Thermal Performance of an Experimental Packed Bed Thermal Energy Storage System," M.S.Thesis, University of Tennessee.

APPENDICES

APPENDIX A

DEVELOPMENT OF THE GOVERNING EQUATIONS
FOR THE SINGLE-PHASE WORKING FLUID IN PACKED BED

The governing equations for the working fluid in a packed bed of spherical particles that accounts for dispersion effects and the temperature gradients in both axial and radial directions can be obtained by performing an energy balance on an incremental fluid control volume of length /x and a radial thickness /r. The rate of energy entering the incremental volume is equal to the rate of energy leaving the volume plus the rate of energy accumulated within the fluid in the incremental volume and rate of energy absorbed by the thermal energy storage material.

In order to form the energy balance for the fluid passing through the incremental control volume, (refer to figure A-1) the following expressions are useful,

1. The energy entering the control volume during / t is

$$\left[\frac{M_f \cdot C_f}{S_{fr}} \cdot T_f^{'} \cdot 2\pi r \cdot \Delta r \cdot \Delta t \right]_x + \left[-K_f^x \cdot \varepsilon \frac{\partial T_f^{'}}{\partial x} \cdot 2\pi r \cdot \Delta r \cdot \Delta t \right]_x$$

$$+ \left[-K_f^r \cdot \varepsilon \cdot \frac{\partial T_f^{'}}{\partial r} \cdot 2\pi r \cdot \Delta x \cdot \Delta t \right]_x$$
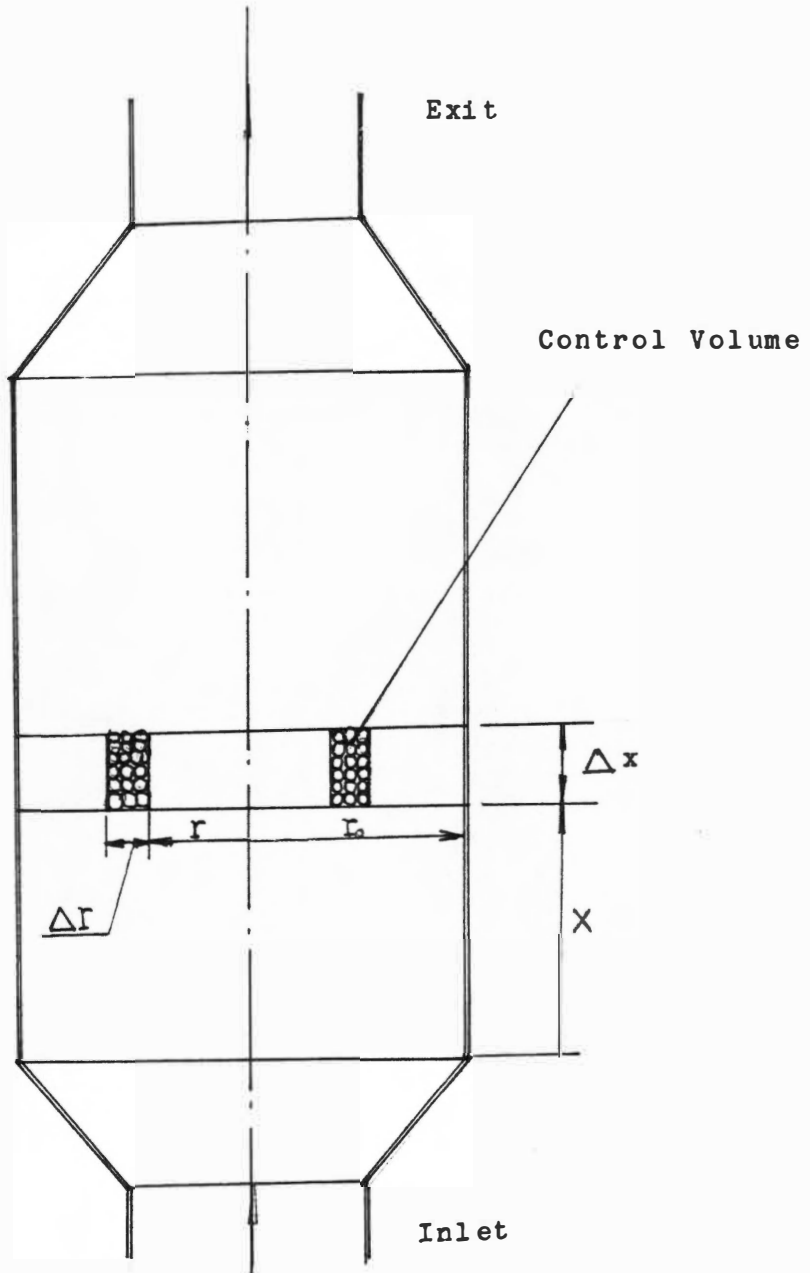
Figure A-1.   Schematic Diagram of Heat Storage Packed Bed

2. The energy leaving the control volume during time $\triangle$t is

$$\left[\frac{M_f \cdot C_f}{S_f} \cdot T_f' \cdot 2\pi r \cdot \Delta r \cdot \Delta t \right]_{x + \Delta x}$$

$$+ \left[-K_f^x \cdot \varepsilon \cdot \frac{\partial T_f'}{\partial x} \cdot 2\pi r \cdot \Delta r \cdot \Delta t \right]_{x + \Delta x}$$

$$+ \left[-K_f^R \cdot \varepsilon \cdot \frac{\partial T_f'}{\partial r} (2\pi r + \Delta r) \cdot \Delta x \cdot \Delta t \right]_{r + \Delta r}$$

3. The energy accumulated by the fluid in the control volume during $\triangle$t is

$$\left[C_f \cdot \rho_f \cdot \varepsilon \cdot 2\pi r \cdot \Delta r \cdot \Delta x \cdot T_f' \right]_{t + \Delta t}$$

$$- \left[C_f \cdot \rho_f \cdot \varepsilon \cdot 2\pi r \cdot \Delta r \cdot \Delta x \cdot T_f' \right]_{t}$$

4. The energy absorbed by the heat storage material in the control volume during $\triangle$t is

$$\frac{hA}{S_{fr} \cdot Lu} (T_f' - T_{sur}') \cdot 2\pi r \cdot \Delta r \cdot \Delta x \cdot \Delta t$$

Now the first law of thermodynamics applied to the control volume is

$$
\begin{bmatrix} \text{Energy entering} \\ \text{Control Volume} \\ \text{during } \triangle t \end{bmatrix} + \begin{bmatrix} \text{Energy exiting} \\ \text{Control Volume} \\ \text{during } \triangle t \end{bmatrix} = \begin{bmatrix} \text{Energy accumulated} \\ \text{in Control Volume} \\ \text{during } \triangle t \end{bmatrix}
$$

$$\text{(A-1)}$$

Substituting the preceding expressions into the equation above and simplifying yields the follow governing equation in general forms

$$
K_f^x \cdot \varepsilon \cdot \frac{\partial^2 T_f'}{\partial x^2} - \frac{M_f \cdot C_f}{S_{fr}} \cdot \frac{\partial T_f'}{\partial x} - K_f^R \cdot \varepsilon \cdot \left(\frac{\partial^2 T_f'}{\partial r^2} + \frac{1}{R} \frac{\partial T_f'}{\partial r} \right)
$$

$$
- \rho_f \cdot C_f \cdot \varepsilon \cdot \frac{\partial T_f'}{\partial t} - \frac{hA}{S_{fr} \cdot Lu} \cdot (T_f' - T_{sur}') = 0 \qquad \text{(A-2)}
$$

The boundary conditions are

$$
T_f' = T_{fi}' \qquad\qquad at \quad x = 0
$$

$$
\frac{\partial T_f'}{\partial x} = 0 \qquad\qquad at \quad x \rightarrow \infty
$$

$$
\frac{\partial T_f'}{\partial r} = 0 \qquad\qquad at \quad r = 0
$$

$$h_w \cdot (T_f{}' - T_{sur}{}') = -K_w \cdot \left. \frac{\partial T_w{}'}{\partial r} \right|_{r=r_o} \qquad\qquad at\ r = r_o$$

and the initial condition is

$$T_f{}' = T_o{}'(x) \qquad\qquad at\ \ t = 0$$

Equation (A-2) can be non-dimensionalized and becomes

$$\frac{1}{PE} \frac{\partial^2 T_f}{\partial X^2} - \frac{\partial T_f}{\partial X} - \frac{\partial T_f}{\partial \eta} - (T_f - T_{sur}) + \kappa \left(\frac{1}{\bar{r}} \frac{\partial T_f}{\partial \bar{r}} + \frac{\partial^2 T_f}{\partial \bar{r}^2} \right) = 0 \qquad\qquad (A-3)$$

in terms of the following non-dimensional parameters

$$X = \frac{hA \cdot x}{M_f \cdot C_f \cdot Lu}$$

$$\eta = \frac{h \cdot A \cdot t}{S_{fr} \cdot \rho_f \cdot C_f \cdot Lu \cdot \varepsilon}$$

$$\bar{r} = \frac{r}{r_o}$$

$$T_f = \frac{T_f{}' - T_o{}'}{T_{fi}{}' - T_o{}'}$$

$$\kappa = \frac{\varepsilon \cdot \ K_f^R \cdot \ Lu \cdot \ S_{fr}}{h \, A \, R_o}$$

$$PE = \frac{(\rho_f \ V_f \ C_f)^2 \ S_{fr} \ Lu \cdot \ \varepsilon}{h \cdot A \cdot K_f^x}$$

For most residential applications, the wall of the heat storage packed bed is well-insulated outside. Even so, the bed wall may still absorb a significant amount of thermal energy, but this usually will not markedly influence the temperature in the bed in the radial direction. Tables A-1 and A-2 list some experimental data of A.G.Graves [45] for the charging mode. The flowrates are 0.25 and 4.0 GPM for Table A-1 and Table A-2, respectively. In these tables point 2 is at the centerline, whereas point 1 and point 3 are one inch from the wall, on either side of the centerline.

TABLE A-1 Experimental Bed Temperature for 'Bed S'
during Charging at Flowrate of 0.25 GPM,
(Ti-To)=45, From [45]

Time(min)	Temperature(F)		
	point 1	point 2	point 3
0.0	82.5	82.5	82.5
10.4	88.6	88.4	88.5
20.8	105.9	105.8	106.0
31.2	115.1	115.0	115.0
41.6	119.5	119.5	119.5
52.0	122.2	122.1	122.2
62.4	124.5	124.5	124.5

TABLE A-2 Experimental Bed Temperature for 'Bed S'

during Charging at Flowrate of 4.0 GPM,

(Ti-To)=40 F, From Graves [45]

Time(min)	Temperature(F)		
	point 1	point 2	point 3
0.0	86.3	86.5	86.7
2.6	114.6	115.9	114.8
5.2	117.7	118.2	117.7
7.8	119.0	119.3	119.1
10.4	119.8	120.1	119.9
13.0	120.1	120.2	120.1

From the experimental data in Tables A-1 and A-2, the assumption of uniform temperature in the bed radial direction appears reasonable, at least for the cases investigated by Graves (op.cit.).

Neglecting the radial temperature gradient, the governing equation (A-2) becomes

$$\frac{1}{PE} \frac{\partial^2 T_f}{\partial X^2} - \frac{\partial T_f}{\partial X} - \frac{\partial T_f}{\partial \eta} - (T_f - T_{sur}) = 0 \qquad \text{(A-4)}$$

with the boundary conditions

$$T_f = T_{fi}(\eta) \qquad \qquad at \quad X = 0$$

$$\frac{\partial T_f}{\partial X} = 0 \qquad \qquad at \quad X \to \infty$$

and initial condition

$$T_f = T_o(X) \qquad \qquad at \quad \eta = 0$$

APPENDIX B

GOVERNING EQUATIONS FOR THE PHASE-CHANGE THERMAL
ENERGY STORAGE MATERIAL

The transient response of a latent heat storage packed bed is governed not only by the energy balance equation for the working fluid but also by the transient energy equations for the heat storage material and the conservation of energy equation at the phase change interface. The energy equations for the phase change material are welll known and are

Liquid region:

$$\rho_l \cdot C_l \frac{\partial T_l'}{\partial t} = K_l \cdot \left(\frac{\partial^2 T_l'}{\partial R^2} + \frac{2}{R} \frac{\partial T_l'}{\partial R} \right) \qquad (B-1)$$

Solid region:

$$\rho_s \cdot C_s \cdot \frac{\partial T_s'}{\partial t} = K_s \cdot \left(\frac{\partial T_s'}{\partial R} + \frac{2}{R} \frac{\partial T_s'}{\partial R} \right) \qquad (B-2)$$

The equation of conservation of energy at the phase change interface is

$$\rho_l \cdot L \cdot \frac{\partial R^*}{\partial t} = -K_l \left. \frac{\partial T_l'}{\partial R} \right|_{R = R^*} + K_s \cdot \left. \frac{\partial T_s'}{\partial R} \right|_{R = R^*} \qquad (B-3)$$

or

$$\rho_s \cdot L \cdot \frac{\partial R^*}{\partial t} = -K_s \cdot \left. \frac{\partial T_s'}{\partial R} \right|_{R=R^*} + K_l \cdot \left. \frac{\partial T_l'}{\partial R} \right|_{R=R^*} \tag{B-4}$$

It is helpful to introduce the following new dimensionless parameters

$$STe = \frac{C_l \cdot (T_m' - T_o')}{L}$$

$$\eta = \frac{K_l \cdot (T_m' - T_o) \cdot t}{R_o^2 \cdot \rho_l \cdot L}$$

$$\overline{R} = \frac{R}{R_o}$$

$$\zeta_1 = \frac{\rho_s \, C_s \, K_l}{\rho_l \cdot C_l \cdot K_s}$$

$$\zeta_2 = \frac{K_s}{K_l}$$

$$\zeta_3 = \frac{\rho_l K_s}{\rho_s K_l}$$

which allow the equations (B-1),(B-2),(B-3), and (B-4) to be simplified to the following non-dimensional forms, respectively

$$STe \cdot \frac{\partial T_l}{\partial \overline{\eta}} = \frac{\partial^2 T_l}{\partial \overline{R}^2} + \frac{2}{\overline{R}} \frac{\partial T_l}{\partial \overline{R}} \tag{B-5}$$

$$STe \cdot \frac{\partial T_s}{\partial \overline{\eta}} = \zeta_1 \cdot \left(\frac{\partial^2 T_s}{\partial \overline{R}^2} + \frac{2}{\overline{R}} \frac{\partial T_s}{\partial \overline{R}} \right) \tag{B-6}$$

$$\frac{\partial \overline{R}^*}{\partial \overline{\eta}} = - \left. \frac{\partial T_l}{\partial \overline{R}} \right|_{\overline{R} = \overline{R}^*} + \zeta_2 \cdot \left. \frac{\partial T_s}{\partial \overline{R}} \right|_{\overline{R} = \overline{R}^*} \tag{B-7}$$

$$\frac{\partial R^*}{\partial \overline{\eta}} = -\zeta_3 \left. \frac{\partial T_s}{\partial \overline{R}} \right|_{\overline{R} = \overline{R}^*} + \frac{\zeta_3}{\zeta_2} \cdot \left. \frac{\partial T_l}{\partial \overline{R}} \right|_{\overline{R} = \overline{R}^*} \tag{B-8}$$

The boundary conditions are

at the center

$$\frac{\partial T}{\partial R} = 0 \qquad\qquad \overline{R} = 0$$

at point 1

$$T_1 = \frac{0.719 \dfrac{K_p}{K_c} \cdot T_{sur}}{\dfrac{1}{E} + 0.719 \cdot \dfrac{K_p}{K_c}}$$

and the initial condition is

$$T_f = T_o(x) \qquad\qquad at\ \eta = 0$$

APPENDIX C

THE GOVERNING EQUATIONS FOR THE PACKED BED
WITH BOTH WORKING FLUID AND HEAT STORAGE MATERIAL
UNDERGOING PHASE-CHANGE

The temperature of the working fluid passing through the packed bed remains constant in the saturation regime if the effect of the pressure drop on the temperature is ignored. The governing equation of the working fluid can be obtained by applying an energy balance on the fluid within the incremental volume with the assumption of no radial gradient of thermodynamic quality. This yields

$$M_f \cdot L_f \cdot \frac{\partial <x>}{\partial x} + \rho_f \cdot L_f \cdot S_{fr} \cdot \varepsilon \cdot \frac{\partial <x>}{\partial t} + \frac{hA}{Lu}(T_f' - T_{sur}') = 0$$

$$(C-1)$$

introducing following non-dimensional variables

$$X' = \frac{h \cdot A \cdot X \cdot (T_m' - T_o')}{M_f \cdot L_f \cdot Lu}$$

$$\eta' = \frac{hA \cdot t (T_m' - T_o')}{\rho_f \cdot L_f \cdot S_{fr} \cdot Lu \cdot \varepsilon}$$

$$T = \frac{T_f' - T_m'}{T_o' - T_m'}$$

the equation (C-1) can be non-dimensionalized and becomes

$$\frac{\partial <x>}{\partial X'} + \frac{\partial <x>}{\partial \eta'} + (T_f - T_{sur}) = 0 \qquad\qquad\text{(C-2)}$$

with the boundary condition

$$<x> = <x>_i (\eta') \qquad\qquad X' = 0$$

and the initial condition

$$<x> = <x>_o (X') \qquad\qquad \eta' = 0$$

The governing equations for the phase-change heat storage material are the same as those given in appendix B.

APPENDIX   D

THE NUMERICAL EQUATIONS
FOR THE PHASE-CHANGE HEAT STORAGE MATERIAL

The purpose of this appendix is to develop the finite difference equations used in modelling the phase change heat storage material. With reference to figure (D-1), the moving boundary at a point in time is shown to be a fractional distance E $\triangle$R between the grid points i $\triangle$R and (i+1) $\triangle$R. The value of E is, of course, between 0 and 1. The figure identifies the points (i-1), i, and the boundary itself, as well as the corresponding temperatures T_{i-1} , T_i , and T_m on the boundary.

In the following sections, the problem is discussed for four different cases

(1)CASE 1:   2< i <20

(1.A) The travel Rate of the Moving Boundary

Forming a Taylor's series expansion about the temperature Tm at the moving boundary for each of the temperatures at the points on either side of the moving boundary yields:

$$T_{i-1} = T_m + (E+1)\Delta\overline{R} \left.\frac{\partial T}{\partial \overline{R}}\right|_{\overline{R}=\overline{R}^*} + \frac{(E+1)^2\Delta\overline{R}^2}{2!} \left.\frac{\partial^2 T}{\partial \overline{R}^2}\right|_{\overline{R}=\overline{R}^*} + 0\,(\Delta\overline{R}^3)$$
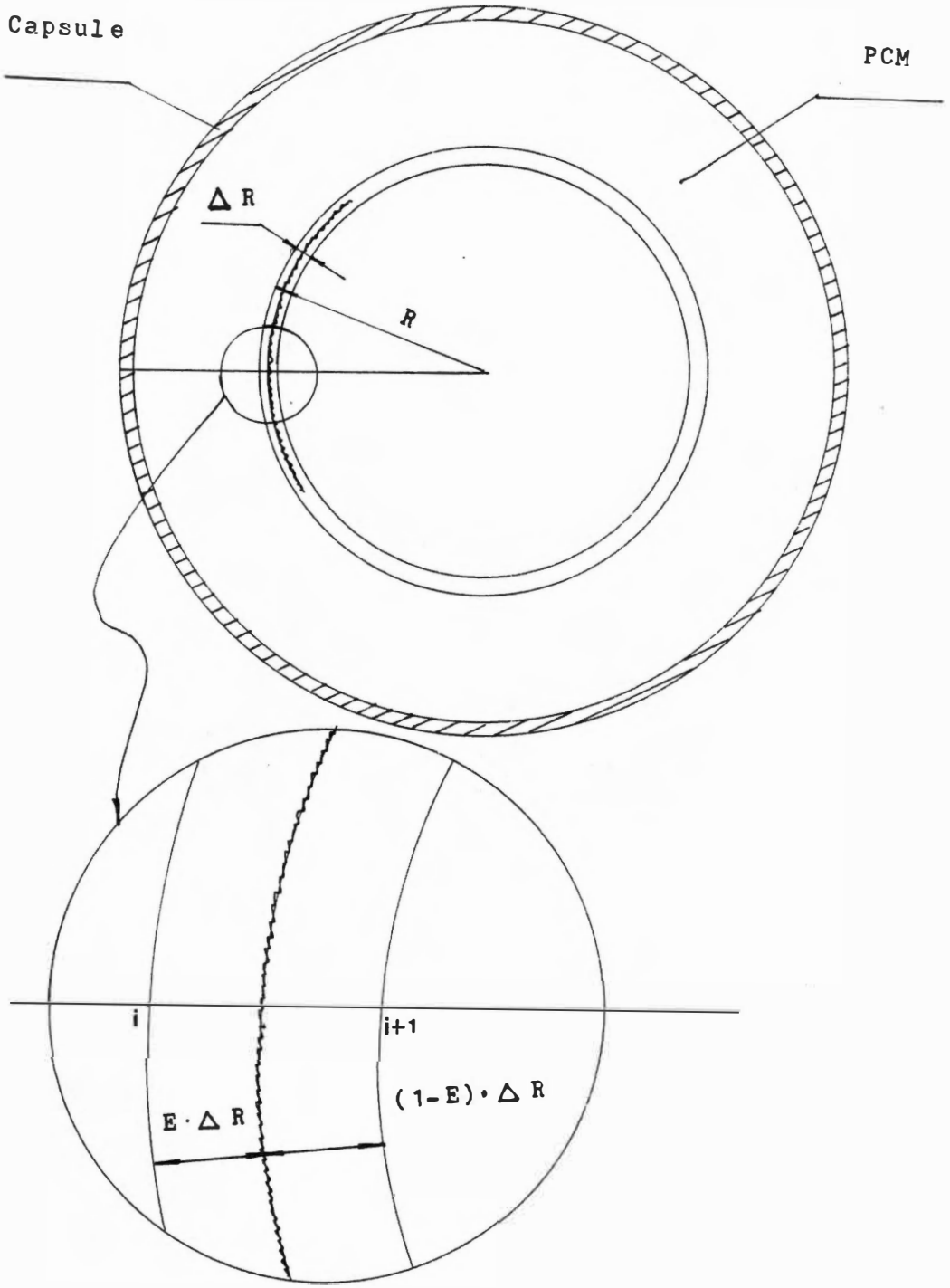
D-1. Schematic Diagram of Encapsulated PCM (CASE 1)

$$T_i = T_m + E \cdot \Delta \overline{R} \cdot \left. \frac{\partial T}{\partial R} \right|_{\overline{R} = \overline{R}^{\bullet}}^{-} + \frac{(E \cdot \Delta \overline{R})^2}{2!} \left. \frac{\partial^2 T}{\partial R^2} \right|_{\overline{R} = R^{\bullet}}^{-} + 0(\Delta \overline{R}^3)$$

$$T_{i+1} = T_m - (1 - E) \Delta \overline{R} \cdot \left. \frac{\partial T}{\partial \overline{R}} \right|_{\overline{R} = \overline{R}^{\bullet}}^{+} + \frac{(1 - E)^2 \Delta \overline{R}^2}{2!} \left. \frac{\partial^2 T}{\partial \overline{R}^2} \right|_{\overline{R} = \overline{R}^{\bullet}}^{+} + 0(\Delta \overline{R}^3)$$

$$T_{i+2} = T_m - (2 - E) \Delta \overline{R} \cdot \left. \frac{\partial T}{\partial \overline{R}} \right|_{\overline{R} = \overline{R}^{\bullet}}^{+} + \frac{(2 - E^2 \Delta \overline{R}^2}{2!} \left. \frac{\partial^2 T}{\partial \overline{R}^2} \right|_{\overline{R} = \overline{R}^{\bullet}}^{+} + 0(\Delta \overline{R}^3)$$

Using these expressions, the temperature gradient on each side of the moving boundary can be obtained. The left-side temperature gradient on the moving boundary thus obtained is

$$\left. \frac{\partial T}{\partial \overline{R}} \right|_{\overline{R} = \overline{R}^{\bullet}}^{+} = \frac{1}{\Delta \overline{R}} \left(- \frac{2 - E}{1 - E} T_{i+1} + \frac{1 - E}{2 - E} T_{i+2} \right) + 0(\Delta \overline{R}^2) \qquad \text{(D-1)}$$

The right-side temperature gradient on the moving boundary is

$$\left. \frac{\partial T}{\partial \overline{R}} \right|_{\Delta \overline{R}}^{-} = \frac{1}{\Delta \overline{R}} \left(\frac{E + 1}{E} T_i - \frac{E}{E + 1} T_{i-1} \right) \qquad \text{(D-2)}$$

By inserting the two temperature gradients given by (D-1) and (D-2) into equation (B-7), one obtains the following expression for the travel rate of the moving boundary

$$\frac{\partial E}{\partial \eta} = \frac{+1}{\Delta \overline{R}^2} \left[-\left(\frac{E+1}{E} T_i - \frac{E}{E+1} T_{i-1} \right) + \zeta_2 \left(\frac{2-E}{1-E} T_{i+1} \right. \right.$$

$$\left. \left. + \frac{1-E}{2-E} T_{i+2} \right) \right] + 0(\Delta \overline{R}) \tag{D-3}$$

THe finite difference form of above equation (D-3) has been shown in equation (4-4)

(1.B) The Temperature at Point i

Expanding the temperature at point (i-1) and that at the moving boundary with respect to the temperature at point i results in

$$T_{i-1} = T_i + \Delta \overline{R} \cdot \left. \frac{\partial T}{\partial \overline{R}} \right|_i + \frac{(\Delta \overline{R})^2}{2!} \left. \frac{\partial^2 T}{\partial \overline{R}^2} \right|_i + 0(\Delta \overline{R}^3)$$

and

$$T_m = T_i - E \cdot \Delta \overline{R} \left. \frac{\partial T}{\partial \overline{R}} \right|_i \frac{(E \cdot \Delta \overline{R})^2}{2!} \left. \frac{\partial^2 T}{\partial \overline{R}^2} \right|_i + 0(\Delta \overline{R}^3)$$

from these two equations, we obtain

$$\frac{\partial T}{\partial \overline{R}} \bigg|_i = \frac{1}{\Delta \overline{R}} \left(\frac{1-E}{E} T_i - \frac{E}{E-1} T_{i-1} \right)$$
(D-4)

and

$$\frac{\partial^2 T}{\partial \overline{R}^2} \bigg|_i = \frac{2}{\Delta \overline{R}^2} \left(\frac{1}{E} T_i + \frac{1}{E+1} T_{i-1} \right)$$
(D-5)

By inserting equations (D-4), and (D-5) into equation (3-4) one obtains

$$\frac{\partial T}{\partial \eta} \bigg|_i = \frac{2}{Ste \cdot \Delta \overline{R}^2} \left[\left[\frac{1}{E} + \frac{1-E}{(K-I)E} \right] T_i \right.$$

$$\left. + \left[\frac{1}{E+1} + \frac{E}{(K-I)(-E+1)} \right] T_{i-1} \right]$$
(D-6)

The finite difference form of equation (D-6), is shown as equation (4-3) in the body of this thesis.

(1.c) The Temperature at Point i+1

Using a similar procedure, we obtain

$$\frac{\partial T}{\partial \eta} \bigg|_{i+1} = \frac{2}{STe \cdot \Delta \overline{R}^2} \left[\left[\frac{1}{(2-E)} + \frac{(E-1)}{(k-i-1)(2-E)} \right] T_{i+2} \right.$$

$$\left. + \left[\frac{2}{E-1} + \frac{E}{(E-1)(K-i-1)} \right] T_{i+1} \right]$$
(D-7)

and the finite difference form of equation (D-7) is shown as equation (4-5).

(2)CASE 2:   i=1

In this case the melting /freezing front lies between point '1' and point '2' (see figure (D-2))

(2.A) The Velocity of the Moving Boundary

Assuming that the temperature profile between point '1' and the moving boundary is linear, the temperature gradient on the left hand side of the moving boundary is

$$\frac{\partial T}{\partial \overline{\overline{R}}}\Bigg|_{\overline{R}=\overline{R}^{\bullet}}^{+} = \frac{T_1}{E \cdot \Delta \overline{\overline{R}}} \tag{D-8}$$

the temperature gradient on the right hand side of the moving boundary can be obtained by substituting i=1 into equation (D-2), thus

$$\frac{\partial T}{\partial \overline{\overline{R}}}\Bigg|_{\overline{R}=\overline{R}^{\bullet}}^{-} = \frac{1}{\Delta \overline{\overline{R}}} \left(\frac{2-E}{1-E} T_2 - \frac{1-E}{2-E} T_3 \right) + 0 \, (\Delta \overline{R}^{\,2}) \tag{D-9}$$

By substituting equation (D-8) and (D-9) into equations (B-7) the expression for the speed of the moving boundary then becomes

$$\frac{\partial E}{\partial \overline{\overline{\eta}}}\Bigg|_{R=R^{\bullet}} = \frac{-1}{\Delta \overline{R}^{\,2}} \left[-\frac{1}{E} T_1 + \zeta_2 \left(\frac{2-E}{1-E} T_2 + \frac{1-E}{2-E} T_3 \right) \right] + 0 \, (\Delta \overline{R}) \tag{D-10}$$
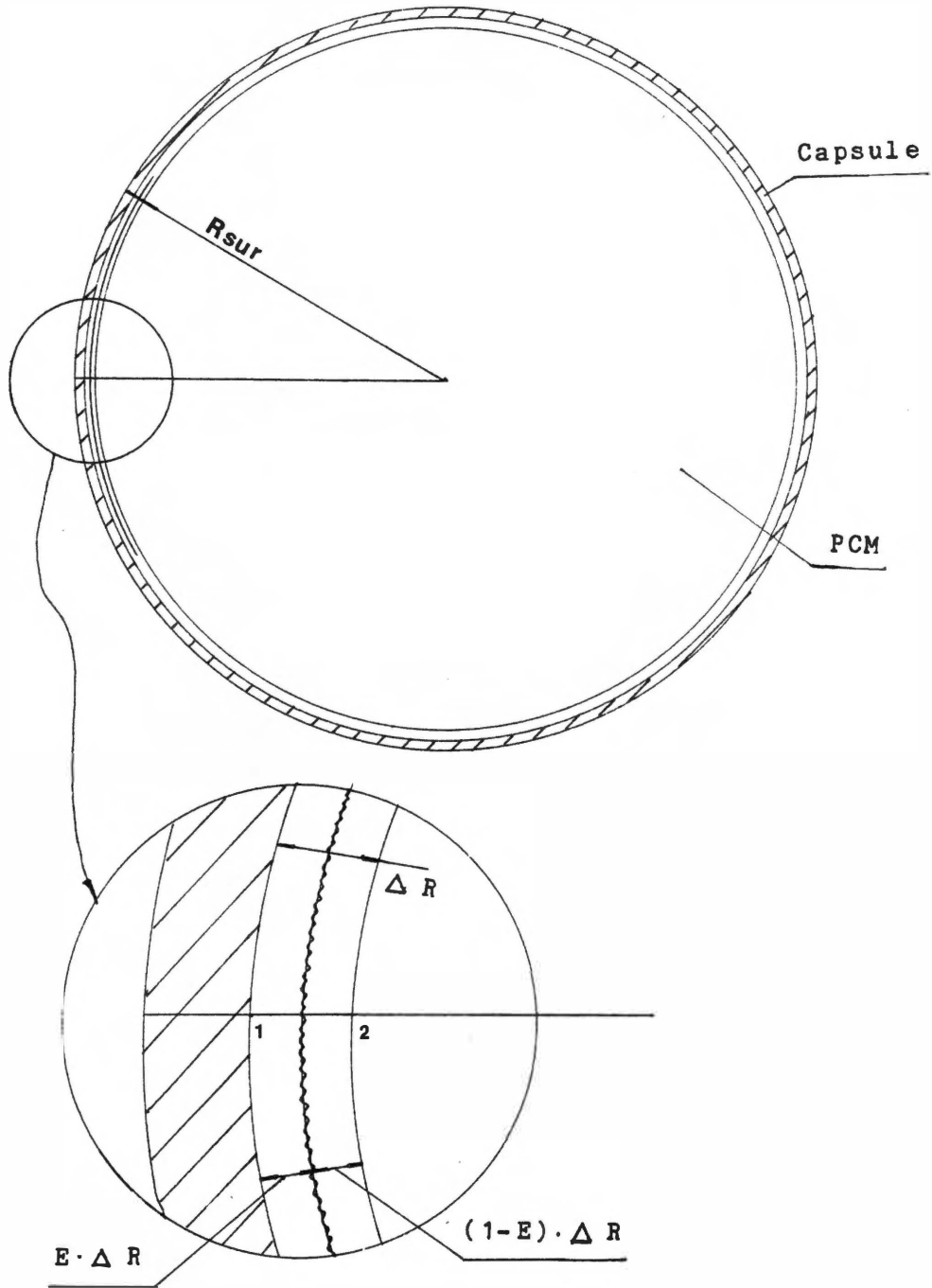
D-2. Schematic Diagram of Encapsulated PCM (CASE 2)

(2.B) The Temperature Gradient at Point 2

From the Taylor series expansion of temperature about point 2, the following expression for the non-dimensional derivative of temperature is obtained

$$\frac{\partial T}{\partial \overline{\eta}}\bigg|_{i=2} = \frac{2}{STe \cdot \Delta \overline{R}^2}\left[\left[\frac{1}{2-E} + \frac{1}{(k-2)} \cdot \frac{E-1}{2-E}\right]T_3 \right.$$

$$\left. + \left[\frac{2}{E-1} + \frac{E}{(E-1)(K-2)}\right]T_2\right] \tag{D-11}$$

(2.C) The Temperature at Point 1

From an energy balance on the capsule (see figure (D-2)) there results

$$T_1 = 0.719\left(\frac{K_p}{K_c}\right) \cdot T_{sur}/\left(\frac{1}{E} + 0.719\frac{K_p}{K_c}\right) \tag{D-12}$$

where the surface temperature of the capsule, which can be determined by the boundary condition at R=Rsur, is

$$T_{sur} = \frac{T_f + \dfrac{T_1}{(Bi)p \cdot \Delta \overline{\overline{R}}}}{1 + \dfrac{1.0}{(Bi)p \cdot \Delta \overline{\overline{R}}}} \tag{D-13}$$

It should be noted that the numerical constant in equation (D-12) depends upon both the capsule diameter and shell thickness.

(3) CASE 3: i=2

The only difference between the expressions for this case and those for case 1 is the equation for the temperature at point 1, which can be obtained by expanding the temperatures at point 2 and at the phase-change interface about point 1 to obtain

$$T_1 = \frac{\dfrac{-(1+E)}{E} T_2 - \dfrac{K_p}{K_c} \cdot \dfrac{T_{sur}}{1.39}}{\dfrac{(2+E)}{(1+E)} - \dfrac{K_p}{1.39 \cdot K_c}} \qquad (D-14)$$

(4) CASE 4: i=20

In this case, the melting/freezing front lies between point '20' and the center point of the capsule.

Speed of the Moving Boundary

The temperature gradient on the left side of the moving boundary can be obtained by substituting i=20 into equation (D-3) to obtain

$$\left. \frac{\partial T}{\partial \overline{R}} \right|_{\overline{R}=\overline{R}^{\bullet}}^{+} = \frac{-1}{\Delta \overline{R}^2} \left[\left[\frac{E+1}{E} T_{20} - \frac{E}{E+1} T_{19} \right] \right] \qquad (D-15)$$

The temperature gradient on the right side is, using (D-2)

$$\frac{\partial T}{\partial \bar{R}}\bigg|_{\bar{R}=\bar{R}^{\bullet}}^{-} = \frac{-T_{21}}{(1-E)\Delta\bar{R}}$$

(D-16)

Applying equation (D-7) the speed of the moving boundary becomes

$$\frac{\partial E}{\partial \eta} = \frac{-1}{\Delta\bar{R}^2}\left[\left[\frac{E+1}{E}T_{20} - \frac{E}{E+1}T_{19}\right] + \zeta_2\left[\frac{-T_{21}}{(1-E)}\right]\right]$$

(D_17)

Finally, the temperature at point '21' must satisfy the following equation (which is obtained from the general governing equation by noting that at this point, R=0)

$$\frac{\partial T}{\partial \eta} = 3\frac{\partial^2 T}{\partial\bar{R}^2}$$

(D-18)

with the boundary condition

$$\frac{\partial T}{\partial R} = 0 \qquad\qquad \bar{R} = 0$$

APPENDIX   E

MELTING AND SOLIDIFYING PROCESSES IN A GLAUBER SALT

(1) Introduction

This appendix describes work to investigate, both theoretically and experimentally, the phase change processes of a Glauber salt developed as a thermal energy storage material. The main objective of the present experiment was to check the melting and solidification behavior and compare the experimental results for the phase-change location in a one-dimensional system with the classical Stefan solution.

The experimental result shows that the location of the moving interface between solid and liquid phases and the temperature distribution along the x-direction agree well with the classical analytical solution due to Stefan [44], and that the freezing temperature is a little lower than the melting temperature.

The Glauber's salt used in the experiment was obtained from encapsuled pellets used in a DoE funded study at the University of Tennessee, Project No. 7685 s-17. A bulk quantity of this material was obtained by cutting away the capsule coating.

(2) Experimental set up and procedure

The experimental set up consisted of a cylindrical test section 1.5 ft long and 2.5 inch in inner diameter; a heater which consisted of a solid aluminum cylinder wrapped with electrical resistance wire, and a three-legged support. The electric A.C. power to the heater was controlled with a powerstat, which allowed adjustment of the temperature at the bottom of the test section. Nineteen thermocouples, ten of them on the inner surface of test section wall and equally spaced in the x-direction, and nine on the centerline with equal x-direction spacing, were used to measure the temperature distribution in the salt and along the wall. The latter nine thermocouples were glued to a 0.15 inch glass tube, and then the tube was inserted in the centerline. All of the thermocouples were connected to a Hewellet-Packard model 9826 computer to record temperatures automatically. The set up is shown schematically in Figure E-1.

In the solidification test, another solid alumimum cylinder six inches long and three inches in diameter was used to replace the heater cylinder. The replacement unit had, of course, no electrical heating wire. In this case half of the aluminum cylinder extended out the bottom of the plastic cylinder and into an ice-water mixture to cool
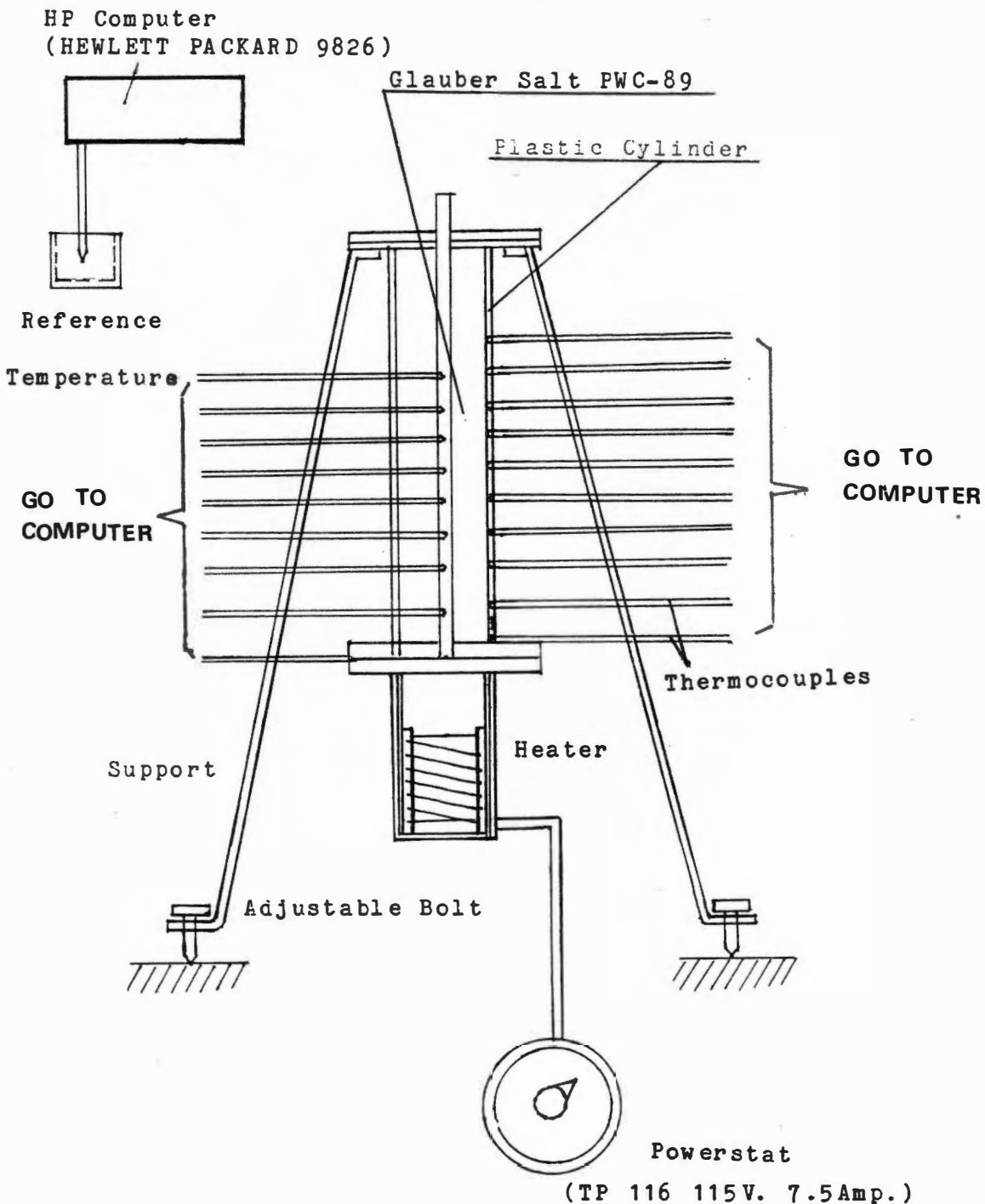
Figure E-1.   Schematic Diagram of Experimental Setup

the bottom of the test section.

(3) Theoretical analysis

This is a one-dimensional phase change problem and can be described after Stefan method [44] by the following set of partial differential equations for the melting case.

For the liquid phase

$$\frac{\partial^2 T_l'}{\partial x^2} = \frac{1}{a_l} \frac{\partial T_l'}{\partial t}$$

(E-1)

and the solid phase

$$\frac{\partial^2 T_s'}{\partial x^2} = \frac{1}{a_s} \frac{\partial T_s'}{\partial t}$$

(E-2)

the coupling conditions at the interface are

$$T_l' = T_s' = T_m'$$

(E-3)

and

$$\zeta_2 \frac{\partial T_s}{\partial x} - \frac{\partial T_l}{\partial x} = \frac{1}{a_l} \frac{\partial x^*}{\partial t}$$

(E-4)

Assuming that the initial temperature equal to the melting temperature

$$T_s' = T_i'(x) = T_m' \qquad\qquad t = 0$$

the equations will be simplified as follows

$$\frac{\partial^2 T_l'}{\partial x^2} = \frac{1}{a_l} \frac{\partial T_l'}{\partial \eta} \qquad\qquad\qquad (E-5)$$

$$-K_l \cdot \frac{\partial T'}{\partial x} = \rho L \frac{\partial x^*}{\partial t} \qquad\qquad x = x^* \qquad\qquad (E-6)$$

With the boundary conditions

$$T_l' = T_l' \qquad\qquad x = 0 \qquad\qquad t > 0$$

$$T_l' = T_m' \qquad\qquad x = x^* \qquad\qquad t > 0$$

The analytical solution(See, for example, reference 43) can be expressed as

$$T_l(x,t) = \frac{erf(x/2(a_l \cdot t)^{1/2})}{erf(\lambda)} (T_m - T_o) + T_o$$

and

$$x^* = \lambda \cdot 2(a_l \cdot t)^{1/2}$$

where λ can be determined from the following transcendental equation

$$\lambda \, e^{\lambda^2} \cdot erf(\lambda) = \frac{C\,(T_o - T_m)}{L\sqrt{\pi}}$$

(4) Results and Discussion

Melting Test:

The bottom temperature was maintained at 180+4 F, and the temperatures were recorded once every 12 minutes. Figure (E-2) shows the measured temperature at the bottom of the test section.

Figure (E-3) shows the transient response of the melting front, which indicates that the experimental results are essentially coincident with the theoretical results, especially in the first run. The difference between the first and the second runs was caused by some initial cavities in the solidified Glauber's salt due to the solidification process in the test apparatus.
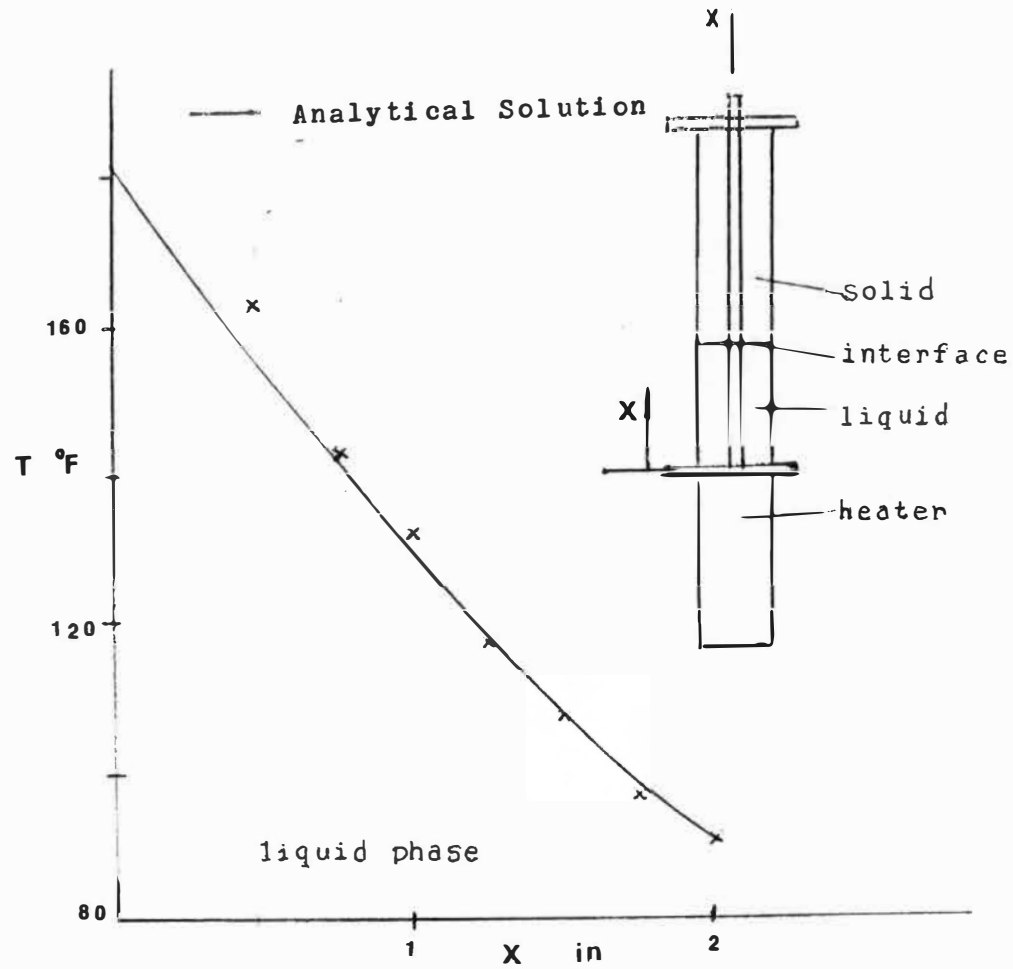
Figure (E-4) shows the temperature distribution along the x-direction. Clearly, good agreement between the experimental results and the analytical results has been found. This, of course, is an indication of the validity of the properties given by the manufacturer for this PCM. Unfortunately, no packed bed results were obtained with
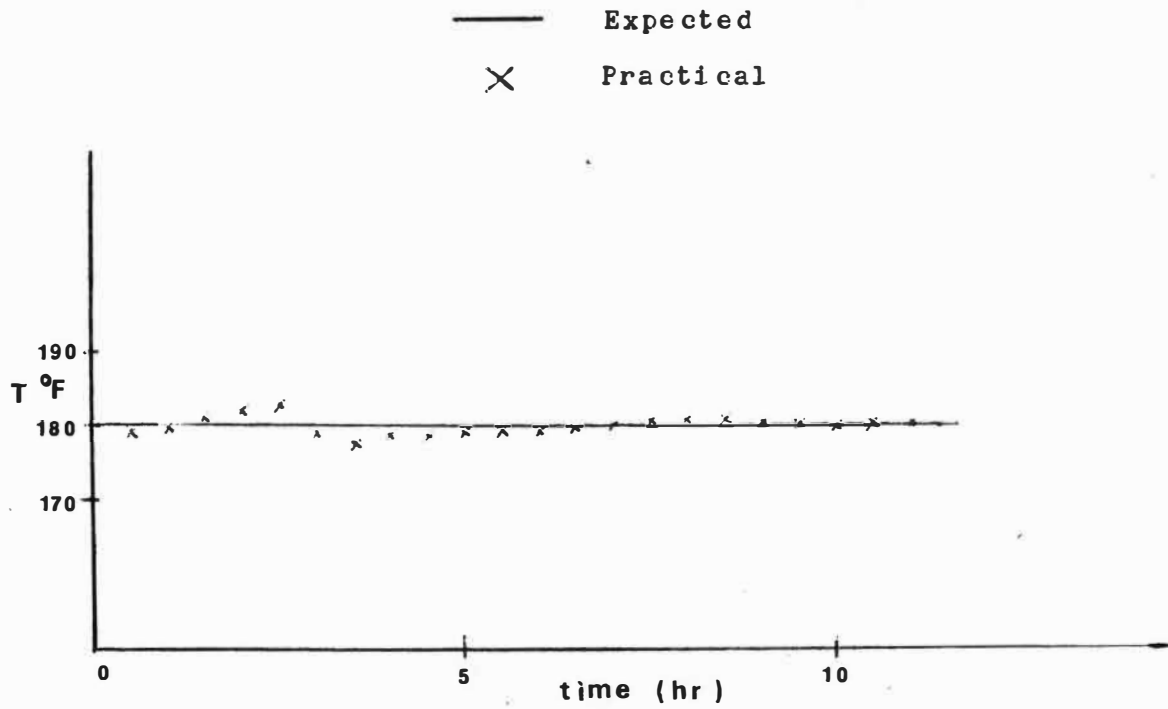
E-2. Input Temperature on Bottom Surface of Test Section
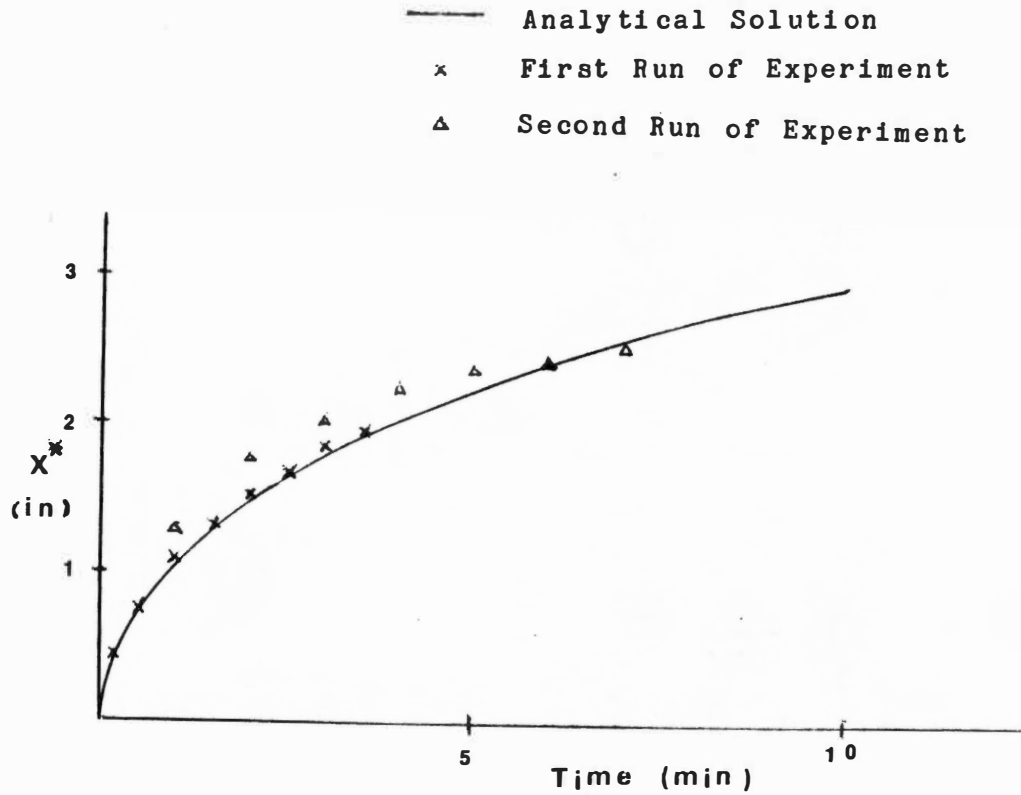
E-3. Transient Response of Melting Front

E-4. Temperature Distribution in Liquid Region
along x-Direction

this material due to mechanical failures of the encapsulating material.

Solidification Test:

The bottom temperature was maintained at 32 ± 0.5 F. The temperature at point A was recorded every 10 minutes except at the beginning and at times near freezing. From the temperature record at point A, the freezing temperature can be estimated to be in the range of 83-84.5 F, which is about 5-6 F lower than the melting temperature. Figure (E-5) indicates the temperature variation at point A with time.

During these tests, visual observation indicated that the phase-change interface was clear and no noticeable "mushy region" was observed in the melting process.
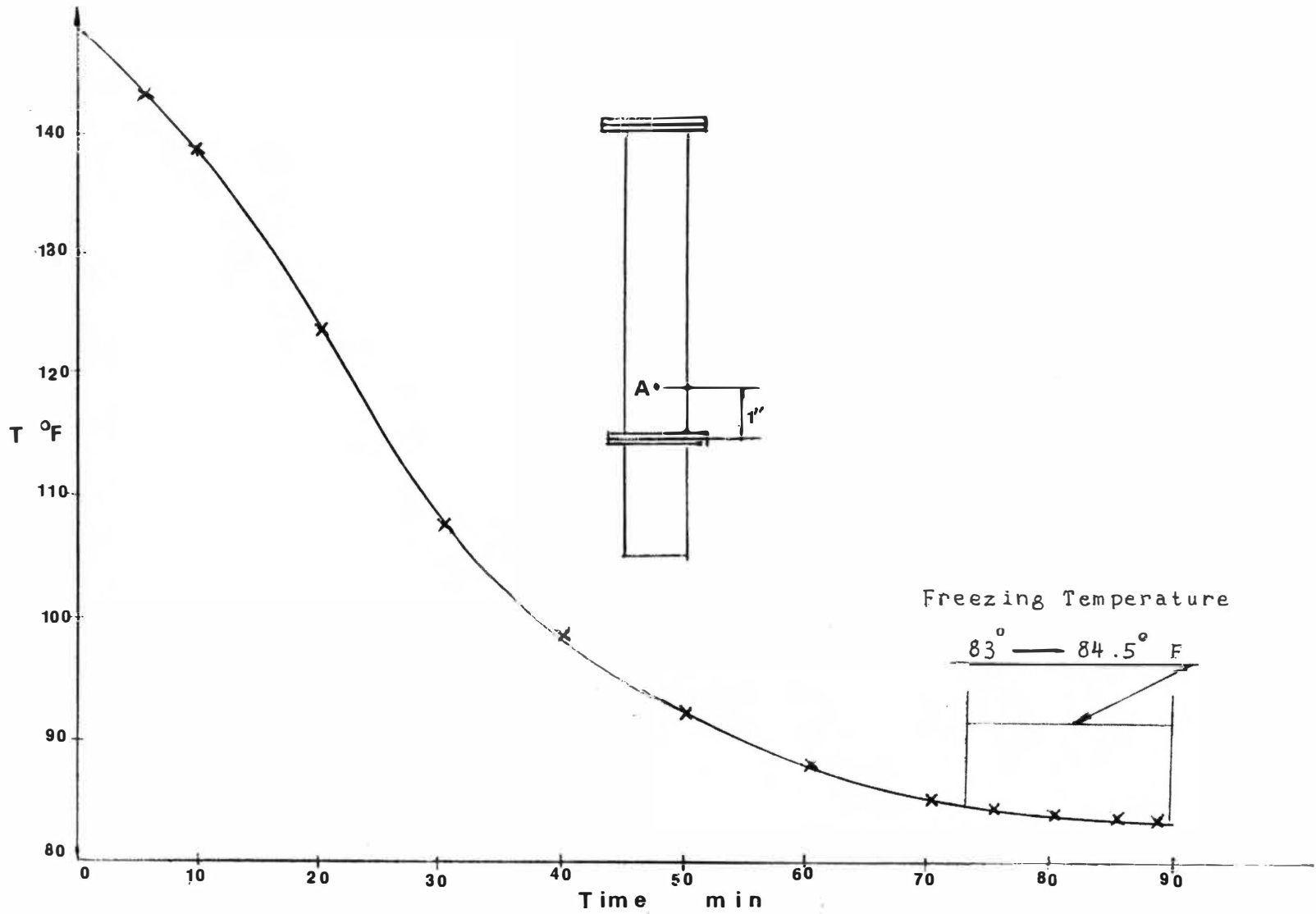
E-5. Variation of Temperature at Point A with Time

VITA

Shi-Hong Ji was born in Taichow, Jiansu province of China(PRC) on November 28,1937. He attended elementary schools in that city and was graduated from Taichow High School in June 1955. The following September he entered Chinhua University, and in January 1961 he received a Bachelor of Science degree in Power Machinery Engineering. In Spring of 1961 he worked as a engineer in Peking Researh Institute. IN 1965 he was promoted to a chief engineer of a research group and now he is a division head in that institute.

The author is a member of Peking Aeronautical and Astronautical society. He will return back to China after graduation.